DESIGN AND VERIFICATION OF SHAPE MEMORY POLYMER EMBOLIZATION DEVICES FOR PERIPHERAL INDICATIONS

A Dissertation

by

TODD LAWRENCE LANDSMAN

Submitted to the Office of Graduate and Professional Studies of
Texas A&M University
in partial fulfillment of the requirements for the degree of

DOCTOR OF PHILOSOPHY

Chair of Committee,	Duncan J. Maitland
Committee Members,	Fred J. Clubb Jr.
	John C. Criscione
	Ruth L. Bush
Head of Department,	Anthony Guiseppi-Elie

August 2016

Major Subject: Biomedical Engineering

ABSTRACT

Polyurethane shape memory polymers (SMPs) have found a variety of uses in the medical industry in the form of self-tightening sutures, suture anchors, ligament fixation devices, vascular stents, and thrombectomy devices. New formulations of polyurethane SMP scaffolds are gaining significant interest for use in vascular embolization procedures. These scaffolds have demonstrated rapid time to occlusion, improved healing, and favorable biocompatibility, and they eliminate the need to implant multiple devices to achieve stable occlusion, significantly reducing procedure times and the total cost of treatment. Described here are various methods used to fabricate SMP scaffolds, indications for SMP scaffold embolization, advantages of using these scaffolds in embolization procedures, results seen in vivo and in vitro to verify the safety and efficacy of the SMP scaffolds, and future directions for SMP scaffolds that will propel the technology to significant use beyond vessel occlusion.

The research described in this work resulted in the creation of novel embolic devices that have the potential to drastically reduce the cost of endovascular embolization procedures by reducing the number of devices required for treatment, radiation time, the need for repeat procedures, and the time to complete healing of the treated vessel. These devices also demonstrated resistance to undesired thromboembolism in vitro, while also exerting negligible radial force on the vessel endothelium to minimize the likelihood of vessel rupture or perforation. In vitro verification testing demonstrated that this device appears to be safe and effective for embolization within the peripheral vasculature. This

work also represented the first verification of the echogenicity of shape memory polymer foam devices in vitro. In addition, this research solidified the designation of polyurethane shape memory polymer foam as a platform technology that can be combined with other material systems to create shape memory occlusive devices with enhanced fluid uptake and bactericidal properties.

ACKNOWLEDGEMENTS

I would like to express my utmost gratitude to my committee chair, Dr. Duncan Maitland, and my committee members, Dr. Fred J. Clubb Jr., Dr. Ruth Bush, and Dr. John Criscione, for their guidance, support, and continued encouragement throughout the course of this research. Dr. Maitland, I am extremely grateful for the educational and professional development opportunities that you have given me throughout my time at Texas A&M. I have had numerous opportunities that most graduate students never have, and I know how lucky I am. When I decided to pursue my Ph.D., my dream was to design a device and see it through FDA approval where it can benefit thousands of patients. Through the work presented here, I have made substantial progress towards realizing that dream, and you are the primary reason that has been possible.

I would also like to thank my friends and colleagues within the Department of Biomedical Engineering, and especially within the Biomedical Device Laboratory. We are truly lucky to have the supportive, challenging environment we were immersed in since our first days in the lab. Together we have created an environment that fosters innovation and excellence in impactful, translational research, and I am a better engineer, researcher, and man because of each member within the lab.

Thank you to my girlfriend, Ashley McCullough, my mom, Bonnie, my dad, Jim, and my brother, Tim, for always supporting me throughout my decade-long endeavor into higher education. You stood by me, encouraged me, and gave me the support I needed to make it through all the stressful and difficult times. I truly would not have made it this far

in my pursuit of becoming a doctor if it were not for you. I love all of you, and I hope I made each of you proud.

Finally I would like to thank the funding sources that helped make my dissertation possible. All of my research was supported in part by the National Institutes of Health, and specifically the National Institute of Biomedical Imaging and Bioengineering (Grant numbers R01EB000462 and R43EB022016) and the National Institute of Neurological Disorders and Stroke (Grant number U01NS089692). I would also like to thank DEP Shape Memory Therapeutics, Inc. for their willingness to support my research and move the peripheral embolization device towards FDA approval and commercialization.

NOMENCLATURE

AAA	Abdominal Aortic Aneurysm
ACDO	Amplatz® Canine Duct Occluder
ACT	Activated Clotting Time
AVM	Arteriovenous Malformation
AVP	Amplatzer Vascular Plug
BDL	Biomedical Device Laboratory
CVI	Chronic Venous Insufficiency
DCM	Dichloromethane
DI	Deionized
DSC	Differential Scanning Calorimetry
EVA	Endovenous Ablation
GDC	Guglielmi Detachable Coils
HDI	Hexamethylene Diisocyanate
HDPE	N,N,N’,N’-Tetrakis(2-hydroxypropyl)ethylenediamine
HIPE	High Internal Phase Emulsion
IFU	Instructions For Use
IVUS	Intravascular Ultrasound
NVP	N-vinylpyrrolidone
PBS	Phosphate Buffered Saline
PCS	Pelvic Congestion Syndrome
PDA	Patent Ductus Arteriosus

PED	Peripheral Embolization Device
PEDGA	Polyethylene Glycol Diacrylate
PFO	Patent Foramen Ovale
PLA	Poly(d,l-lactide)
POSS	Polyhedral Oligomeric Silsesquioxane
PTAH	Phosphotungstic Acid Hematoxylin
PTFE	Polytetrafluoroethylene
PVA	Polyvinyl Alcohol
PVC	Poly(vinyl chloride)
PVP	Polyvinylpyrrolidone
RNE	Recurrent Neurological Events
RO	Reverse Osmosis
SEM	Scanning Electron Microscopy
SMA	Shape Memory Alloy
SME	Shape Memory Effect
SMP	Shape Memory Polymer
TEA	Triethanolamine
THF	Tetrahydrofuran
VI	Venous Insufficiency

TABLE OF CONTENTS

Page

LIST OF FIGURES

Page

LIST OF TABLES

Page

CHAPTER I

INTRODUCTION*

Researchers in the medical industry have been drawn to the advantages of shape memory materials, such as nitinol, since 1971. [1] Until the 1990s, commercially available shape memory materials used in the medical industry were limited to nickel–titanium, copper, and iron-alloy systems. [2] In 1985 Drs. Robert Ward and Judy Riffle of Thoratec Laboratories Corporation, Pleasanton, California, filed a patent titled "Method for making an article with shape-memory properties and some of the thus obtained articles," which is one of the first descriptions of what is considered a shape memory polymer (SMP) today. In 1990 Dr Hayashi of Mitsubishi Heavy Industry, Japan, published his findings on one of the first commercial thermoplastic SMPs. [3] SMPs offer several advantages over traditional shape memory alloys (SMAs). For instance, SMPs can recover up to 400% plastic strain versus only 7–8% for SMAs, they typically cost approximately 10% of the cost of SMAs, SMPs can be fabricated with densities less than 1.25 g/cm3, they can be tuned to have a wide range of transition temperatures for numerous applications, and they have demonstrated biocompatibility in various applications. [4] Since the introduction of SMPs into the marketplace, they have continued to garner significant interest as highly advantageous materials for use in the medical industry.

SMPs are capable of switching between a primary and a secondary shape on the input of an external stimulus, such as heat or UV light. [5, 6] These materials can be

* Parts of this chapter are reprinted with permission from "Embolic Applications of Shape Memory Polyurethane Scaffolds" by Todd L. Landsman, Andrew C. Weems, Sayyeda M. Hasan, Robert S. Thompson, Thomas S. Wilson, Duncan J. Maitland, *Advances in Polyurethane Biomaterials*. Copyright (2016) Elsevier Ltd.

due to the switching segments that undergo thermal transitions during programming while the permanent shape is maintained by the net points of the polymer. [5, 6] Net points are physical or chemical cross-links that provide the shape memory effect (SME) for the polymer.

SMPs can be fabricated using a variety of polymer systems, including poly(ε-caprolactones), acrylates, polynorbornenes, cross-linked polyethylenes, poly(ether ketones), and polyurethanes. [7-12] From 2005 to 2015, polyurethane SMPs have garnered significant interest for use in implantable medical devices. This is primarily because they are easily manufactured in large quantities using conventional polymer fabrication techniques, their mechanical properties and transition temperatures are easily tuned to match specific applications, and they have demonstrated extensive biocompatibility. [4, 13-15] These characteristics of polyurethanes have resulted in their implementation into the design and fabrication of numerous medical devices, such as thrombectomy devices, cardiovascular stents, self-tightening sutures, and kidney dialysis adapters. [16-19] However, perhaps the most intriguing technologies with the potential to compete with current FDA-approved devices are polyurethane SMP foams used in embolization procedures. The goal of embolization, current treatment methods, and how SMP foams can propel these procedures into a new realm of innovation will be discussed in Chapter II. This knowledge was used to design a novel peripheral embolization device that utilizes SMP foam technology. Chapter III details the in vitro verification of the safety and efficacy this device. Chapter IV investigates extending the use of SMP foams into composite devices that also act as a pharmaceutical release platform. This device

incorporated the enhanced swellability and antibacterial properties of an iodine-complexed hydrogel, with the rapid hemostasis and large volume filling capacity of SMP foams to create a new generation of wound dressings to improve patient outcomes in civilian and combat trauma situations.

CHAPTER II

EMBOLIC APPLICATIONS OF SHAPE MEMORY POLYURETHANE SCAFFOLDS*

2.1 Introduction

Researchers in the medical industry have been drawn to the advantages of shape memory materials, such as nitinol, since 1971. [1] Until the 1990s, commercially available shape memory materials used in the medical industry were limited to nickel–titanium, copper, and iron-alloy systems. [2] In 1985 Drs. Robert Ward and Judy Riffle of Thoratec Laboratories Corporation, Pleasanton, California, filed a patent titled "Method for making an article with shape-memory properties and some of the thus obtained articles," which is one of the first descriptions of what is considered a shape memory polymer (SMP) today. In 1990 Dr Hayashi of Mitsubishi Heavy Industry, Japan, published his findings on one of the first commercial thermoplastic SMPs. [3] SMPs offer several advantages over traditional shape memory alloys (SMAs). For instance, SMPs can recover up to 400% plastic strain versus only 7–8% for SMAs, they typically cost approximately 10% of the cost of SMAs, SMPs can be fabricated with densities less than 1.25 g/cm3, they can be tuned to have a wide range of transition temperatures for numerous applications, and they have demonstrated biocompatibility in various applications. [4] Since the introduction of SMPs into the marketplace, they have continued to garner significant interest as highly advantageous materials for use in the medical industry.

* Parts of this chapter are reprinted with permission from "Embolic Applications of Shape Memory Polyurethane Scaffolds" by Todd L. Landsman, Andrew C. Weems, Sayyeda M. Hasan, Robert S. Thompson, Thomas S. Wilson, Duncan J. Maitland, *Advances in Polyurethane Biomaterials*. Copyright (2016) Elsevier Ltd.

synthesized in their primary shape and programmed into an elongated or compact secondary shape via mechanical programming. The SMP maintains this secondary shape due to the switching segments that undergo thermal transitions during programming while the permanent shape is maintained by the net points of the polymer. [5, 6] Net points are physical or chemical cross-links that provide the shape memory effect (SME) for the polymer.

SMPs can be fabricated using a variety of polymer systems, including poly(ε-caprolactones), acrylates, polynorbornenes, cross-linked polyethylenes, poly(ether ketones), and polyurethanes. [7-12] From 2005 to 2015, polyurethane SMPs have garnered significant interest for use in implantable medical devices. This is primarily because they are easily manufactured in large quantities using conventional polymer fabrication techniques, their mechanical properties and transition temperatures are easily tuned to match specific applications, and they have demonstrated extensive biocompatibility. [4, 13-15] These characteristics of polyurethanes have resulted in their implementation into the design and fabrication of numerous medical devices, such as thrombectomy devices, cardiovascular stents, self-tightening sutures, and kidney dialysis adapters. [16-19] However, perhaps the most intriguing technologies with the potential to compete with current FDA-approved devices are polyurethane SMP foams used in embolization procedures. The goal of embolization, current treatment methods, and how SMP foams can propel these procedures into a new realm of innovation will be discussed throughout this chapter.

2.1.1 Scaffold Fabrication Techniques

Numerous fabrication techniques can be used to create porous SMP scaffolds. Each method varies in complexity and results in varying scaffold morphologies, as demonstrated in **Figure 2.1**.

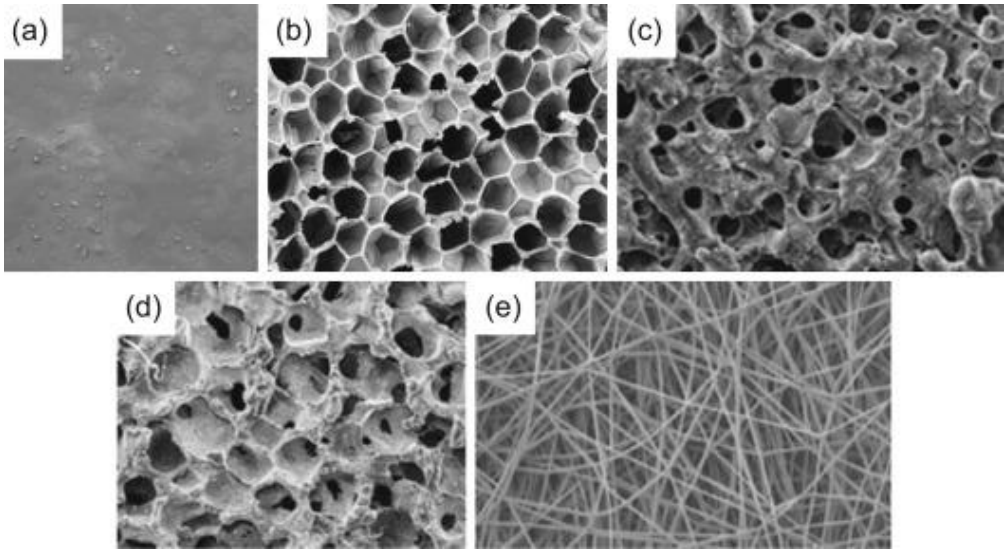

Figure 2.1: SEM image of polymer scaffolds synthesized via (a) solvent casting, [20] (b) gas blowing, (c) emulsion templating, [21] (d) particle leaching, [21] and (e) electrospinning. [6]

The best-suited technique for fabricating a given scaffold depends on the intended application, the polymers being used in the fabrication, and the conditions under which the polymer solutions are cured and maintained. Some of these fabrication techniques include gas blowing, emulsion templating, particle leaching, and electrospinning. Although these are not the only methods that can be used to create a porous polyurethane

scaffold, they are the most widely utilized techniques in industry and academia. Each of these techniques will be described in detail in the following sections.

2.1.1.1 Polymer Film Fabrication

Each foaming technique begins with the preparation of a neat polymer solution. Neat polymer films can be developed by physical treatments such as annealing, elongating the polymer, or by solution casting. [22] Physical elongation of the polymer results in a change in the molecular structure of the polymer, while solution casting allows for the structure to develop at the same time as the membrane formation throughout the scaffold. [22]

Neat polymer fabrication using solvent casting involves thin film formation by dissolving the polymer in an appropriate solvent, casting the polymer/solvent solution onto a solid substrate or mold, and then evaporating out the solvent. This process can result in a uniform, flat surface as shown in **Figure 2.1(a)**. [22] However, solvent selection is an important parameter for controlling film morphology. Ohuno et al. synthesized poly(vinyl chloride) (PVC) films using different solvents and studied the effects of solvent blends on polymer morphology. Tetrahydrofuran (THF) is a good solvent for PVC; however, when water is added the solvent quality decreases, resulting in a decrease in the size of the polymer chains in solution. [22] Additionally, the crystallinity of the polymer may be disrupted with the use of poor or mixed solvents.

Neat polymers have been used extensively for drug delivery applications and as biomaterials that promote cell adhesion. In fact, some of the earliest polymer scaffolds were simply films that promoted cell adhesion and growth. [23] Aljawish et al. synthesized

surface-modified chitosan films and studied the degree of protein adsorption and cell adhesion onto the substrate. Heterogeneous surface morphology of the films improved protein adsorption and subsequently resulted in favorable cell attachment and spreading. [24] Film thickness also played a role in increasing cell viability. It was discovered that thicker films resulted in better cell viability. [24]

2.1.1.2 Gas Blowing

Gas blowing has been a popular synthesis technique used for commercial manufacturing of polyurethane foams for years; however, its use in the biomedical engineering field has grown over the last few years. [21] Gas foaming allows nucleation and growth of gas bubbles that are dispersed within a polymer solution for the development of pores, as shown in **Figure 2.1(b)**. [25] There are two ways to generate bubbles during gas blowing: chemical blowing and physical blowing. Chemical blowing requires a reaction between blowing agents for the generation of gas bubbles, while physical blowing agents can be mixed into the polymer to generate a gas–polymer mixture through vaporization. Gas bubbles nucleate, grow, and coalesce within the mixture resulting in pore development. Carbon dioxide (CO_2) is a widely used blowing agent because of its moderate critical point, nonflammability, and lack of toxicity. [25, 26] CO_2 foaming occurs in two stages: the pressurization stage and the depressurization stage. A gas-saturated polymer phase must be generated followed by pore nucleation, growth, and coalescence. As the foam rises, the gas bubbles trapped in the foam mixture coalesce and the pores grow larger. The processes used in gas blowing are summarized in **Figure 2.2**.

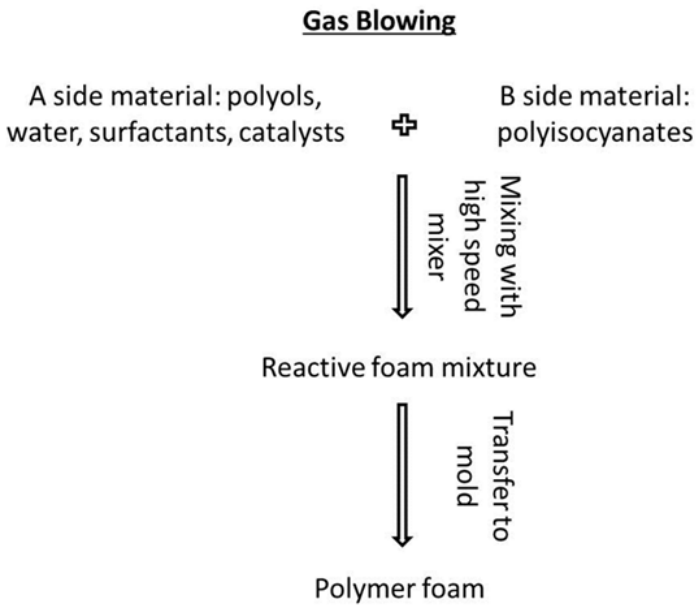

Figure 2.2: Schematic of the steps involved in fabricating porous gas blown scaffolds.

Stabilization of the porous structure can be achieved by chemical cross-linking of the polymer system during foaming, by phase separation, or by cooling it below its glass transition temperature. [27] For polyurethane foams, chain extension with water is effectively used to develop polyurethane ureas. [26] During the foaming step, water is reacted with isocyanate monomers to generate carbon dioxide, resulting in a porous material. Pore structure and interconnectivity can be controlled by varying foaming agent and its concentration in the polymer–gas mixture. [26, 28] A significant advantage of gas blowing is the lack of organic solvents used in the fabrication, which reduces scaffold toxicity for in vivo applications. [21] However, controlling pore sizes and connectivity can be very difficult when using this technique. [21]

Gas blown polyurethane foams have a wide range of biomedical applications as tissue repair scaffolds. Spaans et al. developed biodegradable, biocompatible polyurethane

scaffolds for replacement and repair of the meniscus. The group utilized a 50/50 blend of poly(ε-caprolactone) and poly(l-lactide) for a soft segment, while 1,4-butane diisocyanate constituted the hard segment. [26] The scaffold was synthesized using a combination of CO2 gas blowing and chain extension using adipic acid. CO2 use resulted in interconnected macropores in the final scaffold while chain extension created smaller, homogeneous pores with interconnectivity. [26]

2.1.1.3 Emulsion Templating

Emulsion templating is a popular scaffold fabrication technique that was first utilized in the 1960s. [29] A diagram showing the steps involved in this fabrication technique is shown in **Figure 2.3**. This technique involves the use of two liquid phases, the external and the internal phase. [30] The external phase, also called the nondroplet phase, forms the solid polymeric scaffold while the internal phase, or the droplet phase, consists of oil or water droplets. [31] Simply put, the emulsion of oil in an aqueous/polymer phase allows for the development of a polymer shell around the oil droplets, resulting in a porous scaffold with controlled pore sizes (**Figure 2.1(c)**). Additional components such as surfactants and catalysts are added to stabilize the pores and speed up the reaction kinetics for scaffold synthesis. [30, 32] High internal phase emulsions (HIPEs) are a widely used type of emulsion templating for polymer scaffolds. [30] For this type of emulsion, the droplet phase consists of 70% of the volume of the emulsion and the resulting scaffold has small, interconnected pores. [30] A polymerized HIPE is often called a polyHIPE. To differentiate pore characterization from gas blowing techniques, the spherical cavities generated from the emulsion droplets are called voids.

[33] The voids normally have interconnected holes which are referred to as windows. Synthesis of a polyHIPE consists of mixing reactive monomers, catalysts, and surfactant while slowly adding the droplet phase. [33] Mixing is required to break up the formation of larger droplets due to phase separation. Once the nondroplet phase has cured, the resulting polyHIPE is washed and dried to remove the droplet phase. [33]

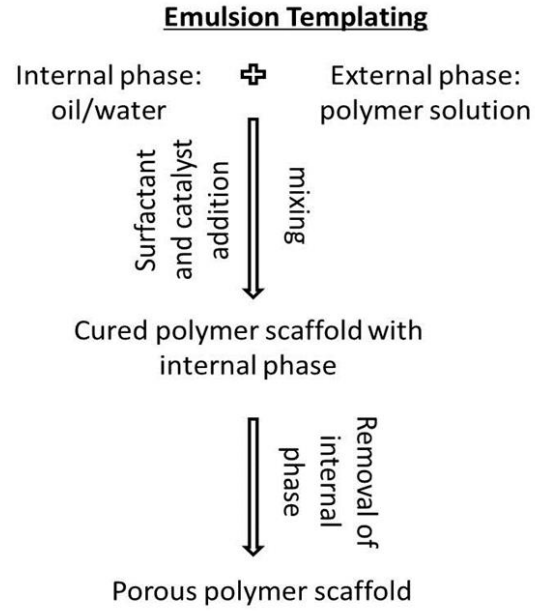

Figure 2.3: Schematic of the emulsion templating process used for fabricating scaffolds.

Void size can be controlled by altering the concentration and viscosity of the external phase and the volume of the internal phase. [29] Surfactant concentration also plays a major role in altering the polyHIPE morphology. [29] Yao et al. studied the effects of a triblock surfactant concentration on polyHIPE morphology. The void structure became more homogeneous and interconnected when surfactant concentration was

increased from 2% to 7% (v/v). [34] Increasing surfactant concentration allows thinning of the polymer films separating adjacent emulsion droplets, allowing for windows to develop in the void structure as the polymer cures. [33] However, one disadvantage of polyHIPEs is the large amount of droplet phase that is required during synthesis. [29] If the droplet phase is organic, further postfabrication cleaning of the scaffold is required to ensure removal of all organic solvents that might cause cell toxicity.

Emulsion freeze drying is another form of emulsion templating that utilizes droplet formation from mixing two immiscible phases as well. [21] However, with emulsion freeze drying the droplet phase is normally water and the emulsion can be frozen quickly once homogeneous voids have been achieved. [21] The scaffold is then freeze-dried to remove the aqueous phase, leaving behind a porous polymer structure. One of the main advantages of this technique is the lack of organic solvents and minimizing the time-consuming drying processes associated with polyHIPEs. [21]

2.1.1.4 Particle Leaching

Particle leaching involves dispersing solid particles into a polymer solution. [35] First, a polymer solution is synthesized at 5–20% concentration in an organic solvent. [36] Then the particles are added to the polymer solution before the solvent is evaporated via air drying, vacuum drying, or freeze drying to embed the solid particles within the polymer matrix. [37] After drying, the polymer/solid composite is immersed in water to dissolve the solid particles, leaving behind a porous polymer scaffold (**Figure 2.1(d)**). This process is summarized in **Figure 2.4**. Most particle leaching techniques utilize salts; however, sugar, ammonium chloride, sucrose, starch, paraffin, and gelatin particles have also been

reported in the literature. [21] Microspheres are preferred for salt leaching because they result in regular pore geometry that enhances the mechanical properties of the scaffold and improves fluid exchange and nutrient supply to cells. [21]

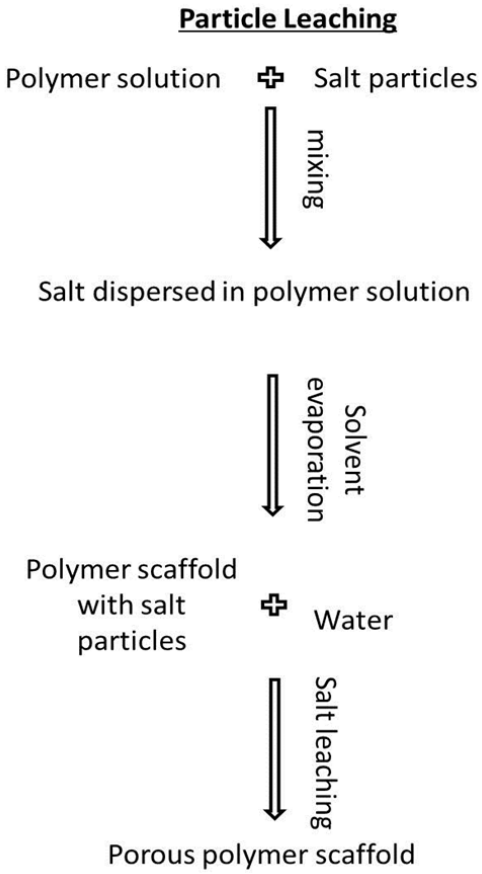

Figure 2.4: Summary of the processes used in creating porous scaffolds by means of particle leaching.

Scaffold porosity can be controlled by varying the particle concentration, while pore sizes depend on the size of the particles added to the polymer solution. [21, 38] If the particle concentration is insufficient, isolated pores will be generated as the polymer

surrounds each particle. Hariraksapitak et al. reported an increase in porosity with higher concentrations of particles (25× to 40×) due to the generation of more voids. However, pore sizes remained in the range of 200–400 μm as a result of the particle size utilized during scaffold synthesis, which indicates that particle size and shape are directly related to the pore size and geometry of the scaffold. [36] Increased particle loading can result in void formation within the scaffold, due to close packing, which will ultimately decrease the overall mechanical properties of the scaffold. [21] Hariraksapitak et al. evaluated compressive and tensile properties for scaffolds with varying porosity. It was reported that higher porosity scaffolds experienced a decrease in both compressive and tensile strength. [36]

An advantage of using particle leaching is the ease of fabrication since no specialized equipment is required for scaffold synthesis. However, the difficulty associated with selecting particle type and size is a disadvantage, because attaining high porosity while maintaining adequate mechanical strength is a challenge. The ability to control and tune the porosity and interconnectivity of a scaffold is especially important for optimizing cell ingrowth and diffusion. [39] Another disadvantage of this technique is that it yields thin materials due to difficulties in leaching salt from large volumes. Organic solvents provide a means of removing salt, although residual solvent may affect cell growth and adhesion.

2.1.1.5 Electrospinning

Electrospinning is a unique scaffold fabrication technique that yields a porous, three-dimensional scaffold that mimics the extracellular matrix (**Figure 2.1(e)**). [40] This

process involves the use of a high voltage power supply applied to the polymer solution to induce jet formation. [40] The basic setup consists of a syringe with a feed pump, high voltage power supply to provide an electrical field, and grounded fiber collector, which is normally a metal plate or a rotating mandrel (**Figure 2.5**). [41] The electrical field generates a charged polymer jet which deforms uniaxially from the needle tip to the grounded collector. [42] During this process, the solvent evaporates, leaving behind dried polymer fibers that form the fibrous scaffold.

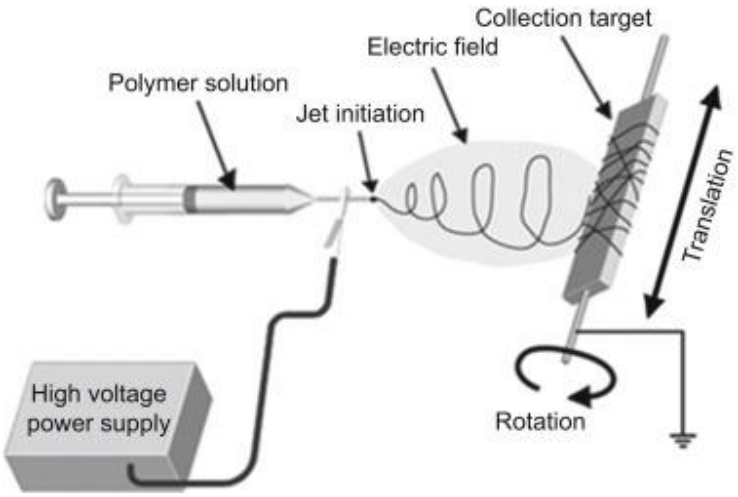

Figure 2.5: Common electrospinning setup used in academia. [41]

Electrospun scaffolds are continuous fibrous scaffolds that result from a polymer melt or solution and have fiber diameters ranging from micro to nanoscale. [40] Electrospinning can be utilized for a wide range of polymers and composite materials, making it a versatile, cost-effective technique for developing biomedical scaffolds with controlled production and easy scale-up. [40] This technique was first used in the 1990s

to develop polymer nanofibers and is currently popular for developing tissue engineering and drug delivery scaffolds. [41] A diagram of a typical electrospinning setup is shown in **Figure 2.5**.

Polymer properties, such as viscosity, surface tension, and conductivity, play an important role in controlling the size, density, and morphology of the electrospun fibers. [40] Solution viscosity is dependent on the polymer molecular weight and degree of entanglements/cross-linking. [42] This affects the development of fibers versus droplets during jet formation, and the subsequent final scaffold could potentially have a combination of both. Lower viscosity solutions generally result in droplet formation while higher viscosity solutions may result in poor jet formation and an increase in fiber diameter. [42] Surface tension of the solution is directly related to the nature of the solvent. A lower surface tension solution may allow the utilization of lower electric fields for fiber formation. [40] However, this may change the solution viscosity and result in droplet formation in the scaffold. Conductivity of the solution is affected by the nature of the solvent and by the incorporation of inorganic salts. [40] Addition of salts, such as sodium chloride, will increase solution conductivity, which in turn increases its mobility under the electric field. [40] This provides greater elongations and thinner diameters of the resulting fibers. Fine-tuning the various parameters of the polymer solution can result in controlled fiber diameters of less than 300 nm for optimal cell infiltration and growth. [43]

2.2 Embolization and Occlusion

2.2.1 Goal of Embolization

In some circumstances blood flow through specific vascular pathways can cause potentially life-threatening complications. In these instances physicians rely on embolization devices to block blood flow to the region. Embolization is a technique in which a physician places a material within a cavity or blood vessel with the intent of completely occluding that region or diverting blood flow from that region. Oftentimes, endovascular embolization supplants highly invasive surgeries used to treat the same morbidity. This is primarily due to reduced treatment costs, recovery time, and patient discomfort, as well as improved clinical outcomes. [44, 45] This type of treatment is used for a wide variety of morbidities, such as arteriovenous malformations (AVM), aneurysms, venous insufficiency, and patent foramen ovale (PFO). [46-50] However, researchers and physicians continue to discover novel indications for endovascular embolization as catheterization technology evolves.

2.2.2 Current Treatment Methods

Although a number of different methodologies exist to exclude vessels from undesired blood flow, such as endovenous ablation, surgical ligation, and sclerotherapy, the following sections describe FDA-approved interventional embolic devices that are most similar to SMP foam scaffolds.

2.2.2.1 Coiling

Embolic coiling involves the placement of a fine coil in a vascular defect to generate and maintain a clot. Initially coils were composed of steel guidewires tipped with

cotton or wool strands that were navigated to the desired location through a catheter under fluoroscopy. This is still the standard procedure used today, but the design of the coils has experienced some changes. [51] The first modern coils were composed of a bare platinum coil and were developed as a method of retaining a clot that was formed by electrothrombosis, a process by which a positive charge is applied to a lead within the aneurysm that attracts negatively charged components of the blood, namely platelets, and forms a clot. Conveniently this same electric current could be used to detach the coil through electrolysis, making a very effective and simple delivery method. [52] Though some alternative detachment methods have been used, most of the variation in embolic coils comes from technologies developed to increase the volume filling and surface area properties of the devices through the addition of hydrogels or fibers, as shown below in **Figure 2.6**. [53-55]

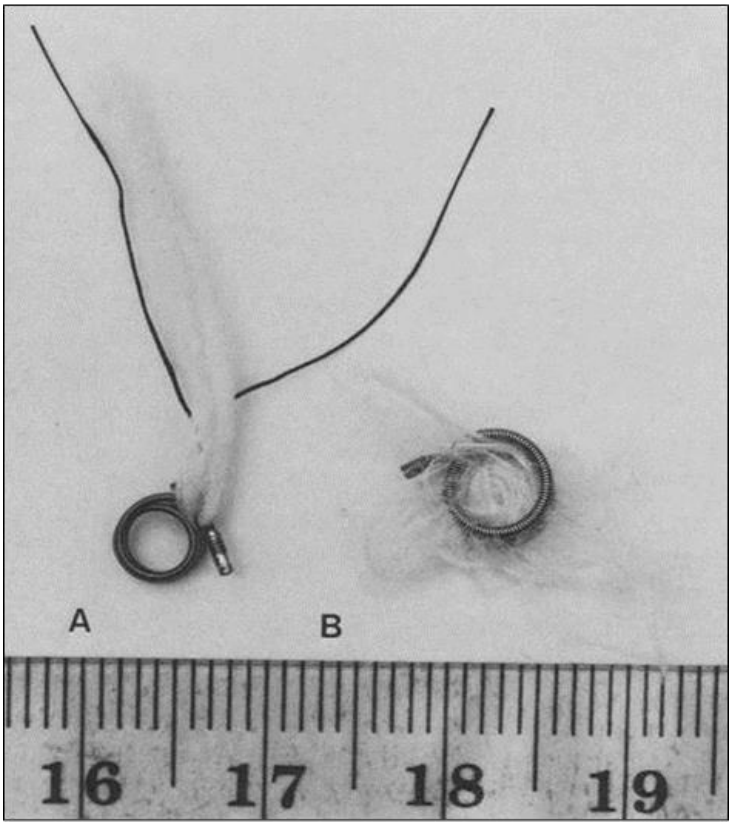

Figure 2.6: (a) Original fibered coils with Dacron fibers attached at the proximal and distal ends of the coil, and (b) the newer style of fibered coils with Dacron fibers attached throughout the length of the coil. [55]

Many coils still use a pushable design that allows them to be delivered using standard guidewires or custom pusher wires. The relative ease of use and low cost of these coils have made them the most popular type of coil in interventional radiology. Detachable coils are still the preferred method where precise positioning is critical for optimal filling, or when coil migration during the procedure is of serious concern. These coils are also typically used when a tortuous pathway may lead to an inability to advance the coil through the entirety of the catheter, which is the case in interventional procedures performed to treat intracranial aneurysms. [56, 57] Endovascular coiling is the most

widely used embolization method but it still has a number of complications. Coils can protrude or fully migrate into the parent vessel and potentially cause a thromboembolism, and the procedure itself is dangerous and can lead to aneurysm rupture. [58] Approximately 20% of aneurysms, particularly those with an internal diameter larger than 25 mm or a neck diameter larger than 4 mm, will experience rebleeding due to coil compaction or device migration. [59] Coiling is typically not well suited for clotting in high flow areas or in areas where the coils could easily migrate. [53, 59, 60]

2.2.2.2 Gelfoam® Plug

Gelfoam®, a gelatin foam available in sheet or powder form that can be formed into a variety of shapes by an interventionalist, is often used off-label to completely occlude specific vessels, although it is not indicated specifically for intravascular embolization. [61] The foam can also be cut into fine segments and mixed with a diluted contrast agent to create a slurry that is injected into the target site, as shown in **Figure 2.7**.

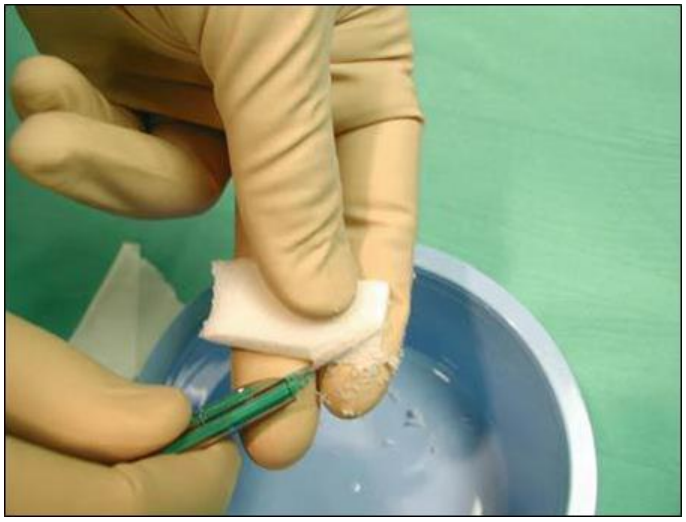

Figure 2.7: A Gelfoam® pledget is shaved with a blade at a 45° angle, allowing the shavings to mix with a contrast agent to produce a slurry that is then injected to the target site. [62]

The device functions as a physical barrier to prevent blood flow through the vessel, but due to the gelatinous and bioabsorbable nature of the foam on saturation, it does not provide a scaffold for clot formation and connective tissue ingrowth. [63] Gelfoam® treatments can lead to downstream embolization due to the nature of the particles and may have a connection with infections, potentially caused by air bubbles trapped in the materials during the mixing process used to prepare the foam. There are also issues with frequent recanalization of treated vessels because the gel is resorbable, and as such, the gel may be fully resorbed before stable fibrosis occurs. Gelfoam® use is often combined with embolic coils so that the gel creates the initial occlusion and the coils are implanted to retain the clot at the treatment region after the body begins resorbing the gelatin. [57, 60]

2.2.2.3 Nitinol Mesh

Nitinol mesh devices, the most notable of which is the Amplatzer Vascular Plug, are a family of endovascular embolization devices that take advantage of nitinol's highly elastic nature to create multiple fine-meshed discs and ovoids that instantly expand on exiting the catheter. One such device is shown below in **Figure 2.8**. The goal of these devices is to provide a sufficiently fine mesh to create flow stagnation and recirculation zones in the device to activate thrombus formation. They have a cost advantage over embolic coils because only one device is used to occlude the target region. However, nitinol mesh devices typically do not create a stable thrombus as rapidly as coils. [57, 64] Newer nitinol mesh devices seek to combine the flexible, self-expanding nature of nitinol with thrombogenic, biocompatible materials like PTFE. One such device is the micro vascular plug system manufactured by Reverse Medical®. This device combines a stent-like structure of nitinol completely covered with PTFE. [65] The inclusion of PTFE seeks to reduce the time to occlusion by forcing the blood flow through the significantly smaller pore sizes of the PTFE cover rather than the nitinol cage.

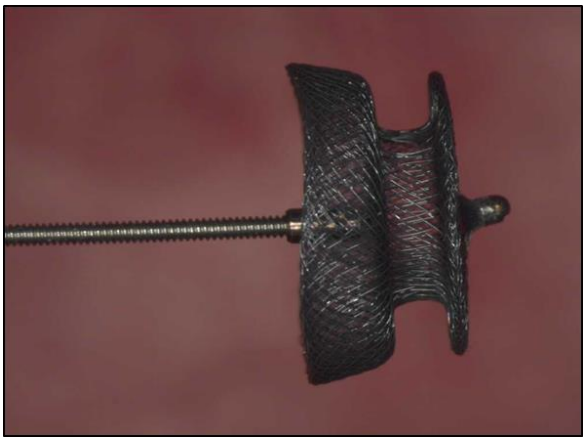

Figure 2.8: Image of an Amplatz® canine duct occluder (ACDO), which shows the fine nitinol wire mesh used as an embolic device to completely occlude patent ductus arteriosus (PDA) in dogs.

2.2.2.4 Polyvinyl Alcohol Foam

Polyvinyl alcohol (PVA) foams can have plastic memory capabilities similar to those of polyurethanes. [66] Currently PVA is mostly used as a foam in a method similar to that of Gelfoam®; it is typically packaged as particles produced from a foam sheet and sorted by size. Typical PVA particles are shown in **Figure 2.9**. PVA foam treatments consist of injecting hundreds to thousands of these particles into the treatment region where they adhere to the vessel wall and produce an inflammatory response resulting in fibrosis. The major issue faced with these PVA treatments is that they can aggregate in the catheter or clot downstream vessels and there have been reports of the foam migrating from the treatment region and causing a pulmonary embolism. [57, 67-69]

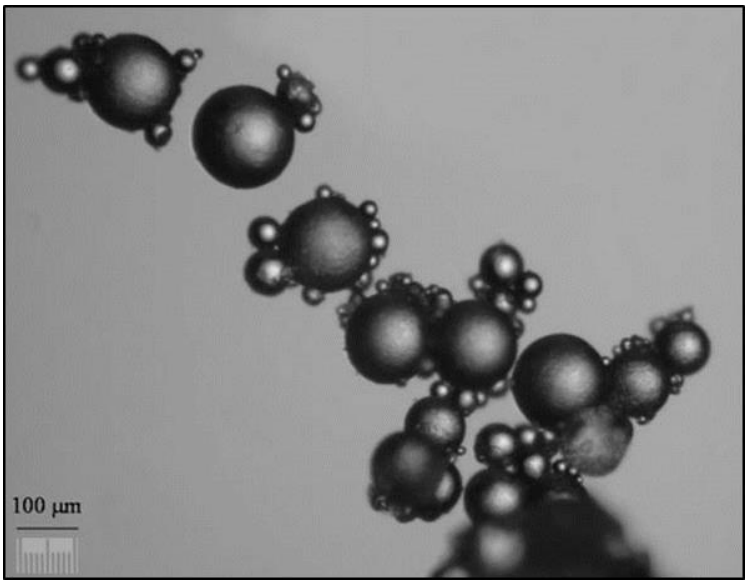

Figure 2.9: Optical microscopy image of unexpanded poly(vinyl acetate)/poly(vinyl alcohol) particles used for embolization in 20 wt% heptane. [70]

2.2.3 Indications for Embolization

2.2.3.1 Arteriovenous Malformations

Vascular malformations, often described as a bag of worms, can occur throughout the body but are most prevalent in the central nervous system. There are many types of vascular malformations, but on their most basic level they are an abnormal connection between an artery and a vein that bypasses or "shunts" a capillary bed. [71] The differentiation in the cellular composition of AVMs varies from distinguishable arterial and venous portions to hyalinized thick and thin-walled portions with no discernable features specific to arteries or veins. [72] Though they are not neoplasms since they possess a nervous parenchyma between the vessels of the malformation, the endothelial cells of the AVM do express higher than normal levels of growth factors and growth factor receptors. [73, 74] These malformations are typically angiographically occult, meaning

that the whole vessel system does not always appear on an angiogram. A typical arteriogram of an AVM is shown below in **Figure 2.10**. This is because the radio-opaque dye used in angiography will follow the straighter, faster paths through the system rather than the more circuitous routes that make up the majority of the malformation. Bruits, unusual sounds in the vasculature caused by turbulence, can sometimes be detected in the presence of these malformations. [75]

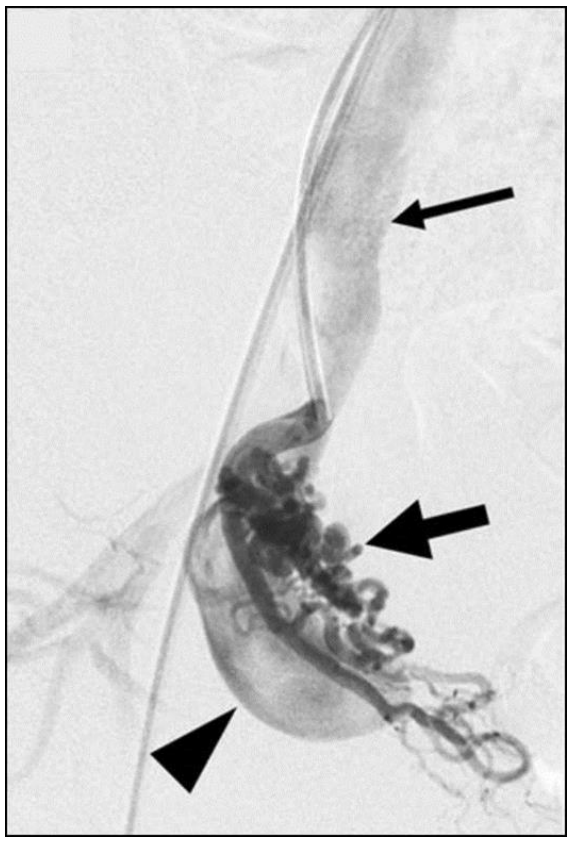

Figure 2.10: Selective vesicle arteriogram showing two right internal iliac arteries feeding an AVM and early drainage to the right internal iliac vein. The nidus of the AVM (black arrow), dilation of the draining vein (black arrowhead), and early drainage of iliac vein (thin black arrow) are shown. [76]

Although these formations are often asymptomatic, they may cause central nervous symptoms such as seizures and ischemia, among other conditions. Localized effects such as hearing and vision loss have also occurred. [77] Treatment for complications associated with AVMs is focused on treating the symptoms of the morbidity. Embolization and resection are used in cases where the physical presence of the AVM poses a concern, such as the structure contacting nerves or, in the presence of endothelium weakening or calcification, a potential for rupture. Treatment typically involves both embolization and resection, sometimes called skeletonization. Embolization is typically done preoperatively to lessen the risk of rupture during the resection procedure and is not usually used as a standalone treatment. [78, 79]

2.2.3.2 Aneurysms

In its simplest form an aneurysm is a dilation of a vessel, typically an artery, at a threshold diameter of about 1.5 times larger than the normal vessel. Abdominal aortic aneurysms (AAA) occur in 5–6% of men and 1–2% of women over the age of 65. The annual mortality rate associated with AAA rupture is approximately 13,000 deaths per year, but this is often thought to be an underestimation. [80-82] Intracranial aneurysms are the second most common aneurysm, occurring in 3% of the adult population, [83] followed by peripheral aneurysms. [84] Like vascular malformations, aneurysms are often asymptomatic but can present with ischemia or other symptoms stemming from increased pressure on the CNS. The most serious complications associated with aneurysms occur when they rupture. Loss of integrity in an intracranial aneurysm can lead to subarachnoid hemorrhage, which has a 30 day mortality rate of 45%, which is mild compared to the

90% mortality rate of a ruptured abdominal aortic aneurysm. [85-87] Treatment is indicated for intracranial aneurysms of any size if they are symptomatic, but oftentimes no intervention is recommended for aneurysms smaller than 10 mm due to a limited likelihood of rupture. The age of the patient is also a significant consideration in determining whether intervention is needed and whether the patient can withstand the trauma associated with surgical intervention.

Currently embolic coils, such as those shown in **Figure 2.11**, are the standard treatment for virtually all aneurysms with the exception of AAAs. [86] Intervention is indicated for abdominal aortic aneurysms if it becomes symptomatic, once the diameter of the aneurysm has reached 5.5 cm, is 250% larger than the patient's normal aortic diameter, or has a growth rate of greater than 1 cm per year. The predominant treatment for an AAA involves the placement of a branched graft spanning a length longer than the dilated portion of the aorta. Occasionally embolic devices are placed in the lumen between the vessel wall and the graft to prevent endoleak, a continued flow of blood into the aneurysm sac rather than through the graft that can potentially lead to aneurysm rupture. [87]

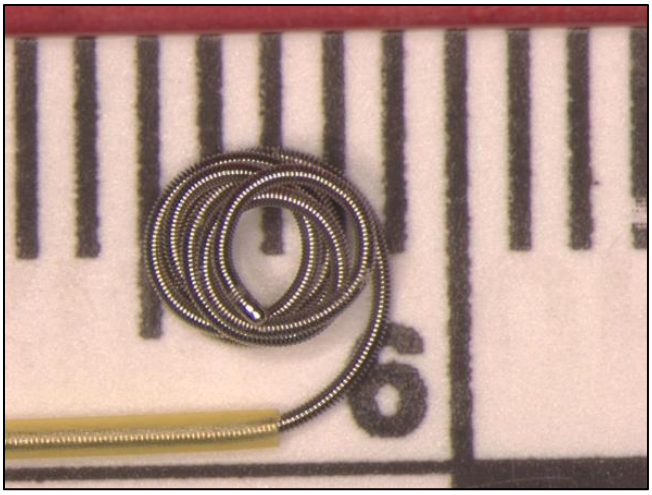

Figure 2.11: Image of a GDC® Ultrasoft detachable coil currently sold by Stryker Corporation. Each line on the scale in the background corresponds to 1 mm.

2.2.3.3 Venous Insufficiency

When venous valves are weakened and allow regurgitation of blood, there is an abrupt increase in venous pressure. [88-90] The increased pressure and resulting venous hypertension are the primary cause of chronic venous insufficiency (CVI). [90-93] The continued prevalence of hypertension leads to dilation of the incompetent veins, resulting in varicose veins like those shown in **Figure 2.12**, the most common manifestation of CVI. [88, 94, 95] If left untreated, CVI can cause dramatic cosmetic changes in skin, lower limb pain, edema, deep vein thrombosis, and ulcers. [95-100] Approximately 400,000–500,000 Americans with CVI have or will develop venous ulcers, typically referred to as venous stasis ulcers. [101-103] Venous ulcers account for the majority of annual health care costs associated with CVI, which are more than 1 billion dollars in the United States and over 650 million dollars in the United Kingdom. [104] The potential consequences of not

treating CVI in a timely manner have prompted physicians to adopt multiple treatment modalities.

Figure 2.12: Pretreatment image of a patient with varicose veins as a result of CVI. [105]

The current gold standard for treating CVI is endovenous ablation (EVA). [100] EVA makes use of a radiofrequency generator or laser energy to denude the endothelium of the target vessel and cause fibrous obliteration of the vessel lumen. [94, 100] Another common technique used to treat CVI is sclerotherapy, in which a liquid or foam detergent is injected into the vessel that chemically damages the endothelium and subsequently

causes fibrosis. [106] Both sclerotherapy and EVA have demonstrated usefulness in treating CVI; however, each treatment comes with its own drawbacks. More than 20% of patients receiving sclerotherapy have to undergo retreatment for recurrent varicose veins, which is greater than the retreatment rate of conventional surgical ligation and stripping procedures. [107, 108] In EVA procedures, multiple injections of local anesthesia are required, followed by injections of tumescent anesthesia. The anesthesia helps prevent pain caused by the laser heating, compresses the vein to make fibrous obliteration of the lumen easier, and also acts as a heat sink around the treatment vessel to minimize thermal damage to surrounding tissue. [109] The number of shots required for this form of treatment results in significant patient pain and discomfort, which is reported in 100% of cases. [100] Although the equipment used in endovenous ablation and the substances used in sclerotherapy continue to evolve, these issues still persist.

2.2.3.4 Patent Foramen Ovale

In utero, there are ostia that allow a patent connection between the left and right atria, which allows oxygenated blood from the maternal circulation to enter the left atrium of the fetus. This connection is known as the foramen ovale, and on the baby taking its first breath, the increased pressure in the left side of the heart permanently fuses the septum primum and septum secundum over the foramen ovale in 80% of cases. In the other 20% of cases, the septa do not completely occlude the foramen ovale, resulting in a condition known as a patent foramen ovale (PFO), which is demonstrated in **Figure 2.13**. [110] PFOs frequently go undiagnosed for a number of years since patients typically show no clinical symptoms. However, if steps are not taken to occlude the PFO, paradoxical

embolisms may occur where emboli from the peripheral veins enter the arterial circulation through the PFO shunt—a well-known cause of cryptogenic stroke. [111, 112] Studies have also shown that PFOs may be to blame for a large percentage of patients who experience migraines. In one study of 162 patients, 35% of individuals diagnosed with a PFO concurrently experienced frequent migraines. [113]

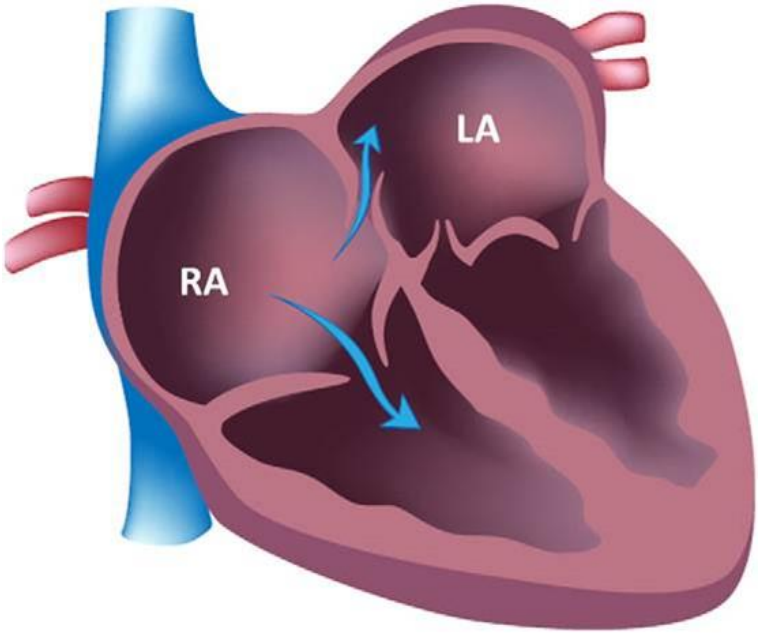

Figure 2.13: Demonstration of the right to left shunt between the atria within the heart caused by a PFO, which can lead to paradoxical emboli and cryptogenic stroke. [114]

To eliminate the risks associated with a PFO, physicians used to attempt surgical closure of the PFO, but this technique is virtually never used in current practice. [114, 115] Instead, PFOs are now treated using a transcatheter approach in which an embolic device is placed between the atria to prevent blood flow from the right atrium directly into the left atrium. [116] This procedure has become known as the simplest procedure in

interventional cardiology, primarily due to the low incidence of surgical complications and the effectiveness of current devices. [117] Reisman et al. have demonstrated that PFO occlusion results in complete resolution of migraine symptoms in 56% of patients 1 year posttreatment, and patients reported having 80% fewer migraine episodes per month. [113] With regard to recurrent neurological events (RNE), such as cryptogenic stroke and transient ischemic attacks from paradoxical thromboembolisms, transcatheter embolization of the PFO resulted in an 84% reduction in RNE compared to medical treatment with only pharmaceuticals. [118] The benefits of PFO closure have illuminated the necessity for percutaneous stable occlusion of PFOs, especially in elderly patients who are more susceptible to peripheral thromboembolisms.

One of the most widely used and successful devices for percutaneous PFO closure is the Amplatzer PFO Occluder (St. Jude Medical Inc., St. Paul, MN), which is a device consisting of two nitinol discs that contain a polypropylene mesh. [119] These types of devices have demonstrated complication rates of less than 5% and procedural success in 100% of cases. [120] However, only 65% of the patients showed complete occlusion of the foramen ovale at 30 day follow-up. New generations of PFO closure devices could benefit from tissue scaffold technologies to allow rapid healing and tissue integration to achieve complete occlusion of PFOs at earlier time points. Another likely trend in future PFO devices is the use of biodegradable materials, which would allow treatment of younger patients since no permanent metallic structure would remain in the heart during its growth and development. The potential to treat patients earlier on would provide

preventative measures that would dramatically decrease the likelihood of cryptogenic stroke and transient ischemic attacks as a result of a PFO.

2.3 Why Shape Memory Polymer Scaffolds?

2.3.1 Biocompatibility

Immediately on implantation and exposure of a material to the host, biocompatibility is primarily dependent on the material, as the cell–polymer and polymer–protein interactions are the dominant causes of host response; after the material begins to degrade, biocompatibility becomes a function of the bulk material. Implant size, geometry, surface chemistry, roughness, surface energy, porosity, composition, sterility, and chemical composition are major factors in determining overall biocompatibility. [121] While many advances have been made to improve thromboresistance or to reduce inflammatory responses of implantable materials, there still exists a great need for understanding how and why the body responds to certain stimuli more intensely compared with others. [122] Without dealing with a specified definition of biocompatibility, several materials are presented that have been proven to be biocompatible.

Polyhedral oligomeric silsesquioxane (POSS) core and poly(d,l-lactide) (PLA) were fabricated into PLA-grafted nanocomposites with shape memory capabilities and implanted into rats. The degradation rate was directly proportional to the length of the PLA segments. These materials exhibited mild inflammatory response on implantation, and a secondary acute response with degradation. At 1 year follow-up, the inflammatory response was resolved and no pathologic abnormalities were found in any organs. The results indicate that these materials have promise as scaffolds for tissue repair and medical

devices. [123] The use of POSS has also been proposed for nanocomposite films on metallic stents for prevention of late stage thrombosis. [124]

SMP foams evaluated by Sokolowski using the Mitsubishi thermoplastic SMP composition have showed no cell lysis, cytotoxicity, or mutagenicity. They also showed good neointimal formation over the aneurysm neck when implanted as a potential aneurysm filling device, and explanted devices showed favorable ingrowth of cells. [125] In a similar study, polyurethane SMPs developed by Wilson et al. have demonstrated biocompatibility, with little variation seen between the thermoplastic and the thermoset compositions. Thermoplastic SMPs showed higher cytokine production compared with thermosets, but both compositions showed no contact activation, thrombin, or plasmin generation. [126, 127] SMP foams based on this composition have also shown excellent biocompatibility when tested using porcine models. These foams demonstrate very low inflammation response compared with FDA-approved silk and polypropylene sutures after 4 weeks. The foams also have organized collagen throughout the entire volume of the foam, and the inflammatory response was substantially reduced compared with the suture materials. [50, 128]

2.3.2 Thrombus Formation

The mechanism of thrombus formation and the effects of polymer surfaces are briefly discussed here. [122, 129-131] Endothelial cells generally produce three thromboregulators: nitric oxide, prostacyclin, and ectonucleotides CD39. These products prevent thrombus formation until they are disrupted. When the endothelium is disrupted, tissue factors and collagen that are exposed to blood flow begin initiating thrombus

formation. This occurs due to the accumulation of activated platelets, a result of the exposed collagen, and the generation of thrombin, which simultaneously activates platelets and converts fibrinogen into a fibrin mesh. A number of other factors interact to allow for platelet adhesion to the injury site, with certain environmental or chemical conditions providing opportunities for either the collagen or the tissue factors dominating the pathway to cause thrombogenesis. Due to these redundancies in the pathway to clotting, this can provide difficulties in preventing clot formation. This also provides a beginning explanation for why prevention of thrombus formation on materials surface is so difficult, even with specialized coatings. [130] When a foreign surface comes into contact with blood, factor XII is converted into factor XIIa, which is a part of the intrinsic clotting system. Eventually, this results in factor X being cleaved into factor Xa, which will in turn cleave prothrombin into thrombin. Thrombin activates the monomer fibrinogen, which polymerizes into fibrin. Fibrin as a polymer is not completely stable until factor XIIIa is present to stabilize it. Additionally, as the clot is forming the matrix will be supported by platelets and fragments attaching to the polymer. The control mechanisms for clot formation include control of local flow, surface-mediated controlled release of catalyst, release of thrombus inhibitors (antithrombin III, tissue factor pathway inhibitor, etc.), and degrading coagulation factor release (fibrinolytic enzyme plasmin, which can degrade fibrinogen and fibrin, as well as inactivate cofactors V and VIII). In this way, blood flow normally does not cause significant clotting to occur until the tissue is damaged, but once damage is detected, clotting can rapidly occur. Due to this, the presence of certain material surfaces can cause continual clotting and result in eventual

failure of the device. By altering the surface chemistry or present local chemical factors near the material, these failures can be mitigated. Several research trends attempting this are presented as well. [132, 133]

At the end of healing, fibrosis or fibrous encapsulation is the ideal response for an embolic device. The process begins with injury to the tissue and implantation of the material. Thrombi, or blood clots, begin to form immediately based on the processes previously described, over the course of minutes to hours. This is enhanced by changes in blood flow patterns, permeability of blood vessels, and composition of the fluid flowing through the area of interest. The thrombus matrix is composed primarily of fibrin, activated platelets, inflammatory cells, and endothelial cells. Platelets in the matrix release a series of factors that contribute to the recruitment of fibroblasts; monocytes and lymphocytes also assist in recruiting fibroblasts. The fibrin in the clot, which has fibronectin bound to it, is cross-linked by factor XII, and other adhesive factors provide a means for cell adhesion and proliferation into the clot. During acute inflammation primarily neutrophils are recruited to the site of device implantation, which will see the initiation of phagocytosis, recruitment and attachment of cells to the foreign material, and the release of degradation-inducing chemicals near the implant surface. This is followed by chronic inflammation, which involves the recruitment of monocytes, lymphocytes, and plasma cells; the other path is the formation of granulation tissue, which begins to occur within days after implantation with the recruitment and proliferation of fibroblasts into the target site. Granulation tissue contains vascular buds, which is recruited by the fibrin present in the thrombus. Collagen and proteoglycans begin to organize in the clot matrix

due to the fibroblasts. As granulation tissue progresses, collagen becomes the dominant tissue type present and begins to contract. Based on the chemical structure of the material and the protein adhesion to the material on implantation, the foreign body response will occur to varying degrees. The number of macrophages present at the site will depend on these factors, as well as the irritation that the material causes. Macrophage fusion into foreign body giant cells, along with remaining clot, will result in encapsulation of the material. The ideal final healing stage for embolic devices is fibrous encapsulation or full reintegration; passive surfaces will have very little or no encapsulation and so will be fully reintegrated into the host. Porous media are an excellent choice for resolutions that do not involve encapsulation, as the porous structure provides a matrix that allows for cellular infiltration and connective tissue proliferation throughout the entire device. [134, 135]

Polyurethanes are a preferred material for blood contacting applications due to superior hemo- and biocompatibility, which are due to the surface properties, chemical structure, interfacial free energy, balance of hydrophobicity with hydrophilicity, and basic surface topography. All of these factors can be tailored in other polymer compositions using a variety of techniques to improve overall compatibility or to tailor the in vivo response to the material. In SMP foams, the scaffold morphology and porosity create areas of low blood shear rates and recirculation zones, which are necessary for rapid clotting. **Figure 2.14** shows SMP foam threaded over nitinol and platinum coil devices that were delivered endovascularly to a porcine sidewall aneurysm. The explant of the devices showed organized, stable thrombus throughout the entire volume of treatment devices, which completely occluded the aneurysm. These porous media structures provide an

effective means of creating flow stasis, but then provide a structural entity to allow rapid cellular infiltration and swift reintegration of the tissue/material matrix with the surrounding tissue. [134] Even with the time required to achieve complete healing at the implantation site, faster stabilization of the clot will create superior clinical outcomes and shorter times until the patient is ambulatory without the risk of thromboembolism.

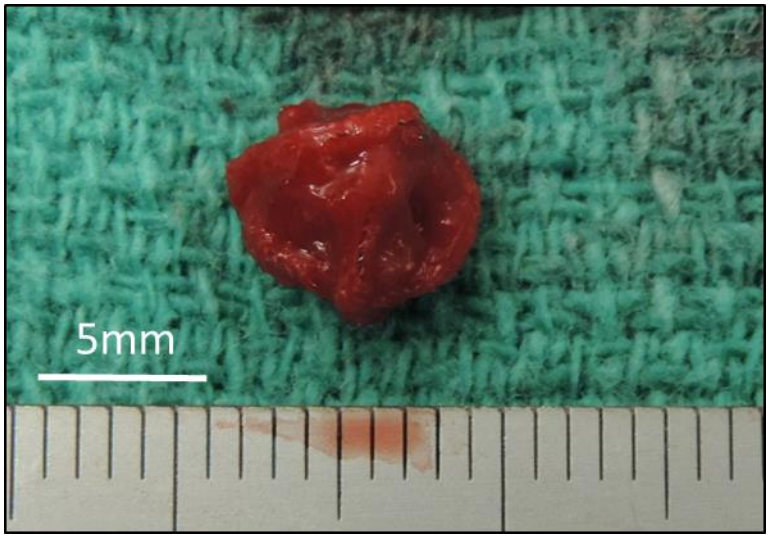

Figure 2.14: Explanted SMP foam-over-coil devices that were delivered using a transcatheter approach to occlude a carotid porcine sidewall aneurysm. Explant occurred less than 2 h after treatment began. Visible throughout the volume of devices is stable thrombus formation.

2.3.3 Recanalization

One of the most concerning complications associated with vascular embolization is recanalization. Recanalization is the reestablishment of blood flow into a formerly occluded region. [136] This phenomenon destabilizes the occluded region and may lead to significant rebleeding at the treatment site. As a common metric used in describing the

efficacy of embolization techniques, recanalization is the primary reason for retreatment procedures. Recanalization rates as high as 34.3% have been recorded for endovascular aneurysm coiling. [137] This statistic highlights the need to continue improving embolization technologies to reduce the prevalence of recanalization.

Experiments have shown that the size of the vascular anomaly being occluded, as well as the total volumetric filling of the embolic device, plays a critical role in the likelihood of recanalization. [138] Recanalization is thought to initiate in the first weeks after treatment. On observing fibrin matrix replacement with a collagen matrix, recanalization can no longer occur out to 3 months. [139, 140] However, until collagen replacement of the fibrin matrix, the potential for angiogenesis and the generation of microvessels that may cause recanalization exists. Some researchers have demonstrated the ability to prevent angiogenesis by using radiofrequency energy to completely denude the endothelium of the implantation site. [139] Although this method proved effective in preventing recanalization, concerns of thromboembolism, long-term efficacy, and overall clinical safety have prevented widespread adoption of this technique.

In preliminary animal studies that sought to treat surgically induced carotid sidewall aneurysms in a porcine model, polyurethane SMP scaffolds proved to be highly advantageous materials to create long-term, stable occlusion without recanalization. [50] The histology performed in this study 90 days postimplantation demonstrated a mature endothelial layer completely isolating the aneurysm from the parent vessel, and dense connective tissue deposition throughout the entire volume of the device, as shown in **Figure 2.15**.

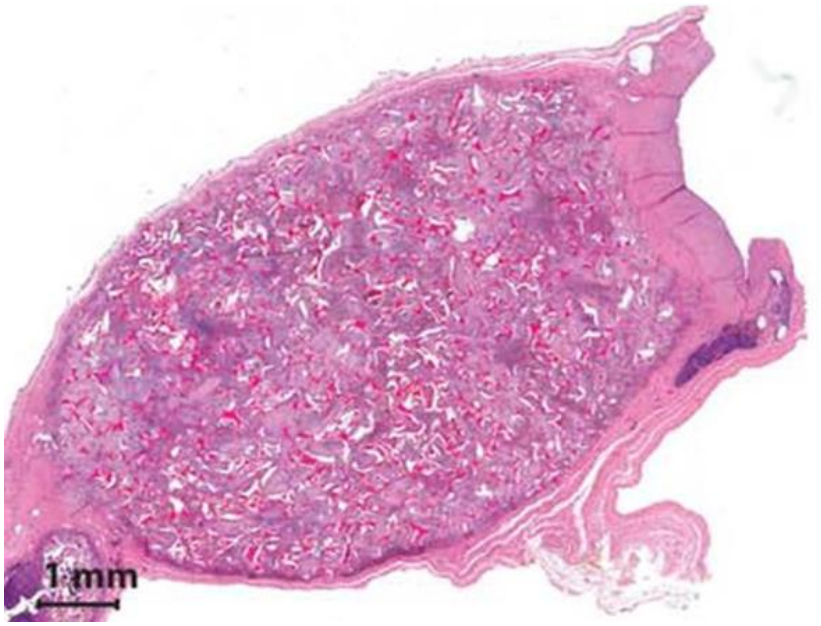

Figure 2.15: H&E stain of a porcine carotid sidewall aneurysm filled with a polyurethane SMP foam 90 days postimplantation demonstrating complete endothelialization across the aneurysm neck and 75% connective tissue within the aneurysm sac. [50]

The organized collagen shown throughout the entire volume of the SMP scaffold and the neointimal layer across the aneurysm neck both support the notion that vascular anomalies treated with this material are highly unlikely to require retreatment as a result of recanalization.

2.3.4 Endovascular Treatments

SMP technology allows devices to be delivered through small catheters and then expand to fill large volumes. Non-SMP foams experience excessive friction when navigated through the catheter, whereas SMP foams can counteract this with the shape memory effect. It has been reported that when technologies like Gelfoam® are delivered

via catheter, it is possible that smaller particles of Gelfoam® embolize and flow downstream creating a thromboembolism. [57] This creates a potential problem for the physician since Gelfoam® is typically cut into numerous pieces before being delivered through a catheter. This methodology prompts the user to cut large enough sections to prevent embolizing downstream of the treatment region on ejecting the Gelfoam® from the catheter, but not large enough to cause excessive friction inside the catheter to prevent advancement to the desired location.

A common problem with expandable implants that are delivered through catheters is failure to deliver the device if it expands too quickly and can no longer be advanced. Because of this complication, a working time must be defined. Working time is the amount of time from device introduction into the catheter to the time at which the device can no longer be retracted or advanced within the catheter. [141, 142] The first generation of HydroCoil® implants (MicroVention, Inc., Tustin, CA) was limited to a 5 min working time, which proved to be an insufficient amount of time to place the implant at the desired location within the neurovasculature. [141] Newer generations of hydrogel-containing coils, such as HydroSoft® (MicroVention, Inc., Tustin, CA), have at least 30 min of working time. As expandable implants, working time must also be considered when designing an SMP scaffold device that will be delivered via catheter. With a 100× volume expansion ratio, SMP foams can exert substantial frictional force on the inner lumen of the catheter if the working time is exceeded. This can lead to an inability to advance the device to the treatment region or improper placement of the device at the target region.

Despite the necessity to adhere to a defined working time when using SMP devices, they offer the enormous advantage of being able to crimp to a diameter of less than 1 mm, be delivered using a minimally invasive catheterization technique, and expand to a final diameter of 10 mm. To put this advantage in terms of surface area, a 1-cm-long SMP scaffold with a 10 mm diameter provides approximately 14,000 mm2 of surface area. A 1 cm length of a typical large bare metal coil used for peripheral occlusion provides approximately 40 mm2 of surface area. Both devices can be delivered through a typical 5 French catheter, but the SMP foam device expands on deployment to provide three orders of magnitude greater surface area than the bare metal coil. It is well known that increased surface area of a procoagulant material results in increased activation of the clotting cascade, which means that an increase in surface area likely results in reduced time to occlusion for these embolic materials. [143] However, a direct comparison of acute time to occlusion has not yet been performed between embolic coils and SMP foams.

2.4 The Future of Shape Memory Polymer Scaffolds

2.4.1 Tissue Engineering Applications

The shape memory behavior of an SMP makes it a very desirable material for use in biomedical applications. Thermally activated SMPs can be programmed and stored in a small secondary shape, and on introduction to the body and water plasticization, recover their large original shape. [144] This property of SMPs can be harnessed for minimally invasive surgery and tissue engineering scaffolds. [144] However, cell compatibility of an SMP biomaterial needs to be extensively understood to determine its feasibility as a short-term or long-term implant and the impact of its SME on cells.

Studying the inflammatory response and biocompatibility of an SMP scaffold was conducted by Filion et al. This group developed SMPs with POSS nanoparticle cores as the net points and PLA with varying chain lengths as the switching segment. [145] SMP degradation and the in vivo inflammatory response were directly related. Longer PLA segments resulted in a more densely packed polymer chain structure that was less prone to hydrolysis. [145] This delayed degradation onset resulted in a late acute inflammatory response, which allowed for tunable degradation profiles that could be useful for numerous tissue engineering applications. [145]

While biocompatibility studies are critical for using SMP as a biomaterial, cell adhesion and proliferation on the material also need to be understood. Davis et al. developed a thermoresponsive 2D cell culture system using the commercially available SMP Norland Optical Adhesive 63 (NOA-63, Norland Products, Cranbury, NJ, USA). This adhesive is a polyurethane that is end-linked with a thiol-based cross-linker using UV click chemistry. [146] The group observed changes in cell behavior as a result of surface shape memory. The substrates were synthesized in a flat topography but shape set so that the secondary shape contained grooves. Mouse embryonic fibroblasts were then seeded onto the grooved substrates. The cells became aligned in the grooved topography but scattered into random alignment after the substrate was actuated such that the topography returned to its flat, primary shape. Nevertheless, the cells maintained 95% viability and no detachment from the substrate was observed. [146] This work demonstrated the use of SMPs to control cell activity and their potential use as tissue engineering scaffolds.

Similarly, Neuss et al. studied different cellular interactions with oligo(ε-caprolactone) dimethacrylate. The group utilized mouse fibroblasts, human mesenchymal stem cells, human omentum majus cells, and rat omentum majus cells for this study. [147] Overall, the cells maintained good viability and attachment over a time period of 3 weeks, supporting the SMP's suitability for medical applications. [147] However, the thermal input and the shear forces necessary for shape change resulted in subconfluent and apoptotic regions. [147] These studies serve as a platform for the development and utility of SMP scaffolds for tissue engineering applications due to their biocompatibility and cell attachment/proliferation. Further investigations may explore whether the shape changing ability of SMPs can drive stem cells down specific lineages or express specific phenotypes. However, optimization of these materials needs to be conducted such that the transition temperature is close to physiological temperature, therefore minimizing adverse effects from overheating the surrounding tissue.

2.4.2 Controlled Pharmaceutical Release

One area where SMPs have a new frontier for innovation is in the design and fabrication of controlled release platforms for pharmaceuticals. Drug-eluting stents have shown reduced rates of restenosis in patients, generally through a polymer-coated stainless steel stent; the drug of choice is sirolimus or paclitaxel, which can limit migration of smooth muscle cells to reduce neointimal hyperplasia. Several good reviews of drug-eluting stents cover topics in greater detail. [148-150] A brief overview of notable studies is presented here. A study by M.C. Chen demonstrated the viability of an SMP stent made from chitosan and epoxy with a heparin coating and sirolimus elution. The surface coating

reduced the platelet adhesion to the stent while providing a diffusion barrier for drug elution that allowed for a sustained release profile for the sirolimus. Significant reduction in neointimal formation was seen when implanted in rabbits compared with noneluting stents. [151]

Another SMP system from star caprolactone cross-linked with hexamethylene diisocyanate that eluted theophylline was synthesized in the same pot as the drug, with up to 20% wt of the drug included in the polymers. This method was used to achieve sustained release for approximately 1 month without bolus release of the drug when tested in an in vitro setup. However, this method of drug loading altered the mechanical and shape memory properties of the material; 20% loading demonstrated decreasing elongation to break below 100% and sufficient rigidity to inhibit shape memory. At approximately 10% loading, there were no significant mechanical changes reported, and the shape fixity and recovery were approximately 99%. Loading of the drug into the polymer did not seem to alter the pore size of the material, as the release profiles were similar for 10% and 20% drug loading. [152] Salicylic acid and adipic acid were also used to produce a bioabsorbable polymer, with sirolimus included as a drug for elution. This stent demonstrated a reduction in angiographic stenosis compared with stents without the sirolimus. [153] It has been suggested the polymers used for drug elution stents may cause inflammation in proportion to the mass of the polymer present. It has been shown that the use of drug-eluting stents lengthen time to resolution of conditions, as fibrin thrombus is often found at time points greater than those seen in untreated arteries during restenosis therapies. Another avenue for the use of drug elution is in cellular migration and

proliferation. Gene suppression therapy has had some success in this regard, using rapamycin and paclitaxel, drugs which can act on a number of cellular targets as well as interrupt cell cycle progression. [154]

The shape memory behavior of SMPs opens new doors for designing controlled release platforms in the pharmaceutical industry. The ability to actuate these polymers via light, heat, or magnetic energy offers the opportunity to implant an SMP containing a pharmaceutical reservoir and actuate the device using noninvasive means. On actuation, miniature SMP doors, latches, apertures, or pores could be opened without requiring the physician to break the patient's skin. This technique could be used to administer multiple boluses of a drug while minimizing patient pain and potentially providing more targeted, local delivery of the drug. The actuation rate of SMPs is also highly tunable. This means that an SMP device loaded with a pharmaceutical agent could be delivered using a minimally invasive endovascular approach, and designed so that it only actuates and releases the pharmaceutical after a given duration of time when the device reaches a specific location in the vasculature. The potential for combining controlled release theories and SMP technology is virtually limitless, and this specialty is likely to be a very active area of research in the future.

2.4.3 Degradable Shape Memory Polymer Scaffolds

SMPs, like other polymers, can be biostable or degradable. A substantial amount of the work done on degradable SMP scaffolds has been performed by Langer or Lendlein, and is too great to be covered sufficiently here. [155-173] A small selection of their work, as well as that of several other significant findings as they relate to cardiovascular

applications, is presented. The Langer group developed a series of poly(polyol sebacate) SMPs, with tailorable transition temperatures between 7 and 40 °C. In vitro degradation and compatibility of these materials showed similar behavior to poly(lactide-co-glycolic acid). These materials would be ideal for a variety of medical devices, including surgical sutures to tighten at body temperature, cardiovascular stents to expand on arrival at the implant site, or other devices that require a transition at body temperature. [174]

A very exciting application of biodegradable polymers is in the field of cardiovascular devices. Guglielmi detachable coils (GDCs) have been the interventional device of choice for intracranial aneurysm filling, but there are problems with healing and recanalization when using these devices. Murayama et al. developed a biodegradable polymer poly(glycolic-l-lactic acid) over a GDC coil and compared this device with standard GDCs in experimentally created aneurysms in porcine models. Despite having a lower packing density in the aneurysm sac after the implantation procedure, the biodegradable GDC hybrids demonstrated complete occlusion of the aneurysm, whereas standard GDCs did not. There was a distinct separation between the parent vessel and the hybrid coil-packed mass using angiography at 3 months, which was not visible when using standard GDCs, indicating improved healing response with the hybrids. Additionally, the hybrid-filled aneurysms were smaller and softer, similar to tissue, 3 months after the implantation. After 3 months, GDC-filled aneurysms were a hard, solid mass distinctly dissimilar from surrounding tissue. Finally, mildly organized connective tissue was present 2 weeks postimplantation, as well as only a mild immune response for hybrid coils.

Standard GDCs showed the same immune response, but no connective tissue organization. [175]

Copolymers of lactide, glycolide, and caprolactone have been synthesized in block copolymer compositions that demonstrated shape memory while also possessing degradability. These materials showed rapid degradation rates in temperature-controlled PBS, with total mechanical property loss within 2 months based on molecular weight of the lactide and glycolide–caprolactone segments. For tissue scaffolds, this is ideal as the loss of mechanical properties could be tailored to allow for material degradation as connective tissue infiltrates the material. [176]

Hyperbranched PCL as a soft segment and hard segment of poly((R)-3-hydroxybutyrate-co-(R)-3-hydroxyvalerate) were compared with linear PCL-based SMPs. These polymers were poly(ester urethanes), using aromatic diisocyanates, showed good biocompatibility, and allowed for cellular attachment and growth on the surface. The use of these materials in stents was examined, showing quick recovery from the secondary shape to the original shape at body temperature, indicating good promise for these materials in stent applications. [177] Other compositions and composite materials have also shown a variety of degradation profiles, thermomechanical properties, and biocompatibilities. [177] Adding a degradation functionality to SMPs provides a means of developing minimally invasive tissue scaffolds and medical devices that do not require a second medical procedure for removal. As the presented works indicate, a wide variety of chemical compositions and properties can be obtained for SMPs, including the mechanism and rate of degradation. For cardiovascular applications, materials can be

produced that have tunable mechanical and thermal properties with selective coagulation and degradation times while promoting cellular ingrowth and proliferation. With SMPs, the promises made by tissue engineering, to provide methods for the body to heal and repair itself with minimal interference from external sources, are becoming realized. As this field progresses, healing responses and clinical outcomes for patients will begin to improve.

CHAPTER III

DESIGN AND VERIFICATION OF A SHAPE MEMORY POLYMER PERIPHERAL OCCLUSION DEVICE

3.1 Introduction

In many cases of venous disease, blood flow through specific vessels can cause extreme pain and high rates of morbidity which greatly affect quality of life for thousands of patients every year. These morbidities include chronic venous insufficiency, pelvic congestion syndrome, varicoceles, and varicosities associated with portal vein hypertension. In each of these cases, incompetent venous valves are weakened and allow regurgitation of blood in peripheral vessels, causing a sudden rise in venous pressure and the subsequent formation of varicose veins. [88, 89, 178, 179] In these instances, physicians rely on peripheral occlusion devices to block or divert blood flow from the susceptible region and force blood flow through healthy vessels- significantly reducing the pain and risk of hemorrhage associated with varicosities. Fibered platinum coils, such as the Nester® Embolization Coils (Cook Medical, Inc., Bloomington, IN), are one common type of embolization device used to permanently occlude peripheral vessels. However, several coils are often required to achieve complete occlusion, and recanalization, or the recurrence of blood flow through a previously occluded vessel, that requires retreatment can occur in up to 20% of patients. [180] Additionally, complete thrombotic occlusion of the target vessel may not occur for up to 19 minutes after treatment with fibered coils, leading to increased procedural costs and radiation exposure. [181]

Hemorrhage as a result of traumatic vessel injury can also be managed using peripheral occlusion devices. In these instances, every minute required to achieve stable vessel occlusion may be critical to the patient's survival. Therefore, the ideal peripheral occlusion device should minimize time to occlusion, require only one device to achieve stable vessel occlusion, minimize the potential for recanalization, and be delivered minimally invasively. To address the prolonged time to occlusion and the need to implant multiple devices, some physicians turn to embolic plugs, such as the AMPLATZER™ Vascular Plugs (AVP, St. Jude Medical, St. Paul, MN). These plugs provide a single device solution to achieve complete vessel occlusion. Embolic plugs typically consist of a fine nitinol mesh with or without a PTFE fabric incorporated into the structure. [182] However, vascular plugs may require up to 20 minutes for stable thrombus formation and they can typically only be used in vessels with limited tortuosity due to the stiffness of the devices. [183] The drawbacks of current coils and vascular plug devices highlight the need to continue improving on peripheral embolization technology.

Shape memory polymer (SMP) foams have been thoroughly investigated as advantageous embolic devices for stabilizing porcine sidewall aneurysms and vascular anomalies. [184-187] Previously, the biocompatibility of SMP foams has been demonstrated in porcine models. [186, 188] In these studies, significant connective tissue infiltration was seen throughout the implant, which caused complete, stable occlusion of the treated aneurysms. Connective tissue deposition and scar formation is a critical step in preventing recanalization. [189, 190] The proposed SMP foams aim to minimize time to mature healing by providing a scaffold morphology that readily supports a healing

response involving the initial clotting of blood within the scaffold then, over time, replacement of the clot with mature connective tissue. With reduced time to mature healing, the risk of recanalization is significantly reduced. This, in turn, decreases the need for follow-up imaging and the overall cost of treatment. SMP foams also have the unique ability to be stored in a compressed geometry and subsequently expand to fill large volumes upon contact with circulating blood. [191] The shape memory capacity of these foams results in an ideal material for minimally invasive devices which provide limited friction during catheter delivery but are still capable of expanding up to ten times their crimped diameter to fill large volumes and create rapid occlusion of vessels with a single device. The affinity for rapid clot formation is primarily due to the high surface area and porous morphology of the foam that creates numerous recirculation and stagnation zones that activate rapid thrombosis. [185, 192]

The following study consists of a series of in vitro tests aimed at verifying the safety and efficacy of a first-generation shape memory polymer peripheral embolization device (PED) used for arterial and venous occlusion in peripheral vessels accessible with a 4-6 Fr guide catheter. Material characterization was conducted on various SMP foam formulations to ensure the proposed formulation would remain crimped at room temperature but allow expansion when exposed to a 37°C aqueous environment. The shape recovery of the PED was also analyzed to ensure the foam expanded slowly enough to allow delivery to the treatment site via catheter. Mechanical analysis was conducted on the foam and coil anchor components of the device (**Figure 3.1**) to ensure the radial force of the device is unlikely to cause vessel perforation or rupture. Then a temperature and

pressure-controlled flow system was used to test the device's susceptibility to migration and undesired thromboembolism. The same flow system was used to perfuse bovine blood through SMP foam devices to investigate the distribution of fibrin and erythrocytes throughout the device over time and ensure that blood is able to penetrate throughout the foam volume. This is critical for ensuring there are no regions devoid of access to circulating blood which may delay healing in the treatment vessel and create a predisposition for recanalization after treatment. Finally, the device was delivered to a vascular phantom by a vascular surgeon and interventional radiologist under ultrasound guidance to determine the overall performance and echogenicity of the device, as researchers have investigated for other occlusive devices. [193, 194]

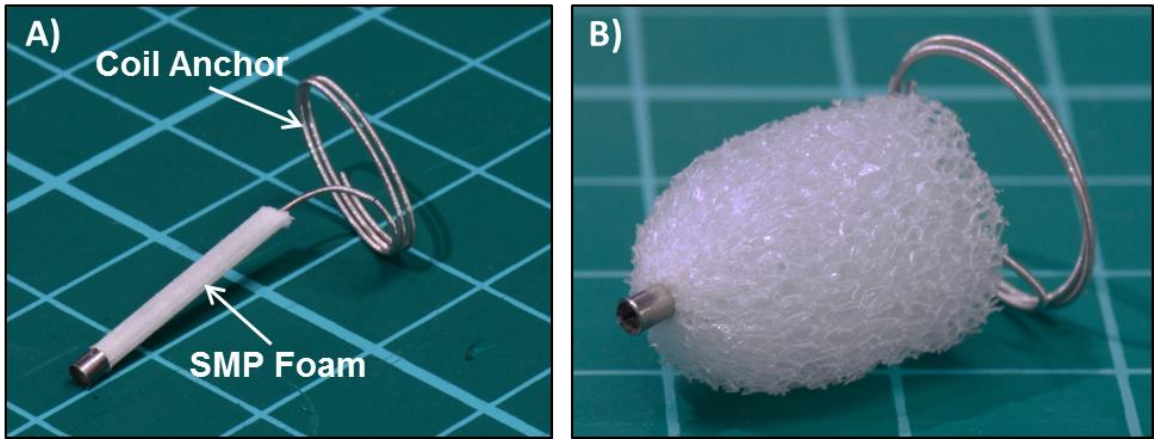

Figure 3.1: Image of the crimped (A) and expanded (B) embodiment of the SMP peripheral occlusion device investigated within this study. The device consists of a distal platinum alloy coil anchor and a proximal length of SMP foam that is crimped for delivery through a guide catheter and subsequently undergoes up to 100X volume expansion to fill large volumes upon deployment.

3.2 Materials and Methods

3.2.1 Foam Fabrication

Each foam composition was fabricated using the three-step protocol described previously (Hasan et al., 2014). In short, isocyanate (NCO) prepolymers were synthesized with appropriate molar ratios of N,N,N',N'-Tetrakis(2-hydroxypropyl)ethylenediamine (HPED, 99%; Sigma-Aldrich Inc., St. Louis, MO), triethanolamine (TEA, 98%; Sigma-Aldrich Inc.), and hexamethylene diisocyanate (HDI, TCI America Inc., Portland, OR). The prepolymers were reacted for 2 days with a temperature ramp from room temperature to 50°C at a rate of 20°C/hr, held isothermally at 50°C for 16 hours, and passively allowed to cool back to room temperature. A hydroxyl (OH) mixture was blended with the remaining molar equivalents of HPED and TEA. This mixture also contained deionized (DI) water (> 17 M Ω cm purity; Millipore water purifier system; Millipore Inc.), and catalysts (T-131 and BL-22, Air Products and Chemicals, Inc., Allentown, PA). During the foaming step, the NCO prepolymer and the OH mixture were combined in a foaming cup along with surfactants (DC 198 and DC 5943, Air Products and Chemicals, Inc., Allentown, PA) and the physical blowing agent, Enovate 245fa (Honeywell International, Inc., Morristown, NJ). This solution was mixed in a FlackTek Speedmixer (FlackTek, Inc., Landrum, SC) and poured into a bucket to form a foam. The foam was cured at 60°C for 5 minutes before passively cooling to room temperature for further processing. Various foam formulations and pore sizes were fabricated to create foams with differing crosslink densities, glass transition temperatures (Tg), rate of moisture plasticization, and subsequent foam expansion rate. Foam formulations are denoted as H20-H60, where the

numerical value appearing after "H" corresponds to the ratio of HPED to TEA equivalents in the polymer premix. Both foam formulation and pore size were used to control the expansion rate of the foams and the resultant working time.

3.2.2 Foam Processing

After fabrication, foams were cut into blocks 2 cm thick, 7 cm long, and 6 cm wide. These blocks were then reticulated using the same method described previously. [186] In short, the foams were penetrated by a floating pin array while subjected to low amplitude, high frequency perturbations, which allowed the creation of pinholes in the foam pore membranes. These pinholes create interconnected pores throughout the foam which allow blood flow and eventual connective tissue deposition to penetrate throughout the entire device. After reticulation, the foams were cut with disposable biopsy punches (Sklar Surgical Instruments, West Chester, PA) for three different device sizes- 6, 8, and 12mm. These device sizes were used to enable delivery through 4, 5, and 6Fr catheters, respectively, and the ability to treat vessels with diameters between approximately 2-11mm. After the foams were cut into their final geometry, they were cleaned to remove any plasticizers and unreacted monomers from the foams. Each cleaning cycle lasted 15 minutes and was performed under sonication in a 40°C water bath. The first two cleaning cycles consisted of submerging the foams in 99% isopropyl alcohol (VWR, Radnor, PA). Then the foams were rinsed with reverse osmosis (RO) water before being cleaned in four cycles of Contrad 70 liquid detergent (Decon Labs, King of Prussia, PA). Each foam was then rinsed with RO water until no Contrad 70 residue was evident. Finally, the foams were cleaned for two cycles in RO water. After cleaning, the damp foams were frozen in

a -20°C freezer for 12 hours before freeze-drying in a FreeZone Freeze Dryer (Labconco, Kansas City, MO) for 24 hours.

3.2.3 Material Analysis

Differential Scanning Calorimetry (DSC) was used to assess the T_g of each foam formulation (H20-H60) through the use of a Q200 DSC (TA Instruments, New Castle, DE), to ensure the crimped devices would remain compressed at typical storage and shipping temperatures. The T_g was also analyzed to verify the tunability of the polymer chemistry, as a higher T_g corresponds to slower shape recovery. Four samples of each foam composition were analyzed using DSC, which provides a simple means of addressing any excessive expansion of the PED while still inside the delivery catheter. This premature expansion can occur as a result of foam contact with blood or saline that plasticizes the foam and depresses the T_g sufficiently to initiate foam expansion at body temperature. Every sample was weighed to ensure a mass of 3-10 mg, cooled -40°C, and heated at a rate of 10°C/min to 120°C. This cycle was repeated twice; the last heating cycle was used for quantification of the T_g for each foam formulation. The T_g was calculated using the half-height method in the TA Instruments software.

3.2.4 Expansion Studies

Expansion studies were conducted to ensure the foams do not undergo premature expansion within the delivery catheter, preventing the device from deploying properly at the target site. Expansion studies were conducted using a water bath heated to 37°C. Foams with pore sizes of approximately 0.5, 1.0, and 1.5 mm were crimped over a 0.010” nitinol wire using the SC250 Stent Crimper (Machine Solutions Inc., Flagstaff, AZ).

Samples were imaged before and after crimping using a Leica MZ16 Digital Video Microscope (Leica Microsystems, Wetzlar, Hesse, DEU) with a Jenoptik CF Scan Camera (Jenoptik AG, Jena, Thuringia, DEU) and loaded into a fixture which held the nitinol wire taut. The entire fixture was submerged in the heated water bath and imaged at 0.5, 1.0, 1.5, and 2.0 minutes, as well as every minute thereafter until 10 minutes had elapsed. Each picture was then converted to a binary image and the 2-D projected surface area of the foam was calculated in each image using MATLAB (MathWorks, Inc., Natick, MA). The projected surface area at each time point was then divided by the length of the sample to obtain an average diameter of the foam at each time point. This analysis aids in determining which foam formulations and pore sizes will provide sufficient working time for physicians to deliver the devices before excessive foam expansion prevents advancing the device through the catheter.

3.2.5 Device Fabrication

Due to the low radial force of the SMP foams, a coil anchor is incorporated into the PED to enable implantation in both arteries and veins with minimal risk of device migration. To fabricate the coil anchors used for in vitro device verification tests, 0.018” diameter 90/10% platinum/iridium coils with an inner diameter of 0.010” were threaded over 0.005”, 0.006”, and 0.008” diameter superelastic nitinol wire for the 6, 8, and 12 mm PED devices, respectively. The coils were then wrapped around a stainless steel mandrel that had been machined to each device diameter and shape-set in a 550°C furnace for 15 minutes. After 15 minutes, the mandrels were immediately quenched in room temperature water to set the final shape of the coil. The coils were removed from the mandrel and a

straight section of the coil was manually threaded through the center of the foam before crimping.

3.2.6 Device Mechanical Analysis

One critical design consideration for a peripheral occlusion device, to prevent vessel perforation or rupture, is to ensure the device does not exert radial forces in excess of the radial strength of the treatment region. To analyze variations in radial strength based on foam formulation and pore size, a J-Crimp Radial Compression Station (Blockwise Engineering LLC, Tempe, AZ) was used with an Instron Model 5966 Dual Column Test System (Illinois Tool Works Inc., Norwood, MA) to perform radial force measurements during foam expansion. For this test, foams were cut into cylinders 4, 6, 8, and 10 mm in diameter and 2 cm in length using biopsy punches. Samples were then crimped to approximately 1 mm in diameter using a SC250 Stent Crimper (Machine Solutions Inc., Flagstaff, AZ). The lumen of the J-Crimp compression station was adjusted such that the expanded diameters of the foam devices were 50% oversized to the lumen, the maximum percentage of oversizing indicated within the Instructions for Use (IFU) for other embolic plug devices like the AVP. Then, each sample was placed inside the J-Crimp compression station while heated to 100°C. Each sample was allowed to freely expand for 20 minutes within the compression station while the radial force of the device was monitored on the Instron.

The radial stiffness of the PED anchor coil was also analyzed and compared to a 14mm AVP and 16mm AVP II. The same J-Crimp Radial Compression Station was used for this analysis. To begin each test, the lumen of the J-Crimp was set to the expanded

diameter of the device of interest. Then the diameter of the J-Crimp was decreased at a rate of 10 mm/min until the expanded device diameter was 50% oversized to the J-Crimp diameter, again aligned with common sizing parameters detailed in the IFU for other embolic devices. The total radial force throughout device compression was continually recorded to determine the maximum force experienced during compression. The maximum force was then divided by the change in diameter to obtain the radial stiffness (k) of each device.

In order to estimate the total surface area of devices in contact with the endothelium of the vessels, a 16mm AVP II and 8mm PED anchor coil were deployed into flexible polyvinyl chloride (PVC) tubing and imaged using the same Leica microscope previously implemented for expansion studies, in conjunction with ImageJ software, to estimate the total surface area of the flexible tubing that was deflected by the radial force of each respective device- providing an estimation of the total surface area of the devices contacting the vessel lumen.

3.2.7 Device Migration and Unintended Thromboembolism

A critical test that must be performed on a new peripheral occlusion device is one that verifies the device will not migrate or dislodge from the treatment region and create undesired thromboembolism. To monitor device stability, samples were delivered and analyzed in the flow loop shown in **Figure 3.2** without the bypass pathway to force flow through a single vessel and represent the worst case scenario with no collateral vessels. Devices were delivered to the test section when the flow system was equilibrated at 37±2°C. The test sections consisted of flexible PVC tubing (McMaster-Carr, Douglasville,

GA) 5, 7, and 10 mm in diameter for the 6, 8, and 12 mm PED, respectively. Each tubing size was chosen so that each device diameter would be approximately 20% oversized to the target vessel- the hypothesized lowest degree of device oversizing that would be indicated for the PED device. Due to limitations in commercial flexible PVC tubing sizes, the 8mm device was only oversized by 14% to the test section, providing a more rigorous stability test than the other device sizes.When the foams were fully expanded in the test section, Pump 1 was set to circulate a 36.7% (vol) glycerol-water mixture at room temperature through the lumen of the mock vein. This glycerol solution was used to ensure the inner diameter of the mock vein was lubricious and the circulating fluid matched the kinematic viscosity of blood. [195] The flow rate was then gradually ramped up in increments of approximately 20 mL/min while maintaining the pressure within the flow system at 207±52 mmHg. At each flow rate interval, the devices were imaged for 2 minutes with a stationary Canon PowerShot SX230 HS Digital Camera (Canon U.S.A., Inc., Melville, NY) positioned above the test section to monitor migration. Displacement of more than 1mm in 2 minutes was deemed a device failure. The flow interval prior to the interval at which failure occurred was noted as the maximum flow rate for each device. This procedure was used for both PED and Cook coils.

3.2.8 Blood Perfusion

In order to monitor the degree of blood infiltration throughout the PED and investigate the potential for zones devoid of blood contact within the foam volume, bovine blood was incorporated into the flow system shown in **Figure 3.2**. Histology was subsequently performed on foam devices to verify blood infiltration throughout the foam.

The histological analysis was also used to investigate the affinity for fibrin deposition within the foam, which serves as a precursor to stable scar formation and the prevention of recanalization. To accomplish this, bovine blood was obtained as part of a tissue share program with the Rosenthal Meat Science and Technology Center at Texas A&M University in College Station, TX. All blood used in this study was obtained from animals euthanized for purposes unrelated to this research. Blood was collected immediately following sacrifice of the animals and citrated in a 5 gallon bucket containing approximately 2.1 liters of 3.2% sodium citrate to prevent clotting, as recommended by Adcock et al. [196] The 3.2% sodium citrate solution was prepared by mixing 2,103 mL of phosphate buffered saline (PBS) with a pH of 7.4 (Sigma-Aldrich Inc.) with 67.3 g of sodium citrate (Santa Cruz Biotechnology Inc., Dallas, TX).

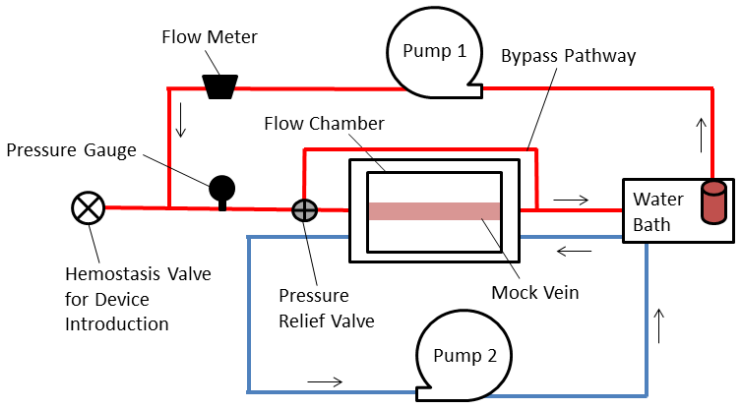

Figure 3.2: Schematic of flow system used for in vitro device stability and blood perfusion studies. Pump 1 is a peristaltic pump which circulates fluid through the test section, and Pump 2 is also a peristaltic pump which circulates heated water into the flow chamber surrounding the mock vein to maintain the test section in a 37°C aqueous environment.

Before perfusing blood through foam devices, Activated Clotting Time (ACT) tests were conducted using a Hemochron® 401 (International Technidyne Corporation, Edison, NJ) and kaolin-activated test vials (Accriva Diagnostics, Piscataway, NJ). ACT tests were conducted to determine the proper amount of 0.1 M calcium chloride ($CaCl_2$, Flinn Scientific Inc., Batavia, IL) to add to the blood to restore the clotting capabilities of the blood. The target ACT value for the bovine blood was between 120 and 180 seconds to mimic normal, healthy ACT of cattle. [197] Various amounts of $CaCl_2$ were added to 2 mL of citrated blood in the kaolin-activated test vials until the ACT fell into the desired range. Ultimately, 105 µL of $CaCl_2$ for every 1 mL of citrated blood resulted in an average ACT of 173 seconds. This ratio of $CaCl_2$ to blood was used throughout the blood flow studies. All blood flow studies were conducted within 24 hours after blood collection, and less than six hours elapsed between the first and last flow study.

To begin the blood flow studies, 37°C PBS was perfused through the flow system for ten minutes to prime the tubing and fittings. The pressure relief valve proximal to the test section was set to approximately 8.7 psi (450 mmHg) to ensure all flow was forced through the test section until the fittings of the flow system were at risk of failure. This pressure setting served as a rigorous test of in vitro clotting of the device as flow would likely be diverted, thereby creating clinical occlusion, from the treatment vessel at much lower pressures in vivo. All tubing used in the flow loop was 1/4”ID x 3/8”OD S-50-HL Tygon®, an ISO 10993 certified, non-pyrogenic, non-hemolytic, non-toxic tubing commonly used in biologic applications. [198-200] While the flow system was primed, 500 mL of citrated blood was warmed within a container inside a water bath until it

reached 37°C. When the flow system and blood had equilibrated at 37°C, 105 µL of $CaCl_2$ was added for every 1 mL of blood in the warmed container. The blood and $CaCl_2$ was lightly stirred for 5 seconds before the inlet of peristaltic pump 1 was inserted into the blood container to begin perfusion through the flow system. Foams were perfused with blood for 30, 90, 150, 210, and 270 seconds at a flow rate of 40mL/min. Perfused blood was then captured in a waste container after exiting the test section so that it would not recirculate through the test system. At each time point, the tubing within the flow chamber was cut proximal and distal to the foam and quickly rinsed with PBS to remove any non-adherent cells. Each sample was then fixed in formalin for 7 days.

3.2.9 Histological Analysis

After fixation, each sample was transected perpendicular to the long axis at three points to obtain cross-sections through the sample from proximal, middle, and distal regions relative to the direction of flow. Each section was dehydrated in increasing concentrations of ethanol and cleared with Pro-Par Clearant (Anatech Ltd., Battle Creek, MI) using the Citadel 1000 Tissue Processor (Shandon Inc., Pittsburgh, PA). Samples were then infiltrated with and embedded in paraffin wax using the Citadel 1000 tissue processor and Tissue-Tek TEC III Tissue Embedder (Miles Laboratories Inc., Naperville, IL). Paraffin blocks were sectioned at 5µm thicknesses on a Microm HM355S Rotary Microtome (Thermo Fisher Scientific Inc., Waltham, MA), placed on the M7654-1 SP Tissue Flotation Bath (Cardinal Health, Dublin, OH) set to 45°C, floated onto glass slides, and dried in a Lipshaw Model 218 Slide Dryer (Shandon Inc., Pittsburgh, PA). Once slides were dry, they were deparaffinized with xylenes, rehydrated, and stained with

Hematoxylin and Eosin (H&E) and Phosphotungstic Acid Hematoxylin (PTAH). Slides were then imaged with a virtual microscope using a 40x objective (Olympus Corporation, Tokyo, JPN).

To analyze the percent of fibrin coverage on each histology slide, Adobe Photoshop was used to isolate the fibrin, stained bluish purple by the phosphotungstic acid, from the erythrocytes and foam struts, stained pinkish red by the hematoxylin. When each stain was isolated, the slides were converted to binary images and analyzed for the surface area of pixels corresponding to each stain using ImageJ. H&E was used as a counterstain to aid in verifying the presence of fibrin and leukocytes.

3.2.10 Ultrasound Investigation

Two physicians with over 15 years of experience in their respective fields performing various peripheral embolization procedures delivered the PED into the flow system shown in **Figure 3.2**, where a homemade ultrasound phantom was inserted in place of the mock vein. The ultrasound phantom was created by bringing 3 cups of water to a boil, mixing in nine 0.25 ounce packets of gelatin and 4 tablespoons of sugar free Metamucil, and pouring the mixture into a greased circular mold containing a ¼" PVC tube that would create a lumen through the phantom upon removal. The mold was placed in a refrigerator for 12 hours before the phantom was removed from the mold and placed into the flow system. While circulating the same 36.7% (vol) glycerol-water solution used for device migration studies through the vascular phantom, an M-Turbo® SonoSite ultrasound machine was used with a HFL38x planar probe (FUJIFILM SonoSite, Inc.,

Bothell, WA) to image a device delivery procedure and analyze the efficacy and echogenicity of the PED.

3.3 Results

3.3.1 Material Analysis

DSC was used to assess the ability to control the activation temperature of the proposed devices, which corresponds to the T_g of the materials under investigation. It is critical that the actuation temperature of these devices is greater than the temperature at which they are stored to prevent premature expansion of the foams. The T_g for all foam formulations ranged between 49 and 70°C. **Figure 3.3** shows representative thermograms for each foam composition used in this study, where H20-H60 correspond to foam compositions with 20-60% molar equivalents of HPED. The thermograms demonstrate a single transition with no indication of a secondary transition, as well as a nearly linear relationship between increasing T_g as the ratio of HPED to TEA also increases. The average T_g found for each foam formulation and the corresponding standard deviations are shown in **Table 3.1**.

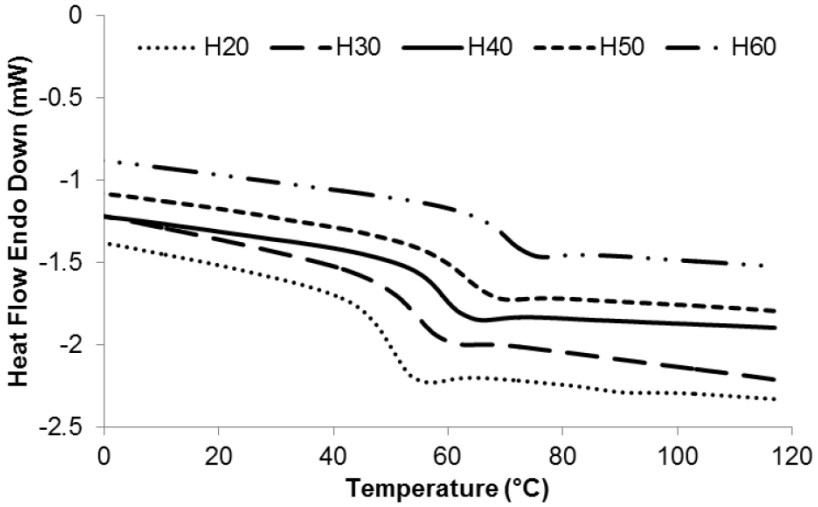

Figure 3.3: DSC thermograms showing increased glass transition temperatures with increasing ratios of HPED to TEA.

Table 3.1: Average glass transition temperature and standard deviation for each foam formulation based on analysis of four samples of each foam formulation.

Foam Composition	Average Tg (°C)	Standard Deviation
H20	49.84	0.15
H30	53.33	0.58
H40	58.83	0.28
H50	62.49	0.26
H60	69.44	0.39

Based on pilot expansion and delivery studies, devices fabricated using H20 and H30 formulations expanded too rapidly to allow delivery of devices via catheter. For this reason, only devices fabricated from H40, H50, and H60 foams were investigated further as potential foam formulations to incorporate into the peripheral occlusion device. **Figure 3.4** shows the results from the expansion studies conducted in 37°C water. As expected, there is a general trend of decreasing expansion rate, within the first three minutes of

submersion in 37°C water, as the crosslink density of the foam increases (higher HPED content). The first three minutes of exposure to aqueous environments is critical as the PED is designed to be delivered within three minutes after first contacting blood or saline. Pore size also had a dramatic effect on expansion rate, as shown in **Figure 3.4**, where expansion rate decreased as the pore size decreased due to increased foam density delaying water diffusion into the foam matrix. However, regardless of pore size and foam composition, all samples experienced 100% shape recovery in less than 20 minutes.

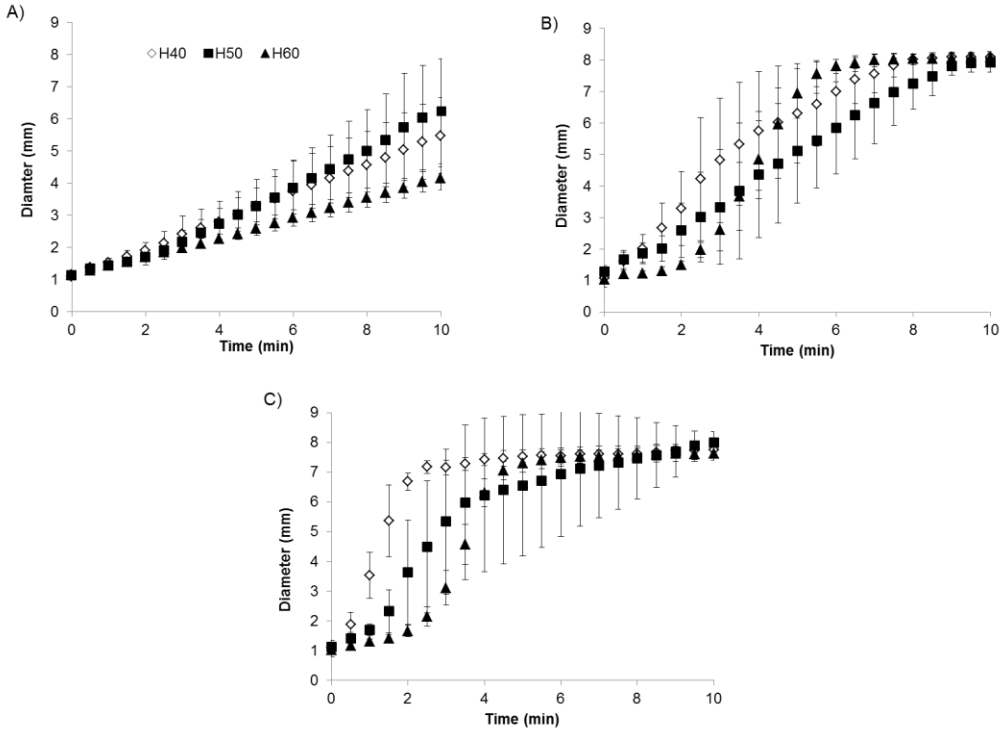

Figure 3.4: Average expanded diameter of crimped 8mm foam cylinders with 0.5 mm pores (A), 1.0 mm pores (B), and 1.5 mm pores (C) at 30 second intervals after immersion in 37°C water (mean ± one standard deviation, n = 5). Foams demonstrated controllable expansion rates based on varying foam composition and pore size. Again for reference, H40, H50, and H60 refer to foam compositions with 40%, 50%, and 60%, respectively, molar equivalents of HPED.

3.3.2 Device Mechanical Analysis

Radial force tests demonstrated that the radial force of foam devices consistently increased as the device diameter increases. The results for the radial force tests are summarized below in **Table 3.2**. These tests show the radial force of SMP foams with varied foam chemistries (H40, H50, H60). A pore size of 0.5 ± 0.1 mm was chosen for analysis of all chemistries after testing the radial force of foam samples with 0.5, 1, and 1.5mm pore sizes, which revealed that foams with the smallest pore size exert the greatest radial force due to increased foam density. Constrained recovery tests demonstrated that the maximum force exerted on the vessel walls by foam expansion when the foam is 50% oversized to the target vessel is significantly lower than the 107 N of force required to rupture autologous veins commonly used in bypass procedures, if we assume a uniform cylindrical surface area of the foam. [201]

Table 3.2: Maximum radial force (mean ± one standard deviation, n = 5) exerted by H40 (A), H50 (B), and H60 (C) foams during actuation when the foam expanded diameter is 50% oversized to the target vessel. Graph shows a positive relationship between device diameter and the maximum radial force of the foam.

Foam Composition	Device Diameter (mm)	Vessel Diameter (mm)	Radial Force (N)
H40	4	2.7	0.08 ± 0.03
	6	4.0	0.16 ± 0.03
	8	5.3	0.24 ± 0.05
	10	6.7	0.30 ± 0.05
H50	4	2.7	0.13 ± 0.07
	6	4.0	0.17 ± 0.04
	8	5.3	0.21 ± 0.04
	10	6.7	0.25 ± 0.03
H60	4	2.7	0.20 ± 0.04
	6	4.0	0.29 ± 0.07
	8	5.3	0.38 ± 0.05
	10	6.7	0.36 ± 0.09

The radial stiffness of each different sized anchor was compared to the stiffness of two vascular plugs currently on the market in **Figure 3.5**. During radial force testing to determine device stiffness values, the 8mm devices exerted an average maximum radial force of 4.0 N, while the AVP II exerted an average maximum radial force of 15.8 N when oversized by 50% to the target vessel. Microscopic imaging of the 8 mm PED anchor coil revealed that approximately 30% of the coil surface area is in contact with the vessel endothelium, which corresponds to 0.43 cm^2 of surface area. Given the estimated surface area of coils in contact with the vessel lumen, the PED anchor would exert a pressure of approximately 700 mmHg on the vessel endothelium- less than half the pressure required to cause rupture in an autologous vein graft. [201] When a 16 mm AVP II was deployed within a flexible PVC tube with an inner diameter of 10 mm, it was estimated that approximately 0.85 cm^2 of device surface area was in contact with the inner diameter of the tubing, resulting in a radial pressure of approximately 1,400 mmHg. Given the proven safety and efficacy of the AVP II device that led to its FDA approval, and the markedly reduced radial force and pressure exerted by the PED anchor, it is unlikely that the PED coil anchor would cause vessel rupture or perforation in vivo. Prior to verification tests, it was hypothesized that the coil anchor would account for the vast majority of the radial force exerted by the PED. Radial stiffness testing revealed that this was indeed the case, as demonstrated by a maximum radial force of less than 0.5 N for any foams tested.

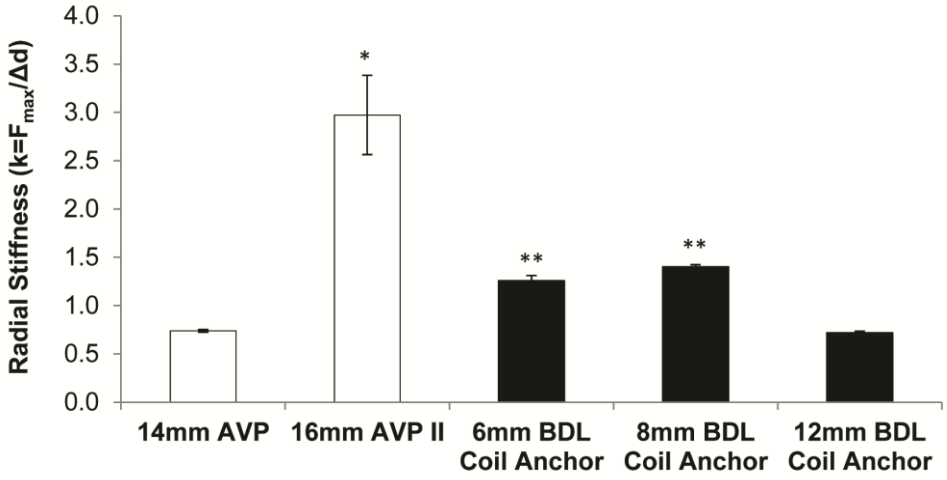

Figure 3.5: Maximum radial stiffness (mean ± one standard deviation, n = 5) in N/mm of a 14 mm AVP and 16 mm AVP II (St. Jude Medical, Inc.) compared to platinum alloy coils fabricated within the Biomedical Device Laboratory (BDL) at Texas A&M. The maximum radial force was measured while each device was radial compressed until the lumen diameter corresponded to a vessel size for which each device is 50% oversized. The maximum radial force was then divided by the change in diameter to produce a device stiffness constant that enables estimations of the total radial force exerted by each device when implanted in any sized vessel. *p<0.05 vs. all other devices, and **p<0.05 vs. 14 mm AVP for a two-tail paired Student's t-test.

3.3.3 Device Migration and Unintended Thrombosis

To ensure the PED has a limited risk of migrating downstream and causing unintended thrombosis, studies were conducted in which the maximum flow rate was determined for each PED size for comparison to one of the market-leading embolic coils, Cook Medical's Nester® Embolic Coil. **Figure 3.6** summarizes the results from this analysis, which showed the PED can withstand equivalent or higher flow rates than Nester® coils. This analysis was also performed with only one Nester® coil within the mock vein, whereas at least three coils are typically implanted to achieve complete vessel occlusion in the clinic. [202] If three coils were implanted into the test section, the pressure

drop across the device mass would drastically increase, and the maximum flow rate for these coils would likely decrease further.

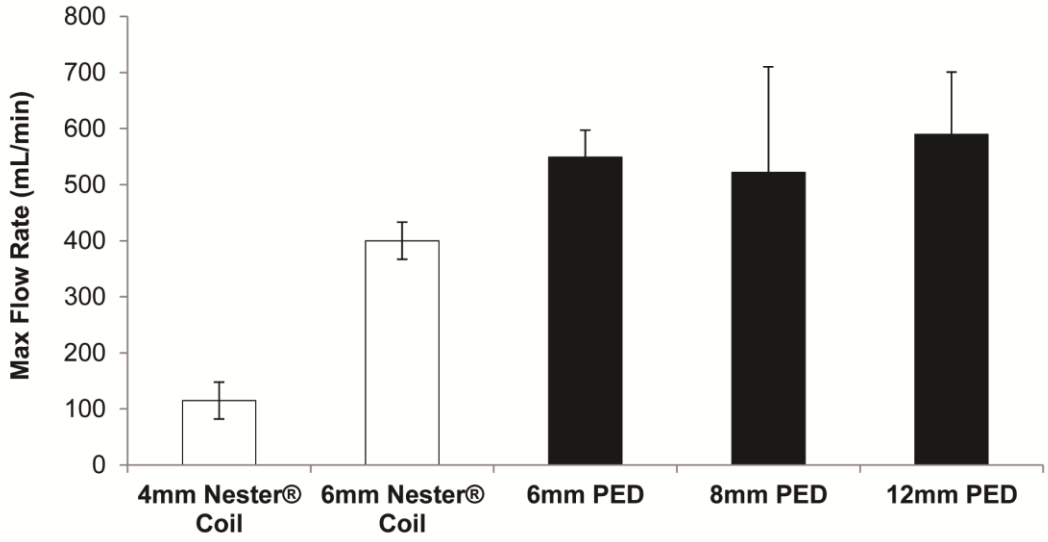

Figure 3.6: Comparison of the maximum flow rate (mean ± one standard deviation, n = 3 for Nester® Coils and n = 4 for PED devices) commercial embolic coils and the PED technology under investigation can withstand without migrating downstream and causing undesired thromboembolism.

3.3.4 In Vitro Clotting and Histological Analysis

During in vitro blood flow studies, complete occlusion of the foam device was observed at 270 seconds. Complete occlusion was evidenced by flow diverting through the pressure relief valve. At this point, the pressure within the vein model created by thrombus formation exceeded the pressure relief valve setting and flow was diverted through the bypass pathway. In order to show the most dramatic change in cellular deposition throughout the foam device, **Figure 3.7** shows a histologic comparison between samples perfused with blood for 30 and 270 seconds.

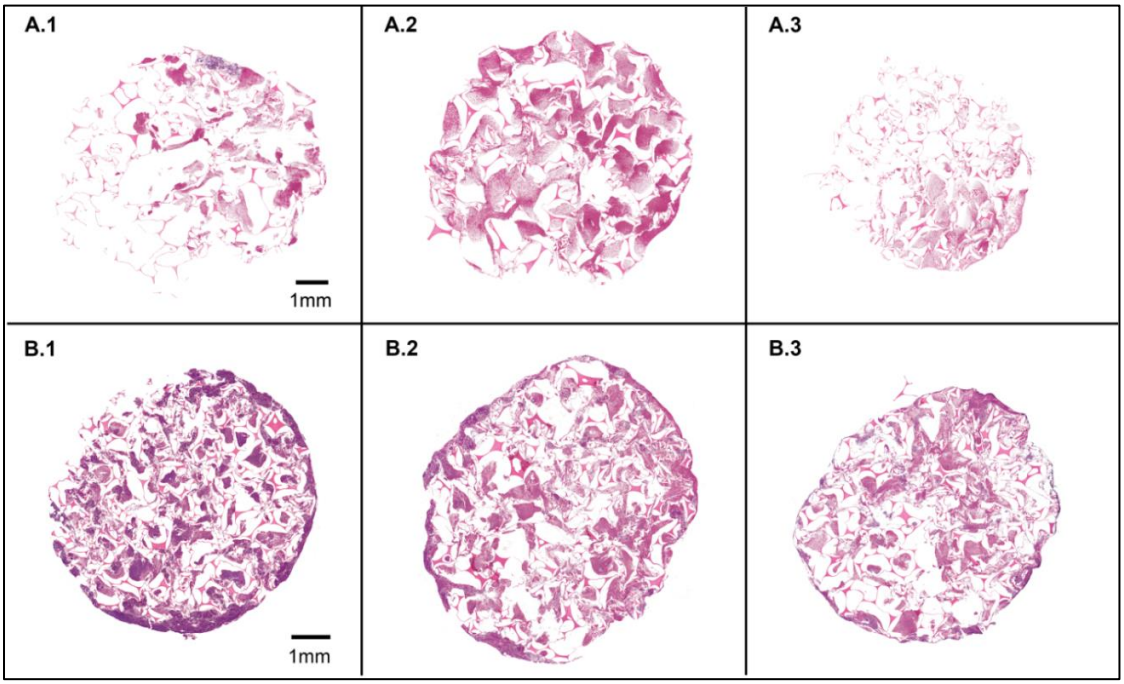

Figure 3.7: Histology results showing foam samples perfused with blood for 30 sec in row A, and samples perfused for 270 sec in row B. Samples 1, 2, and 3 correspond to proximal, middle, and distal locations within the device, respectively. All samples were analyzed using a PTAH stain to highlight erythrocytes pinkish red and fibrin and leukocytes purple.

Each image sequence shows blood is penetrating throughout the entire volume of the foam device, demonstrating the effectiveness of reticulation in creating interconnected pathways along the length of the device. After 30 seconds of blood perfusion, each cross section consists of primarily erythrocytes enmeshed in loose, interspersed fibrin. At 270 seconds, approximately 50% of the proximal section of foam consisted of dense fibrin (**Figure 3.8**), which likely contributed to the complete vessel occlusion which occurred at this time point.

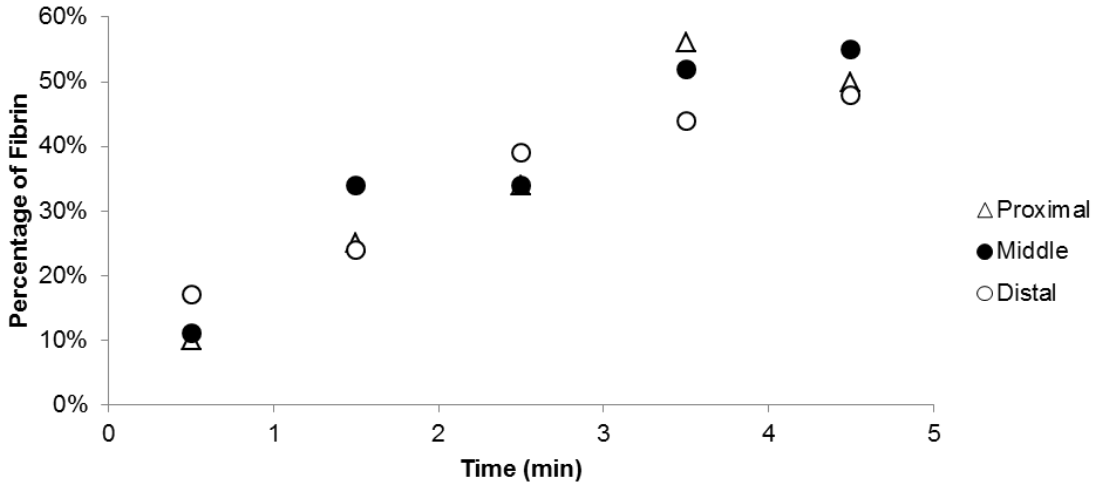

Figure 3.8: Average percentage of fibrin at proximal, middle, and distal locations within the SMP foam device perfused with bovine blood for varying durations of time. Percentage of fibrin quantified using colorimetric analysis.

3.3.5 Ultrasound Investigation

When delivering the PED under ultrasound, both the SMP and platinum coil anchor provided sufficient echogenicity to allow visualization, as shown in **Figure 3.9**. Image A shows the platinum coil anchor exiting the catheter, and image B shows the foam's natural echogenicity allowing easy device visualization. In image C a cross section of the vessel is shown with flow before foam expansion, as indicated by the blue and red colorations typical of flow when using Doppler ultrasound. [203] Flow stagnation and the reduction of flow beyond detectable limits are shown in image D, as indicated by the lack of color mapping within the image after foam expansion. This image also shows significant acoustic shadowing indicative of an acoustically dense material, providing further evidence that the PED is likely to cause rapid occlusion upon expansion in vivo.

This shadowing is the same phenomenon used by physicians to identify dense, calcified lesions within arteries with intravascular ultrasound (IVUS). [204]

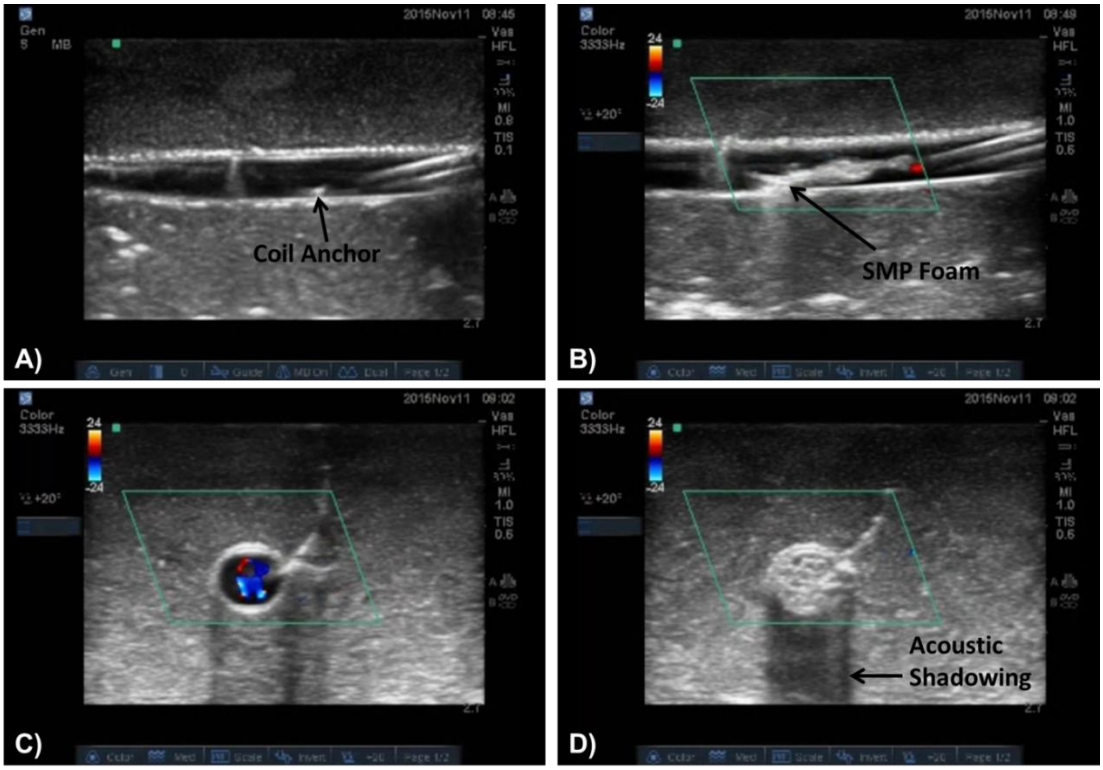

Figure 3.9: Doppler ultrasound images showing the catheter tip and coil anchor deployment (A), foam expansion and the parallel hyperechoic lines indicating the placement of the delivery sheath (B), a cross-sectional view of the mock vessel with flow (C), and a cross-sectional view of the vessel showing flow stagnation and significant acoustic shadowing after foam expansion (D).

3.4 Discussion

Through the use of DSC, precise control of the actuation temperature of SMP foams by altering the ratio of HPED to TEA was verified, which has been demonstrated previously by Wilson et al. and Singhal et al. [191, 205] The increase in T_g as the amount

of HPED increases is a result of the increased crosslink density associated with additional HPED and the steric hindrance provided by the molecular structure of HPED which limits chain mobility. The values obtained in this study for the T_g of each formulation were slightly higher than reported by Singhal et al. [191] This is likely due to the extensive foam cleaning protocol incorporated into this study which removes any unreacted surfactants and catalysts that may have plasticized the previous samples. The ability to control the T_g of SMP foam devices is highly useful for controlling the actuation rate of the device when exposed to circulating blood. This provides a simple means of altering the expansion kinetics of the foam to satisfy the unique specifications required by clinicians for different device indications.

Since the activation of SMPs is entropy-driven and body temperature is lower than the T_g of each foam formulation, the polymers must experience plasticization in the blood or saline injection inside the delivery catheter in order to depress the T_g sufficiently to initiate expansion. Although the transition temperature of these foams are significantly greater than 37°C, the T_g of the foams is depressed to approximately 10°C when exposed to 100% humidity, as shown previously. [206] This transition temperature depression is what allows the foams to expand in the 37°C aqueous environment within the body. However, one potential complication of this actuation method is premature expansion of the foam within the delivery catheter and the inability to successfully deliver the implant. The expansion studies demonstrated the ability to tune the working time of the proposed device, defined as the point at which the expanded diameter of the foam is four times the inner diameter of the delivery catheter. By altering the ratio of HPED to TEA during foam

fabrication and the foam pore size, devices can be fabricated with working times varying from one to five minutes, which is within the working time confines of the first hydrogel-containing coils used in clinical embolization procedures. [207]

Konig et al. found the average burst pressure of human saphenous veins to be approximately 1,575 mmHg. [201] Based on this burst pressure and a PED 8 mm in diameter and 2 cm long device, the radial force of the foams must not exceed 107 N to prevent vessel rupture in the venous system. This maximum radial force assumes a uniform distribution of radial force exerted along the length and circumference of the device. Based on this information, radial force tests demonstrated that the SMP foams exert a radial force on the vessel wall that is drastically smaller than would be required for vessel rupture. This is also considering that the foams are oversized by 50% to the inner diameter of the vessel, which is the common sizing practice when selecting an appropriately sized vascular plug. [208, 209] This test demonstrated that the risk of rupturing the target vessel with this device as a result of foam expansion is extremely low, regardless of which foam formulation is used. The more likely device component to cause vessel perforation or rupture is the coil anchor. Although the radial force of the coil exceeds that of foam, it exerts nearly an order of magnitude less force than commercially available vascular plugs used for peripheral occlusion and less than 50% of the pressure required to rupture saphenous vein grafts, implicating that the risk of vessel rupture as a result of the coil anchor is also low.

In vitro blood perfusion studies and the subsequent histological analysis of SMP foam devices revealed that blood penetrated throughout the device. No foam sections

appeared to be devoid of thrombus deposition, and a dense fibrin mesh was clearly visible at proximal, middle, and distal locations of the device at the moment in which complete vessel occlusion occurred. Complete occlusion was witnessed after 270 seconds of blood perfusion through the device. The pressure setting used in this experiment (450 mmHg) served as a rigorous test of in vitro clotting of the device as flow would likely be diverted, thereby creating clinical occlusion, from the treatment vessel at much lower pressures in vivo. Considering the absence of tissue factor VII and any influence from the extrinsic clotting cascade on thrombus formation, complete occlusion in less than five minutes is a significant achievement; especially considering certain FDA-approved peripheral embolization devices may require more than 5 minutes to achieve vessel occlusion. [210, 211] However, this clotting time may have been affected by clotting activation during blood collection, as well as activation of the clotting cascade from contact with the tubing and storage container in the flow system. In certain clinical settings, the time to occlusion would also likely be increased due to heparin administration.

Although in vitro studies using animal blood cannot be directly correlated to clinical clotting times in humans, previous in vivo studies using the same SMP foam formulation as the devices investigated here demonstrated complete vessel occlusion in less than 90 seconds in a porcine model. [186] This finding was similar to the clotting times reported in porcine studies investigating the clotting efficacy of the AVP II; [212] indicating the SMP foam device under investigation would likely result in analogous occlusion times to the AVP II device.

3.5 Conclusions

This research verified the mechanical properties of the shape memory polymer PED device are safe and unlikely to cause vessel perforation or rupture. At the same time, these studies demonstrated that the likelihood of device migration and undesired thromboembolism to be minimal. The PED accomplished this while also demonstrating a significant reduction in overall device stiffness compared to commercially available vascular plugs, which allows the PED to be delivered to tortuous vessels that may not be accessible using conventional embolic devices. The results of this work also verified the efficacy of the PED in causing complete vessel occlusion and encouraging rapid thrombus formation, as well as ease of visualization of the PED using ultrasound. However, the safety and efficacy of this device must also be verified through in vivo studies and extensive biocompatibility testing before it can be recommended for clinical use.

CHAPTER IV

A SHAPE MEMORY FOAM COMPOSITE WITH ENHANCED FLUID UPTAKE AND BACTERICIDAL PROPERTIES AS A HEMOSTATIC AGENT

4.1 Introduction

Hemorrhage control remains a significant concern of military and civilian trauma centers across the world. Uncontrolled hemorrhage accounts for over 30% of trauma deaths world-wide and over half of these occur before emergency care can be reached. [213] Current hemostatic treatments often rely on compression wraps or gauze as the standard of care. These treatment options are effective in ceasing the hemorrhage but are often ineffective for deep wounds that are irregularly shaped and not amenable to tourniquet application. Newer treatment options include alginates, polymer sponges, chitosan, and gauze impregnated with procoagulants, such as zeolite and kaolin. [214, 215] However, these newer technologies focus primarily on acute cessation of blood flow, rather than long-term healing and infection prevention. The three primary wound dressing technologies employed in Iraq during Operation Iraqi Freedom were HemCon® (HemCon Medical Technologies, Inc., Portland, OR), QuikClot® (Z-Medica Corporation, Wallingford, CT), and CELOXTM (SAM Medical, Tualatin, OR). [216]

HemCon® is a chitosan-based wafer which adheres to tissues upon contact with blood to effectively seal the wound boundary. This dressing has proven to be successful in establishing hemostasis in specific wounds, but the stiffness of the bandage makes packing small, narrow wounds very difficult. [217, 218] CELOXTM is another chitosan-based hemostat in which granules are poured or injected into the wound which gel together

upon contact with blood to provide a physical seal that promotes hemostasis. Although CELOXTM is often deployed in civilian and military trauma situations, re-bleeding and mortality rates of 25% and 13%, respectively, have been reported. [219] QuikClot® Combat Gauze is a device consisting of gauze impregnated with kaolin, an inorganic material that has demonstrated the ability to enhance blood coagulation without causing thermal injury to wound tissue. [220] However, re-bleeding rates as high as 37% have been reported for deep, narrow wounds treated with QuikClot® Combat Gauze. [221] Although each device has proven highly effective in preventing exsanguination in the battlefield, they have proven less useful for smaller, deep wounds incurred by small-caliber firearms and improvised explosive devices. [216] Current dressings are also only indicated for a number of hours, and as such, require frequent changes to prevent bacterial and fungal infection. To address the risk of infection, the standard of care has become the use of a broad spectrum antibiotic regimen; however, bacterial and fungal resistance has forced a series of alternative antibiotics. [222]

New hemostatic technologies, such as XStatTM (RevMedx, Inc., Wilsonville, OR) have demonstrated significantly improved time to hemostasis, ease of application, and survival rates compared to conventional hemostats. [223] The XStatTM device is an applicator filled with numerous compressed cellulose sponges that rapidly expand to fill and apply pressure to deep, non-compressible wounds. Despite the numerous advantages of the XStatTM technology, the nature of inserting approximately 92 miniature sponges into an open wound can lead to a 22-fold increase in device removal time compared to conventional gauze due to the need to remove each individual sponge from the wound

bed. [224] This may cause patient discomfort during prolonged device removal, as well as increased procedural time and costs.

Shape memory polymer (SMP) foams have previously demonstrated exceptional biocompatibility and hemostatic properties in porcine aneurysms. [187, 188] In acute porcine studies, SMP foams have demonstrated hemostasis within an artery in less than 90 seconds after device deployment, as determined by cessation of contrast flow past the device under x-ray. [225] The rapid hemostasis provided by the large surface area and porous morphology of the foams make them strong candidates for controlling hemorrhage. Furthermore, the ability of SMP foams to recover over >400% plastic strain during expansion would enable insertion of a small, crimped device into the wound that would rapidly expand upon contact with blood until the device is completely apposed to an irregular-shaped wound boundary, **Figure 4.1**. However, SMP foams have an inherently limited capacity for absorbing fluid. [206] In the realm of hemostatic wound dressings, the ability to absorb blood and wound fluid is critical for rapid hemostasis, wound healing, and preventing bacterial infection. [226]

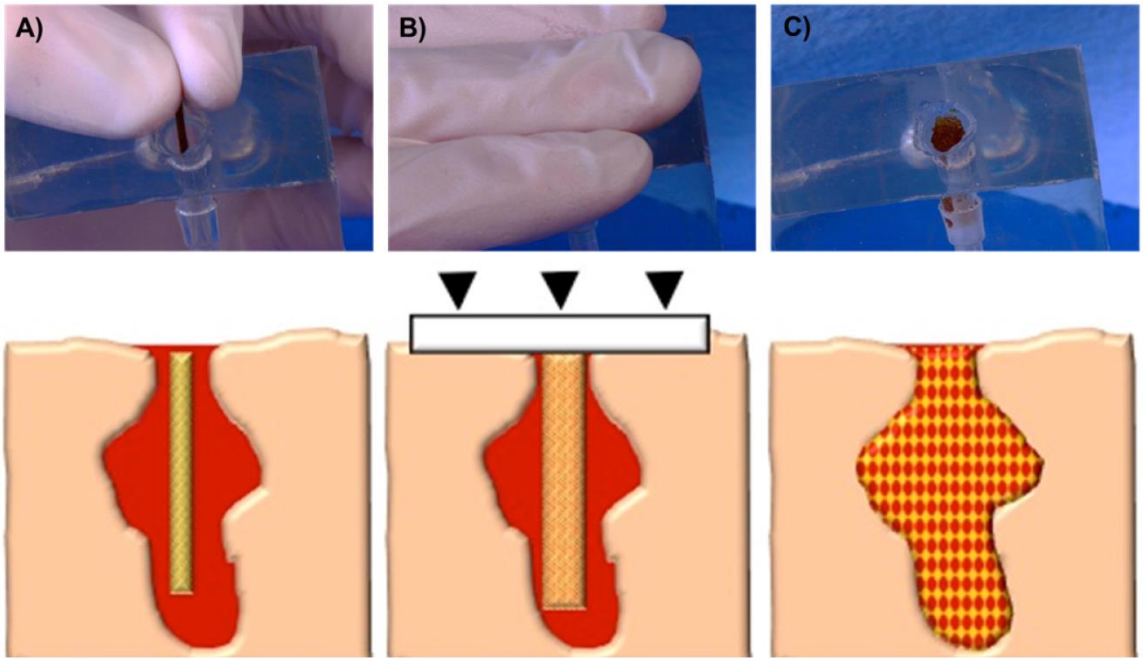

Figure 4.1: Schematic of the envisioned delivery procedure for the hydrogel-SMP foam composite. The first step is to insert the crimped device into the wound (A). Then apply manual compression over the wound site to prevent the device from exiting the wound before expansion (B). Finally, the composite expands to completely fill and conform to the wound cavity and establish rapid blood clotting and hemostasis (C).

In this study, an antimicrobial hydrogel coating was applied to the SMP foam to create a foam-hydrogel composite with enhanced fluid uptake. Specifically, the SMP foam was coated with an n-vinylpyrrolidone (NVP) and polyethylene glycol diacrylate (PEGDA) hydrogel. In addition to increasing the fluid uptake of the composite, the hydrogel is able to directly complex with iodine to form a povidone-iodine (PVP-I_2) complex, which is one of the most widely used iodine antiseptics in surgical care. PVP-I_2 is a stable complex of polyvinylpyrrolidone (PVP) and elemental iodine that is used to kill a variety of viruses, bacteria, fungi, protozoa, and yeast, and there have been no documented cases of microbial resistance to PVP-I_2. [227] The composite presented here

combines the volume filling and rapid hemostasis of SMP foams with the fluid uptake and bactericidal action of iodine-doped hydrogels to create a highly advantageous hemostatic wound dressing prototype. The primary goal of this study was to ensure that the advantageous characteristics of the hydrogel and SMP foams were successfully combined in the composite wound dressing.

4.2 Materials and Methods

4.2.1 Materials

All chemicals were used as received and purchased from Sigma Aldrich (Milwaukee, WI) unless otherwise noted. Foams were fabricated using N,N,N′,N′-Tetrakis(2-hydroxypropyl)ethylenediamine (HPED), 2,2′,2″-nitrilotriethanol (TEA, 98%; Alfa Aesar Inc., Ward Hill, MA), 1,6-diisocyanatohexane (HDI; TCI America Inc., Portland, OR), surfactants DC 198 and DC 5943 (Air Products and Chemicals, Inc., Allentown, PA), and deionized (DI) water (>17MΩ cm purity; Millipore water purifier system; Millipore Inc., Billerica, MA). The CellTiter 96® AQueous One Solution Proliferation Assay (Promega Corp., Madison, WI) was used for antibacterial studies to obtain a quantitative value for the absorbance of bacterial units after being cultured with iodine-containing hydrogel films.

4.2.2 Hydrogel Preparation

Polyethylene glycol diacrylate (PEGDA) was synthesized according to a method adapted from Hahn, et al. Briefly, 4 molar equivalents of acryloyl chloride were added dropwise to a solution of PEG (6 kDa; 1 molar equivalent) and triethylamine (2 molar

equivalents) in anhydrous dichloromethane (DCM) under nitrogen. After the addition was complete, the reaction was stirred for 24 hours. The resulting solution was washed with 2M potassium bicarbonate (8 molar equivalents). The product was precipitated in cold diethyl ether, filtered, and dried under vacuum. FTIR spectroscopy and proton nuclear magnetic resonance (1H-NMR) spectroscopy were used to confirm functionalization of PEGDA. Control and functionalized polymers were solution cast directly onto KBr pellets to acquire transmission FTIR spectra using a Bruker ALPHA spectrometer. Successful acrylation was indicated by an ester peak at 1730 cm^{-1} and loss of the hydroxyl peak at 3300 cm^{-1} in the spectra. Proton NMR spectra of control and functionalized polymers were recorded on Mercury 300 MHz spectrometer using a TMS/solvent signal as an internal reference. All syntheses resulted in percent conversions of hydroxyl to acrylate endgroups of greater than 90%. 1H NMR (CDCl3): 3.6 ppm (m, -OCH2CH2-), 4.3 ppm (t, -CH2OCO-) 5.8 ppm (dd, CH=CH2), 6.1 and 6.4 ppm (dd, -CH=CH2).

PEGDA-polyvinylpyrrolidone (PEG-PVP) hydrogels were prepared by dissolving PEGDA and N-vinylpyrrolidone (NVP) (1:96 molar ratio) to a 5 wt% solution in deionized water with a thermal initiator (1% azobisisobutyronitrile, AIBN). Hydrogels for bactericidal studies were fabricated by pipetting the precursor solution into a mold and heating to 70°C for 30 min. Iodine doping of hydrogels was conducted by placing hydrogel specimens in distilled water with 10 wt% elemental iodine for 2 hours at 50°C. Afterwards, the doped hydrogel specimens were rinsed three times with ethanol, three times with distilled water, and then placed under vacuum to dry prior to characterization. Raman spectroscopy was utilized to confirm successful iodine complexation with the PVP.

Raman spectra were recorded using a Thermo Scientific DXR Raman Microscope with a 780 nm excitation laser (max power 24 mW, 830 lines/mm gratings). Control hydrogels (PEG-I_2, PEG-PVP, PEG-PVP-I_2 no heat) were also fabricated for comparison.

4.2.3 Hydrogel Bactericidal Characterization

For bactericidal studies, Staphylococcus aureus USA 300 was cultured in tryptic soy broth overnight at 37°C while shaking at 220 RPM. Cells were diluted 1:100 in fresh tryptic soy broth and cultured for 2 hours. Cut hydrogels (PEG-PVP, PEG-PVP-I_2, 4 mm diameter) were placed in the bottom of 96 well plates. Gels were washed with 100 μL sterile water, 100 μL 70% ethanol, and 200 μL sterile water. $1x10^7$ cells were added to each well in 100 μL media. Cells and gels were incubated for 1 hr at 37°C. After incubation, cell media was removed and the gels were washed with 100 μL sterile water. Next, 100 μL fresh tryptic soy broth was added to each well and viability assessed with the MTT assay. 20 μL/well CellTiter 96 Aqueous One tetrazolium reagent was added to each well and incubated for 4 hrs at 37°C. Absorbance was read at 490 nm per the manufacturer's instructions. In addition, bacterial suspensions from each well were diluted, plated, and counted for colony forming units after 18 hr incubation on tryptic soy broth agar plates.

4.2.4 SMP Foam Synthesis and Processing

Polyurethane SMP foams were fabricated using a three-step gas blowing process that has been described previously. [191] In short, an isocyanate premix of HDI (63 wt%) was made with 39% hydroxyl groups consisting of HPED and TEA and allowed to cure for 2 days at 50°C. Then a second hydroxyl premix was made with the remaining

molecular equivalents of HPED and TEA. DI water was added to the hydroxyl premix to serve as a chemical blowing agent at 3 wt%. HPED and TEA concentrations for the foam were each 13 wt%. Surfactants DC 198 and DC 5943 were added to the hydroxyl premix at 4 wt% and 3 wt%, respectively. Catalysts T-131 and BL-22 (Air Products and Chemicals, Inc., Allentown, PA) were added to the reaction mixture at 0.3 wt% and 0.5 wt%, respectively. Finally, the premixes were combined and mixed with a physical blowing agent, Enovate (4 pph). The resulting foam was cured for 20 minutes at 90°C, followed by a cold cure cycle of 24 hours at room temperature, after which the foam was processed to create interconnected pores and remove any residual unreacted species within the polymer.

The first processing step the foams undergo after curing is mechanical reticulation, a process described previously by which the residual thin membranes separating the pores of the foam are removed. [225] This results in interconnected pores and the ability for fluid to penetrate the entire volume of the foam. After reticulation, the foams were cut into cylinders 10 mm in diameter and 2 cm in length using a 10 mm biopsy punch and resistively-heated hot wire cutter. After reticulation and cutting to the desired geometry, the foam samples were extensively cleaned in a series of solutions while under sonication. This procedure included two 15 minute cycles in isopropyl alcohol (99.9% purity), four 15 minute cycles in Contrad 70® (Decon Labs, Inc., King of Prussia, PA), and two 15 minute cycles in reverse osmosis (RO) purified water. After all steps were completed, the foams were frozen in a -4°C freezer for 12 hours and subsequently freeze-dried to remove all moisture from the samples.

4.2.5 Composite Fabrication and Characterization

SMP foams were placed in molds (10 mm diameter x 25 mm length) and PEG-PVP precursor solutions were pipetted into the molds. A poragen mixture of dextran and saccharin was added to the hydrogel precursor solution (200 mg/mL) prior to addition to introduce pores into the hydrogel coating (particle size ~ 40-200 microns). Hydrogel-foam composites were cured at 70°C for 6 hours and the poragen leached out over the course of 2 days in deionized water. The hydrogel-foam composites were then frozen at -20°C and lyophilized. Iodine doping of composites was conducted by placing hydrogel-foam composites in distilled water with 10 wt% elemental iodine for 6 hours at 70°C. Subsequently the iodine-doped composites were frozen at -20°C in the mold and then lyophilized. Water uptake was measured on composite specimens that were first dried under vacuum for 48 hours at 60°C and weighed to assess dry (polymer) mass (Wd). The composites were then swollen in RO water for 24 hours and weighed to determine the equilibrium swelling mass (Ws). The equilibrium mass swelling ratio, Q, was calculated using the following equation:

$$Q = \frac{W_s}{W_d} \qquad (1)$$

Excess fluid was removed from the exterior of each sample with a clean Kimwipe (Kimberly-Clark Worldwide, Inc., Roswell, GA) prior to weighing the specimen.

To determine whether the incorporation of hydrogel hindered the shape memory behavior of the foam, expansion studies were conducted to determine the shape recovery and expansion of the composites. To conduct these studies, the average composite diameters were measured before and after crimping using ImageJ software. Samples were

then submerged in 37°C water and imaged at 30 second intervals for a total of 15 minutes. Shape recovery was calculated according to the following equation used by Dr. Tao Xie:

$$Shape\ Recovery\ \% = 1 - \frac{D_n - D_E}{D_c - D_E} \quad (2)$$

where D_n is the diameter of the foam at a given time point during expansion, D_E is the diameter of the expanded device before crimping, and D_c is the crimped diameter of the device. [228] To measure the average diameter of each sample, the 2-D projected surface area of the foam at each time point was divided by the length of the sample. Images were captured at each time point using a Canon PowerShot SX230 HS (Canon USA, Inc., Melville, NY) digital camera. The volume expansion of each composite was also analyzed using equation 3 below:

$$Volume\ Expansion = \left(\frac{D_n}{D_c}\right)^2 \quad (3)$$

Scanning electron microscopy (SEM) was used to assess the morphology of the wound dressing before and after hydrogel incorporation into the composite. To perform this analysis, uncoated SMP foams and iodine-doped composites were gold sputter-coated and placed on double-sided carbon tape for imaging in a NeoScope JCM5000 (Jeol USA, Inc., Peabody, MA) scanning electron microscope.

The expansion force of composite devices was analyzed before and after the hydrogel coating was applied by following a method based on ISO 25539-2. For this test, devices were radially crimped to approximately 1.5 mm in diameter and placed between two compression platens within a waterproof environmental chamber attached to an Instron Model 5966 Dual Column Test System (Illinois Tool Works Inc., Norwood, MA).

A preload of approximately 0.15 N was applied to the crimped devices before the test was initiated. After preloading, 50°C water was added to the environmental chamber to initiate device expansion until the compression platens were completely submerged. The distance between the compression platens remained constant throughout the test, while the force exerted by the expanding device was continuously measured for 15 minutes. The buoyancy force exerted by the water on the compression platens was also measured using the same method with no device between the platens. The expansion forces reported for each device are the result of subtracting the buoyancy force from the raw force measurements.

4.3 Results

4.3.1 Iodine Doping

Raman spectroscopy peaks indicated the presence of the antibacterial polyvinylpyrrolidone-iodine (PVP-I_2) complex in the PEG based hydrogels, **Figure 4.2**. At lower wavenumbers, the generation of the PVP-I_2 complex is visible at 112 cm^{-1}. For PEG-PVP-I_2 complexation without heating, the peak at 112 cm^{-1} is indicative of the v1 vibrations of I_3- complexed to PVP [21]. Upon exposure to heat, peak intensity increases and additional bands appeared around 145 cm^{-1} and 167 cm^{-1} that correspond to v2 vibrations of I_3- and I_5-, respectively. [229] No iodine bands were visible for PEG-I_2 which suggests the importance of the PVP to generate an antibacterial iodophor. Additionally, no bands were visible for the PEG:PVP copolymer at lower wavenumbers since C-C peaks of this polymer are generally identified using Fourier transform infrared spectroscopy at 400 cm^{-1} and higher.

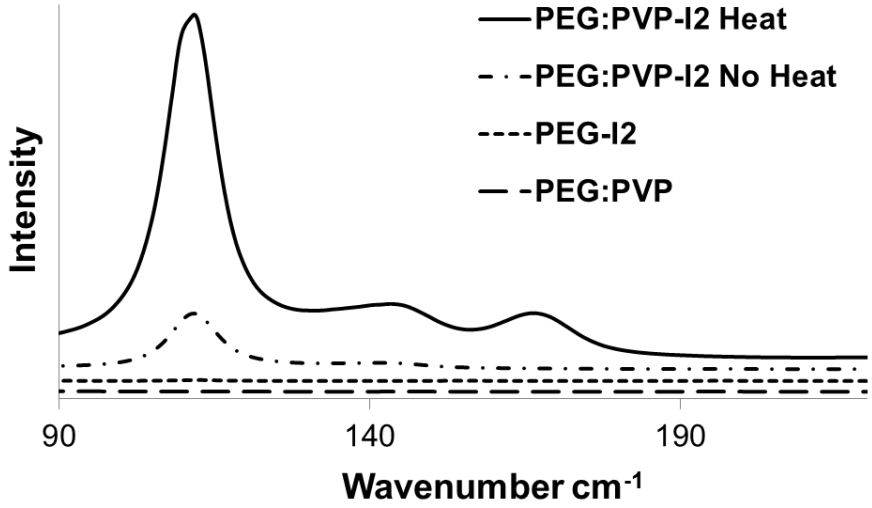

Figure 4.2: Raman spectra of iodide doped hydrogels under various conditions. Successful complex of PVP and iodide is indicated by the presence of a peak at 110 cm-1. A control PEG-PVP gel with no iodide is shown to confirm the lack of convolution due to the chemical composition. PEG-I2 was run to confirm that the complex was due to the interactions with PVP. The heated PEG-PVP shows the greatest amount of iodide complexed to the gel.

4.3.2 Bactericidal Properties

Iodine-doped hydrogel specimens were cultured with Staphylococcus aureus USA 300, a methicillin resistant strain, to determine the potential bactericidal properties of the composite. Log-phase bacterial suspensions (~1 x 10^7) were incubated with hydrogel specimens for 1 hr followed by quantification of bacterial viability and dilution plating of the bacterial suspension. An approximate 80% reduction in bacteria viability was observed after exposure to the iodine-doped hydrogel as compared to the positive control and the hydrogel without iodine doping, **Figure 4.3**. Results of dilution plating corroborated the viability assay (data not shown). The starting culture contained ~1 x 10^7 staphylococci,

which is equivalent to more than 1 x 10^8 bacteria per gram of tissue if we consider the hydrogel surface analogous to tissue. Previous studies have shown bacteria levels exceeding 1 x 10^5 colony forming units per gram of tissue dramatically increase the risk of infection and skin graft failure. [230, 231] Hence, the concentration of staphylococci used in these studies is representative of the bioburden typically found in wounds prone to infection and provides a rigorous test for efficacy. The rapid reduction of viable bacteria within an hour of exposure to the iodine-doped hydrogel indicates the potential bactericidal activity of the composites.

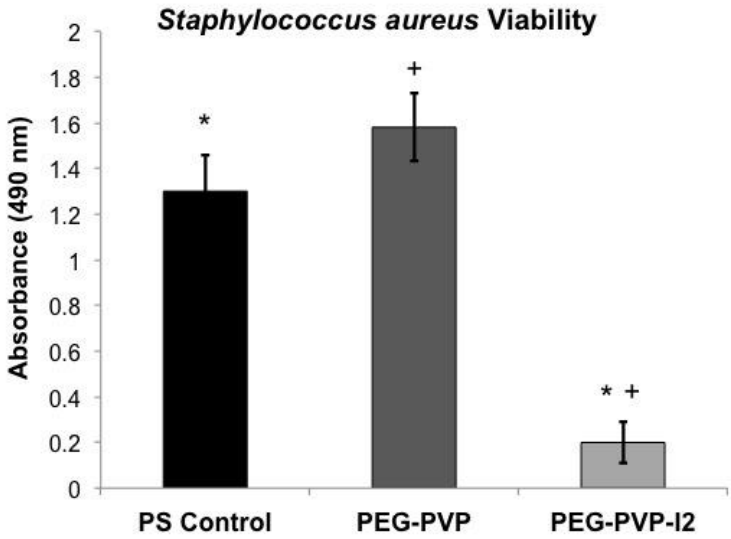

Figure 4.3: Effect of the PEG-PVP hydrogel with and without iodine doping on growth of Staphylococcus aureus measured by the MTT assay in comparison to a positive control. Data shown as mean ± standard deviation. * denotes statistical significance ($p \leq 0.05$) according to one-tailed Student's t-test.

4.3.3 Composite Water Uptake

The swelling ratios of the composites were analyzed to investigate the ability to absorb wound exudate that may lead to bacterial infection and prevent healing. [226] It was also hypothesized that a higher absorptive capacity of the wound dressing will concentrate clotting factors within the dressing and enhance the rate of hemostasis. [217] **Figure 4.4** shows SEM images of the morphology of the wound dressing before and after the hydrogel coating is applied, which shows the extent to which the hydrogel coats the struts and membranes of the foam pores to allow for enhanced fluid absorption. With the incorporation of hydrogels into the wound dressing device, there was a 19X improvement in the swelling ratio of the hydrogel-foam composite as compared to the uncoated SMP foam, **Figure 4.5**. This increase in swelling ratio directly relates to potential wound fluid uptake of the device that is critical for its function as a hemostatic agent.

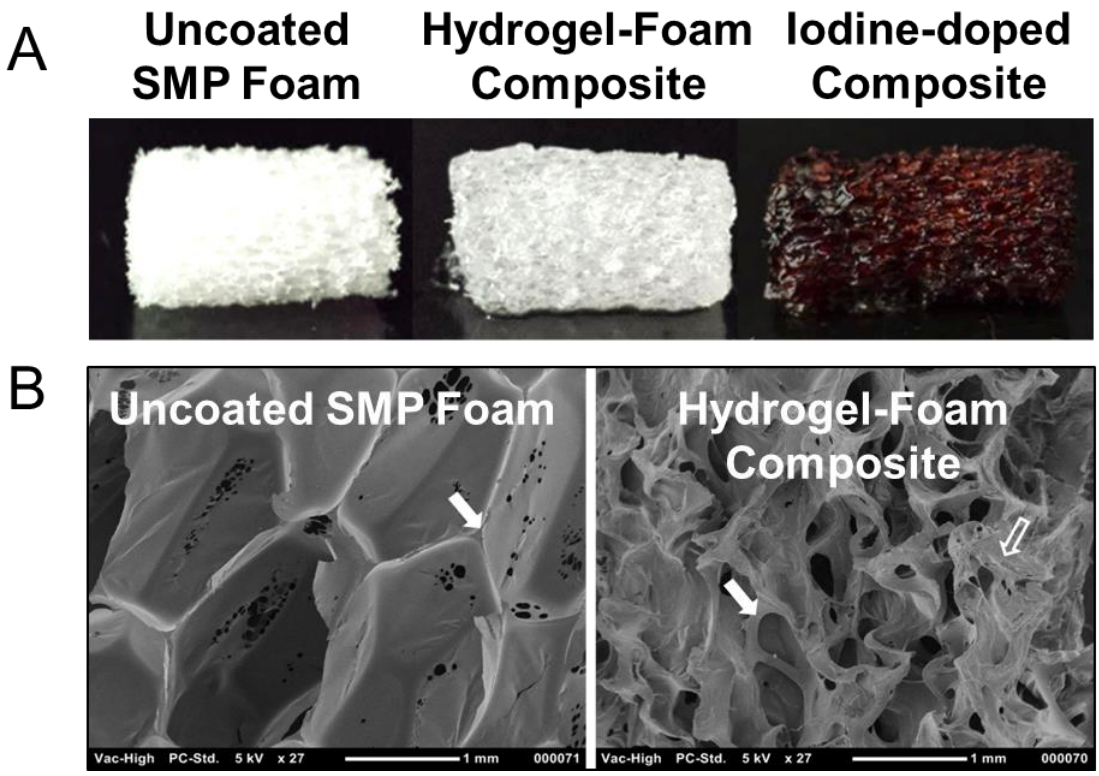

Figure 4.4: A) Image of uncoated SMP foam, hydrogel-foam composite, and iodine-doped composite; B) SEM images of a SMP foam before (left) and after (right) hydrogel incorporation into the composite. After hydrogel incorporation, foam struts (solid arrow) are coated and hydrogel deposits (hollow arrow) are seen throughout the composite.

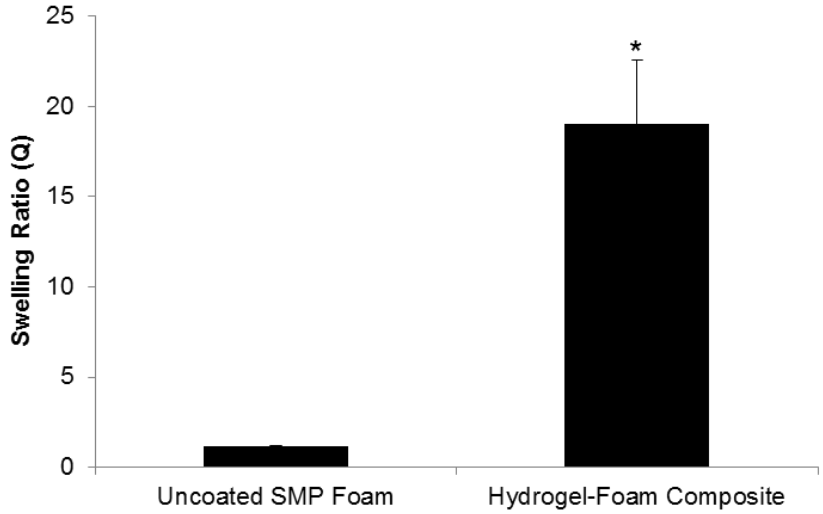

Figure 4.5: Average swelling ratio of the hydrogel-foam composite compared to uncoated SMP foams. The swelling ratio directly correlates to fluid uptake (mean ± standard deviation, n = 5). *denotes statistical significance, $p \leq 0.05$ according to one-tailed Student's t-test.

4.3.4 Shape Recovery and Expansion Ratio

In order to ensure the composites retained the shape memory behavior of the SMP foams, expansion studies were conducted in 37°C water. The results from this analysis are shown in **Figure 4.6(b)**. A typical crimped and expanded composite is shown in **Figure 4.6(a)**. The device would be delivered to the wound in the crimped state and would change shape to the expanded geometry upon contact with physiologic fluid at 37°C. This is possible because of the plasticization of the SMP foam upon contact with moisture, which reduces the transition temperature of the foam to approximately 10°C such that the shape memory effect will occur within the body. Expansion studies demonstrated that the composite devices retain the shape memory behavior of the SMP foams. After 15 minutes of exposure to 37°C water, the composites experienced an average shape recovery of

approximately 74%. Within this time frame the device diameter more than triples, resulting in more than a 1200% increase in device volume. The volume expansion of this device over short periods of time would allow for easy delivery into narrow, penetrating wounds, and subsequent expansion to completely fill abnormal wound boundaries with a single device.

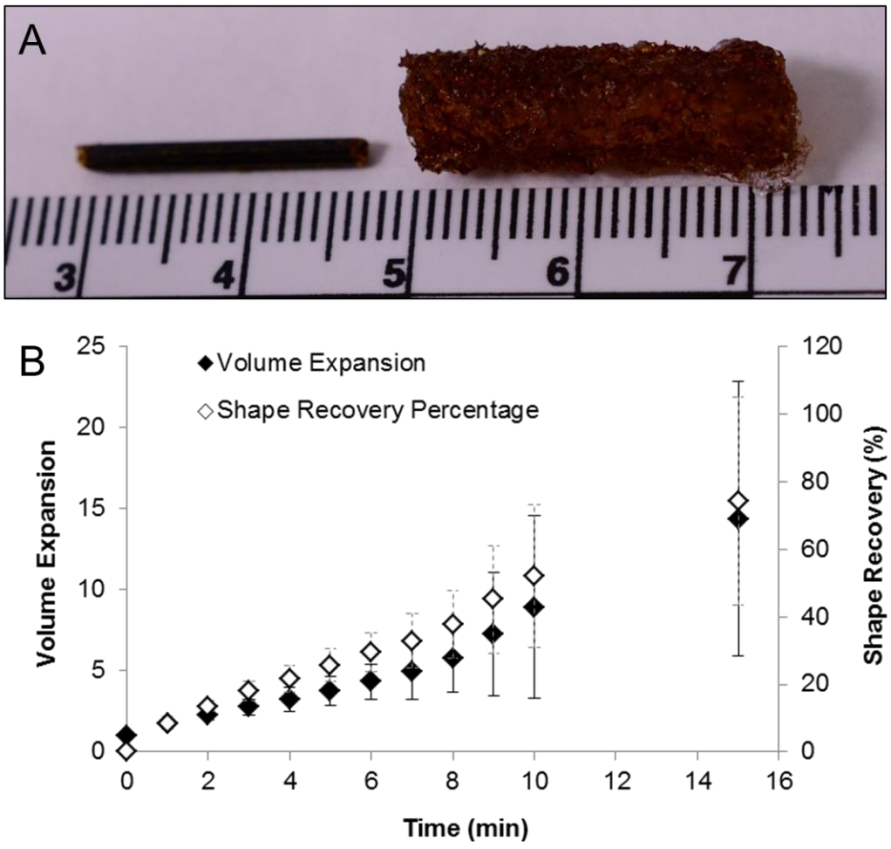

Figure 4.6: A) Representative image of the appearance of a dry, crimped composite (left) and a saturated composite (right). Scale bar is in centimeters. B) Volume expansion ratio and shape recovery analysis of the wound dressing composite after submersion in water at 37°C, (mean ± standard deviation, n = 5).

4.3.5 Expansion Force

An important feature of devices used to treat penetrating wounds that are not amenable to tourniquet application is the ability to apply sufficient radial force to prevent exsanguination around the device and dislocation from the wound bed under physiologic blood flow and pressure. However, the device also should not impart excessive force that may cause damage to the surrounding tissue. The forces exerted by the composites during expansion in 50°C water are summarized in **Figure 4.7**. Force measurements demonstrated an approximate 20% increase in expansion force in the composites compared to uncoated foams. The average maximum expansion force for the composite device was 0.58 N. Assuming a uniform cylindrical surface area of the crimped device, this force equates to a pressure of approximately 6.12 kPa, which is roughly equivalent to the pressure exerted by gauze within a gelatin wound model. [224]

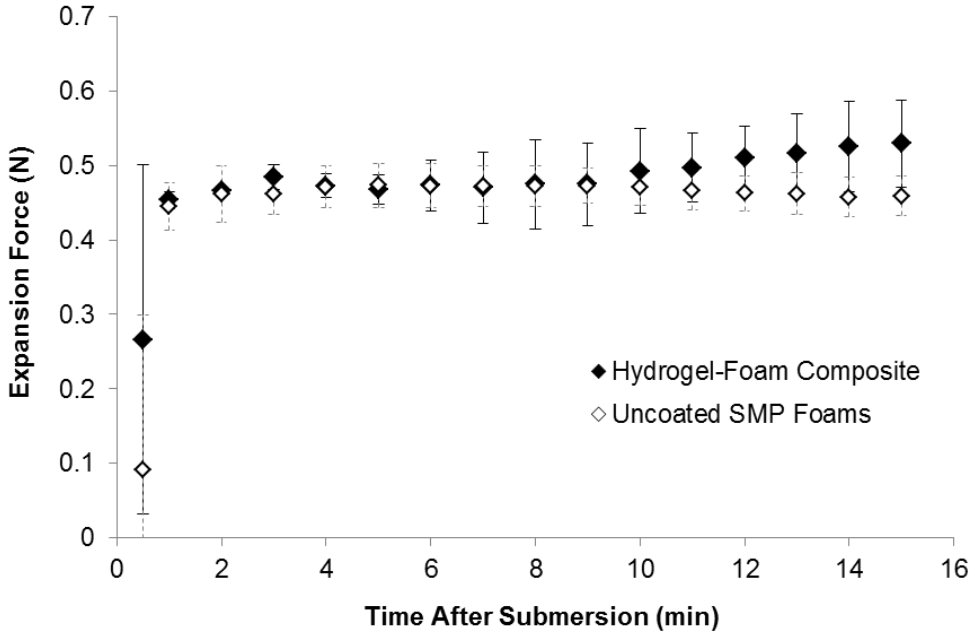

Figure 4.7: One dimensional force exerted by the hydrogel-foam composite and uncoated SMP foams during expansion in 50°C water.

4.4 Discussion

The ideal hemostat is capable of providing hemostasis after trauma to large vessels, requires no special preparation, is simple to apply, lightweight and durable, stable in extreme environments, causes no injury to surrounding tissues, and is inexpensive. [232] None of the dressings currently used in the field satisfy all of these criteria. The FDA approval of the XStat® (RevMedX, Wilsonville, OR) device in 2015 represents an exciting leap forward in addressing hemorrhage control with expandable devices. However, this device does not address potential infection issues and is only indicated for implantation for up to four hours. After this time, each of the individual sponges implanted into the body must be manually removed from the wound. The proposed SMP foam-

hydrogel composite device is a promising technology that may achieve rapid hemostasis with a single device that is also antibacterial. The antibacterial properties of this device could drastically reduce the risk of infections incurred in the battlefield before topical disinfectants can be applied to the wound within a medical facility.

The incorporation of hydrogels into the wound dressing allows this device to absorb substantially more fluid than standard surgical gauze and more fluid than many of the new hemostatic wound dressings under investigation. [224, 232] In future iterations, the swelling capacity of the composite can be improved further through incorporating a higher percentage of hydrogel into the composite, or investigating alternative superabsorbent hydrogel formulations. [233, 234] It is also possible that reduced weight percentages of PEGDA in the hydrogel precursor solution would further improve the swelling capacity of the wound dressing.

Although current wound dressings incorporate chitosan for its hemostatic and antimicrobial effects, it is only effective against certain bacterial species and in specific pH environments. [235, 236] During this work, Raman spectroscopy revealed successful complexation of iodine into the composite to form the common surgical scrub PVP-I_2, typically sold under the brand name Betadine® (Purdue Products L.P., Stamford, CT). There have been no reported instances of microbial resistance to PVP-I_2, and as such, it makes an excellent broad spectrum antiseptic that has proven to be less of an irritant than pure iodine. [227] In antimicrobial studies investigating the effectiveness of the PVP-I_2 complexed hydrogel, there was approximately an 80% reduction in the viability of Staphylococcus aureus in direct contact with the hydrogel compared to the hydrogel

containing no iodophors. The antibacterial results demonstrated by this hydrogel system are equivalent to the results seen in other studies investigating the antibacterial properties of silver-containing hydrogels used in medical applications. [237, 238] A limitation of this study was that the bactericidal activity of the composite device was not assessed. It is likely that the kill zone would be smaller than that seen in this study due to the porous geometry of the device and specific regions of the device that would not be in contact with the bacteria in vitro. However, in vivo this would likely be overcome by the diffusion of unbound iodine from the device into the surrounding area within the wound.

Expansion studies revealed that the composite device retained the shape memory behavior of the SMP foams. This allows the device to be delivered to a wound site in a small, crimped geometry and undergo more than 15X volume expansion to fill large volumes, which is more than five times greater volume expansion than new hemostatic wound dressings on the market. [223] The composites showed an average shape recovery of 74% after 15 minutes of immersion in 37°C water, which is slower shape recovery than previously demonstrated in the same composition of uncoated SMP foams. [239] When dry, the hydrogel acts as an additional moisture diffusion barrier that is likely the reason for delayed plasticization of the SMP foam and subsequent slower shape recovery. The large standard deviation during expansion studies is primarily attributable to the effects of the randomness in hydrogel orientation throughout the composite device. Agglomeration of the hydrogel in some samples at the periphery of the composite will slow the plasticization of the SMP foam and delay shape recovery compared to other samples. In order to increase the effectiveness of this device as a potential hemostat, future iterations

of this device will investigate means of enhancing the rate of composite expansion. One method to accomplish this would be to reduce the amount of hydrogel used in the composite. However, this would coincidentally reduce the swelling capacity of the device. Another method to enhance the rate of expansion without affecting the swelling capacity of the device would be to isolate the hydrogel within the central core of the device so as to not cause any diffusive resistance at the periphery of the device.

Analysis of the force exerted by the composite wound dressing demonstrated an average expansion force of 0.58 N, which is approximately 20% greater than the average expansion force of uncoated SMP foams. One of the limitations of the parallel plate analysis conducted is that it only evaluates the force at the points of the device in contact with the parallel plates and ignores the total radial force exerted by the device. According to previous studies, parallel plate evaluations of the radial force of stents are approximately 10-14% of the total radial force. [240] With this understanding, the total radial expansion force of the composite may be up to 6 N- less than 20% of the radial force exerted by common vascular stents. [240] This is also assuming the wound being treated has the same diameter as the crimped device, which would likely not be the case. Given the generally accepted safety of stents and lack of adverse events related to vessel perforation, it is highly unlikely that the hydrogel-coated SMP foam composite would cause significant damage to the wound bed during expansion.

4.5 Conclusions

In this feasibility study, we successfully created a hydrogel-coated SMP foam that retains the advantages of each respective material system to form a composite device for the treatment of traumatic hemorrhage. This technology is capable of absorbing more fluid than many new hemostatic wound dressings currently under investigation, can undergo up to 15X volume expansion upon contact with 37°C fluid to fill large volumes, and demonstrates antibacterial properties in vitro. This work resulted in an initial proof-of-concept device that has shown highly valuable attributes for use as a hemostatic sponge. The composite studied here could lead to a vastly improved technology for treating hemorrhage in the battlefield and civilian trauma arena. Future studies using relevant animal models of hemorrhage will be used to further assess the potential of this device.

CHAPTER V

CONCLUSIONS

5.1 Summary

This research thoroughly investigated and discussed the goal of embolization in various regions of the human vasculature, current treatment methodologies, and how SMP foams can improve current treatment methods. This work also discusses the projected future of embolic scaffolds and the direction in which research is likely to progress. The knowledge gained from extensive literature reviews of embolization technology and the associated indications led to the design, development, and verification of novel embolic technologies targeting the peripheral vasculature.

The first investigation detailed within this work verified the mechanical properties of the shape memory polymer PED device are safe and unlikely to cause vessel perforation or rupture. At the same time, these studies demonstrated that the likelihood of device migration and undesired thromboembolism to be minimal. The PED accomplished this while also demonstrating a significant reduction in overall device stiffness compared to commercially available vascular plugs, which allows the PED to be delivered to tortuous vessels that may not be accessible using conventional embolic devices. The results of this work also verified the efficacy of the PED in causing complete vessel occlusion and encouraging rapid thrombus formation, as well as ease of visualization of the PED using ultrasound. However, the safety and efficacy of this device must also be verified through in vivo studies and extensive biocompatibility testing before it can be recommended for clinical use.

After verifying the safety and efficacy of a device which incorporated unaltered SMP foam, the second investigation focused on creating a proof-of-concept SMP foam-hydrogel composite device with enhanced fluid uptake and bactericidal properties. In this feasibility study, a hydrogel-coated SMP foam was successfully created that retains the advantages of each respective material system to form a composite device for the treatment of traumatic hemorrhage. This technology is capable of absorbing more fluid than many new hemostatic wound dressings currently under investigation, can undergo up to 15X volume expansion upon contact with 37°C fluid to fill large volumes, and demonstrates antibacterial properties in vitro. This work resulted in an initial proof-of-concept device that has shown highly valuable attributes for use as a hemostatic sponge. The composite studied here could lead to a vastly improved technology for treating hemorrhage in the battlefield and civilian trauma arenas. Future studies using relevant animal models of hemorrhage will be used to further assess the potential of this device.

5.2 Significance of Work

The research described in this work resulted in the creation of novel embolic devices that have the potential to drastically reduce the healthcare costs of endovascular embolization procedures by reducing the number of devices required for treatment, radiation time, the need for repeat procedures, and the time to complete healing of the treated vessel. In addition to the potential clinical impact of this research, there have also been a number of contributions to the scientific literature.

Within this work, numerous testing methodologies and test apparatuses were designed and fabricated for verification testing of novel embolic devices that utilize

polymeric material systems. Novel devices typically require custom testing procedures and apparatuses, and this work has made significant contributions to the design and fabrication of this type of equipment. This work also represents the first verification of the echogenicity of SMP foams, which presents opportunities for minimally invasive devices consistently entirely of foam without the need for radiopaque fillers or components. To the knowledge of the author, this work also represents the first instance of quantifying acute fibrin deposition in an embolic device. The ability to conduct in vitro flow studies with anticoagulated bovine blood was also investigated in this study, which provides a valuable tool for researchers interested in conducting blood contacting device research in vitro.

Finally, the work presented in Chapter IV represents a potential solution to persistent complications and shortcomings associated with commercial hemostatic wound dressings by providing rapid hemostasis in conjunction with inherent bactericidal properties. This research also solidified the ability to incorporate SMP foams with other material systems to create advantageous composite devices with shape memory behavior.

5.3 Future Work

The research presented here provides significant building blocks for commercializing shape memory medical devices. Along these lines, the technology discussed in Chapter III is currently being pursued for commercialization by Shape Memory Medical, Inc. At the time of this manuscript, GLP large animal implant studies for the PED technology have already begun. In the coming weeks, GLP ISO 10993 testing

will also begin on the PED technology to verify the biocompatibility of the device. This will be the first SMP foam device submitted to the FDA for 510(k) clearance.

Future work on the composite SMP foam-hydrogel device will focus on enhancing the rate of expansion of the device without compromising its bactericidal properties. The hydrogel within the device acts as a diffusion barrier, which delays plasticization and the subsequent expansion of the SMP foam. However, for hemorrhagic applications, expansion time is critical to achieve rapid hemostasis. Isolating the hydrogel within the core of the device will be investigated as an effective means of decreasing the time to expansion, as well as the use of superabsorbent hydrogels.

REFERENCES

[1] Funakubo H. Shape memory alloys. New York: Gordon and Breach Science Publishers; 1987.

[2] Huang WM, Ding Z, Wang CC, Wei J, Zhao Y, Purnawali H. Shape memory materials. Mater Today 2010;13:54-61.

[3] Hayashi S. Technical Report on Shape Memory Polymers. Nagoya Research and Development Center: Mitsubishi Heavy Industries, Inc.; 1990.

[4] Sokolowski W, Metcalfe A, Hayashi S, Yahia L, Raymond J. Medical applications of shape memory polymers. Biomedical Materials 2007;2:S23-7.

[5] Zhang D, George OJ, Petersen KM, Jimenez-Vergara AC, Hahn MS, Grunlan MA. A bioactive "self-fitting" shape memory polymer scaffold with potential to treat cranio-maxillo facial bone defects. Acta Biomaterialia 2014;10:4597-605.

[6] Tseng LF, Mather PT, Henderson JH. Shape-memory-actuated change in scaffold fiber alignment directs stem cell morphology. Acta Biomaterialia 2013;9:8790-801.

[7] Defize T, Riva R, Raquez JM, Dubois P, Jerome C, Alexandre M. Thermoreversibly Crosslinked Poly(epsilon-caprolactone) as Recyclable Shape-Memory Polymer Network. Macromol Rapid Comm 2011;32:1264-9.

[8] Hearon K, Gall K, Ware T, Maitland DJ, Bearinger JP, Wilson TS. Post-Polymerization Crosslinked Polyurethane Shape Memory Polymers. J Appl Polym Sci 2011;121:144-53.

[9] Khonakdar HA, Jafari SH, Rasouli S, Morshedian J, Abedini H. Investigation and modeling of temperature dependence recovery behavior of shape-memory crosslinked polyethylene. Macromol Theor Simul 2007;16:43-52.

[10] Sakurai K, Takahashi T. Strain-Induced Crystallization in Polynorbornene. J Appl Polym Sci 1989;38:1191-4.

[11] Wu XL, Huang WM, Ding Z, Tan HX, Yang WG, Sun KY. Characterization of the Thermoresponsive Shape-Memory Effect in Poly(ether ether ketone) (PEEK). J Appl Polym Sci 2014;131.

[12] Yakacki CM, Shandas R, Lanning C, Rech B, Eckstein A, Gall K. Unconstrained recovery characterization of shape-memory polymer networks for cardiovascular applications. Biomaterials 2007;28:2255-63.

[13] Cabanlit M, Maitland D, Wilson T, Simon S, Wun T, Gershwin ME, et al. Polyurethane shape-memory polymers demonstrate functional biocompatibility in vitro. Macromolecular Bioscience 2007;7:48-55.

[14] Lendlein A, Kelch S. Shape-memory polymers. Angewandte Chemie 2002;41:2035-57.

[15] Metcalfe A, Desfaits AC, Salazkin I, Yahia L, Sokolowski WM, Raymond J. Cold hibernated elastic memory foams for endovascular interventions. Biomaterials 2003;24:491-7.

[16] Lendlein A, Langer R. Biodegradable, elastic shape-memory polymers for potential biomedical applications. Science 2002;296:1673-6.

[17] Ortega JM, Small W, Wilson TS, Benett WJ, Loge JM, Maitland DJ. A shape memory polymer dialysis needle adapter for the reduction of hemodynamic stress within arteriovenous grafts. IEEE T Bio-Med Eng 2007;54:1722-4.

[18] Small W, Wilson TS, Benett WJ, Loge JM, Maitland DJ. Laser-activated shape memory polymer intravascular thrombectomy device. Opt Express 2005;13:8204-13.

[19] Wache HM, Tartakowska DJ, Hentrich A, Wagner MH. Development of a polymer stent with shape memory effect as a drug delivery system. J Mater Sci-Mater M 2003;14:109-12.

[20] Boateng JS, Matthews KH, Auffret AD, Humphrey MJ, Stevens HN, Eccleston GM. In vitro drug release studies of polymeric freeze-dried wafers and solvent-cast films using paracetamol as a model soluble drug. Int J Pharmaceut 2009;378:66-72.

[21] Janik H, Marzec M. A review: Fabrication of porous polyurethane scaffolds. Mat Sci Eng C-Mater 2015;48:586-91.

[22] Okuno H, Renzo K, Uragami T. Influence of Casting Solution Additive, Degree of Polymerization, and Polymer Concentration on Poly(Vinyl Chloride) Membrane-Properties and Performance. J Membrane Sci 1993;83:199-209.

[23] Ito Y, Liu SQ, Imanishi Y. Enhancement of Cell-Growth on Growth Factor-Immobilized Polymer Film. Biomaterials 1991;12:449-53.

[24] Aljawish A, Muniglia L, Jasniewski J, Klouj A, Scher J, Chevalot I. Adhesion and growth of HUVEC endothelial cells on films of enzymatically functionalized chitosan with phenolic compounds. Process Biochem 2014;49:863-71.

[25] Ji CD, Annabi N, Hosseinkhani M, Sivaloganathan S, Dehghani F. Fabrication of poly-(DL)-lactide/polyethylene glycol scaffolds using the gas foaming technique. Acta Biomaterialia 2012;8:570-8.

[26] Spaans CJ, Belgraver VW, Rienstra O, de Groot JH, Veth RPH, Pennings AJ. Solvent-free fabrication of micro-porous polyurethane amide and polyurethane-urea scaffolds for repair and replacement of the knee-joint meniscus. Biomaterials 2000;21:2453-60.

[27] Frerich SC. Biopolymer foaming with supercritical CO2-Thermodynamics, foaming behaviour and mechanical characteristics. J Supercrit Fluid 2015;96:349-58.

[28] A.G. Dement'ev TKK, A.I. Demina, P.A. Zinger. Structural-physical properties of foam polyurethanes with various foaming agents. Polymer Science USSR 1991;33:2125-34.

[29] Kimmins SD, Cameron NR. Functional Porous Polymers by Emulsion Templating: Recent Advances. Adv Funct Mater 2011;21:211-25.

[30] Silverstein MS. Emulsion-templated porous polymers: A retrospective perspective. Polymer 2014;55:304-20.

[31] Silverstein MS. PolyHIPEs: Recent advances in emulsion-templated porous polymers. Prog Polym Sci 2014;39:199-234.

[32] Sarvi MN, Stevens GW, Gee ML, O'Connor AJ. The co-micelle/emulsion templating route to tailor nano-engineered hierarchically porous macrospheres. Micropor Mesopor Mat 2012;149:101-5.

[33] Cameron NR. High internal phase emulsion templating as a route to well-defined porous polymers. Polymer 2005;46:1439-49.

[34] Yao CH, Qi L, Jia HY, Xin PY, Yang GL, Chen Y. A novel glycidyl methacrylate-based monolith with sub-micron skeletons and well-defined macropores. J Mater Chem 2009;19:767-72.

[35] El-Kady AM, R.A. Rizk, B.M. Abd El-Hady, M.W. Shafaa, M.M. Ahmed. Characterization, and antibacterial properties of novel silver releasing nanocomposite scaffolds fabricated by the gas foaming/salt-leaching technique. Journal of Genetic Engineering and Biotechnology 2012;10:229-38.

[36] Hariraksapitak P, Suwantong O, Pavasant P, Supaphol P. Effectual drug-releasing porous scaffolds from 1,6-diisocyanatohexane-extended poly(1,4-butylene succinate) for bone tissue regeneration. Polymer 2008;49:2678-85.

[37] Yoon JJ, Kim JH, Park TG. Dexamethasone-releasing biodegradable polymer scaffolds fabricated by a gas-foaming/salt-leaching method. Biomaterials 2003;24:2323-9.

[38] De Nardo L, Bertoldi S, Cigada A, Tanzi MC, Haugen HJ, Fare S. Preparation and characterization of shape memory polymer scaffolds via solvent casting/particulate leaching. J Appl Biomater Func 2012;10:119-26.

[39] Heijkants RGJC, Van Tienen TG, De Groot JH, Pennings AJ, Buma P, Veth RPH, et al. Preparation of a polyurethane scaffold for tissue engineering made by a combination of salt leaching and freeze-drying of dioxane. J Mater Sci 2006;41:2423-8.

[40] Rogina A. Electrospinning process: Versatile preparation method for biodegradable and natural polymers and biocomposite systems applied in tissue engineering and drug delivery. Appl Surf Sci 2014;296:221-30.

[41] Sell SA, Bowlin GL. Creating small diameter bioresorbable vascular grafts through electrospinning. J Mater Chem 2008;18:260-3.

[42] Jiang T, Carbone EJ, Lo KWH, Laurencin CT. Electrospinning of polymer nanofibers for tissue regeneration. Prog Polym Sci 2015;46:1-24.

[43] Jing X, Mi HY, Peng J, Peng XF, Turng LS. Electrospun aligned poly(propylene carbonate) microfibers with chitosan nanofibers as tissue engineering scaffolds. Carbohyd Polym 2015;117:941-9.

[44] Carradice D, Mekako AI, Mazari FAK, Samuel N, Hatfield J, Chetter IC. Clinical and technical outcomes from a randomized clinical trial of endovenous laser ablation compared with conventional surgery for great saphenous varicose veins. Brit J Surg 2011;98:1117-23.

[45] Molyneux A, Kerr R, Stratton I, Sandercock P, Clarke M, Shrimpton J, et al. International Subarachnoid Aneurysm Trial (ISAT) of neurosurgical clipping versus endovascular coiling in 2143 patients with ruptured intracranial aneurysms: a randomised trial. Lancet 2002;360:1267-74.

[46] Bendok BR, Levy EI, Hanel RA, Qureshi AI, Guterman LR, Hopkins NL. Brain AVM Embolization. Operative Techniques in Neurosurgery 2003;2:64-74.

[47] Knerr M, Bertog S, Vaskelyte L, Hofmann I, Sievert H. Results of Percutaneous Closure of Patent Foramen Ovale With the GORE (R) Septal Occluder. Catheter Cardio Inte 2014;83:1144-51.

[48] Min RJ, Almeida JI, McLean DJ, Madsen M, Raabe R. Novel vein closure procedure using a proprietary cyanoacrylate adhesive: 30-day swine model results. Phlebology 2012;27:398-403.

[49] Qureshi SA, Reidy JF, BinAlwi M, Lim MK, Wong J, Tay J, et al. Use of interlocking detachable coils in embolization of coronary arteriovenous fistulas. Am J Cardiol 1996;78:110-&.

[50] Rodriguez JN, Clubb FJ, Wilson TS, Miller MW, Fossum TW, Hartman J, et al. In vivo response to an implanted shape memory polyurethane foam in a porcine aneurysm model. J Biomed Mater Res A 2014;102:1231-42.

[51] Gianturco C, Anderson JH, Wallace S. Mechanical Devices for Arterial-Occlusion. Am J Roentgenol 1975;124:428-35.

[52] Guglielmi G, Vinuela F, Sepetka I, Macellari V, Strother CM. Electrothrombosis of saccular aneurysms via endovascular approach Part 1: Electrochemical basis, technique, and experimental results. Journal of Neurosurgery 1991;75:1-7.

[53] Chuang VP, Wallace S, Gianturco C, Soo CS. Complications of Coil Embolization - Prevention and Management. Am J Roentgenol 1981;137:809-13.

[54] Kallmes DF, Fujiwara NH. New expandable hydrogel-platinum coil hybrid device for aneurysm embolization. Am J Neuroradiol 2002;23:1580-8.

[55] Miller FJ, Mineau DE. Transcatheter Arterial Embolization - Major Complications and Their Prevention. Cardiovasc Inter Rad 1983;6:141-9.

[56] Park S, Lee SJ, Lee M, Lee MS, Kim GM, Kim MD, Won JY, Lee DY. Prospective randomized trial comparing pushable coils and detachable coil during percutaneous implantation of port-catheter system for hepatic artery infusion chemotherapy. Abdominal Imaging 2015;40:595-600.

[57] Vaidya S, Tozer KR, Chen J. An overview of embolic agents. Seminars in Interventional Radiology 2008;25:204-15.

[58] Bilbao JI, Martinez-Cuesta A, Urtasun F, Cosin O. Complications of embolization. Seminars in Interventional Radiology 2006;23:126-42.

[59] Currie S, Mankad K, Goddard A. Endovascular treatment of intracranial aneurysms: review of current practice. Postgraduate Medical Journal 2011;87:41-50.

[60] Lubarsky M, Ray CE, Funaki B. Embolization agents-which one should be used when? Part 1: large-vessel embolization. Seminars in Interventional Radiology 2009;26:352-7.

[61] Patel AA, Solomon JA, Soulen MC. Pharmaceuticals for Intra-arterial Therapy. Seminars in Interventional Radiology 2005;22:130-8.

[62] Golzarian J. Embolization Tools. New York: Springer; 2006.

[63] Speakman TJ. Internal Occlusion of a Carotid Cavernous Fistula. J Neurol Sci 1964;1:303.

[64] Tuite DJ, Kessel DO, Nicholson AA, Patel JV, McPherson SJ, Shaw DR. Initial clinical experience using the amplatzer vascular plug. Cardiovasc Inter Rad 2007;30:650-4.

[65] Pellerin O, Maleux G, Dean C, Pernot S, Golzarian J, Sapoval M. Microvascular Plug: A New Embolic Material for Hepatic Arterial Skeletonization. Cardiovasc Inter Rad 2014;37:1597-601.

[66] Tadavarthy SM, Moller JH, Amplatz K. Polyvinyl alcohol (Ivalon)--a new embolic material. The American Journal of Roentgenology, Radium Therapy, and Nuclear Medicine 1975;125:609-16.

[67] Derauf BJ, Hunter DW, Sirr SA, Cardella JF, Castanedazuniga W, Amplatz K. Peripheral Embolization of Diffuse Hepatic Arteriovenous-Malformations in a Patient with Hereditary Hemorrhagic Telangiectasia. Cardiovasc Inter Rad 1987;10:80-3.

[68] Thompson NP, Scheuer PJ, Dick R, Hamilton G, Burroughs AK. Intraperitoneal ivalon mimicking peritoneal malignancy after plugged percutaneous liver biopsy. Gut 1993;34:1635.

[69] Whiting JH, Morton KA, Datz FL, Patch GG, Miller FJ. Embolization of Hepatic Arteriovenous-Malformations Using Radiolabeled and Nonradiolabeled Polyvinyl-Alcohol Sponge in a Patient with Hereditary Hemorrhagic Telangiectasia - Case-Report. J Nucl Med 1992;33:260-2.

[70] Peixoto LS, Melo PA, Nele M, Pinto JC. Expanded Core/Shell Poly(vinyl acetate)/Poly(vinyl alcohol) Particles for Embolization. Macromol Mater Eng 2009;294:463-71.

[71] Stapf C, Mohr JP, Pile-Spellman J, Solomon RA, Sacco RL, Connolly ES, Jr. Epidemiology and natural history of arteriovenous malformations. Neurosurgical Focus 2001;11:e1.

[72] McCormick WF. The pathology of vascular ("arteriovenous") malformations. Journal of Neurosurgery 1966;24:807-16.

[73] Jabbour MN, Elder JB, Samuelson CG, Khashabi S, Hofman FM, Giannotta SL, et al. Aberrant angiogenic characteristics of human brain arteriovenous malformation endothelial cells. Neurosurgery 2009;64:139-46.

[74] Noran HH. Intracranial Vascular Tumors and Malformations. Arch Pathol 1945;39:393-416.

[75] Lanzino G, Jensen ME, Kongable GL, Kassell NF. Angiographic Characteristics of Dural Arteriovenous-Malformations That Present with Intracranial Hemorrhage. Acta Neurochir 1994;129:140-5.

[76] Koganemaru M, Abe T, Iwamoto R, Suenaga M, Matsuoka K, Hayabuchi N. Pelvic arteriovenous malformation treated by superselective transcatheter venous and arterial embolization. Jpn J Radiol 2012;30:526-9.

[77] Lasjaunias P, Chiu M, Terbrugge K, Tolia A, Hurth M, Bernstein M. Neurological Manifestations of Intracranial Dural Arteriovenous-Malformations. Journal of Neurosurgery 1986;64:724-30.

[78] Gupta A, Periakaruppan A. Intracranial dural arteriovenous fistulas: A Review. The Indian Journal of Radiology & Imaging 2009;19:43-8.

[79] Ogilvy CS, Stieg PE, Awad I, Brown RD, Jr., Kondziolka D, Rosenwasser R, et al. Recommendations for the management of intracranial arteriovenous malformations: a statement for healthcare professionals from a special writing group of the Stroke Council, American Stroke Association. Circulation 2001;103:2644-57.

[80] Brown PM, Zelt DT, Sobolev B. The risk of rupture in untreated aneurysms: The impact of size, gender, and expansion rate. J Vasc Surg 2003;37:280-3.

[81] Kent KC. Abdominal Aortic Aneurysms. New Engl J Med 2014;371:2101-8.

[82] Norman PE, Powell JT. Site Specificity of Aneurysmal Disease. Circulation 2010;121:560-8.

[83] Morita A. Current perspectives on the unruptured cerebral aneurysms: origin, natural course, and management. Journal of Nippon Medical School 2014;81:194-202.

[84] Lawrence PF, Lorenzorivero S, Lyon JL. The Incidence of Iliac, Femoral, and Popliteal Artery Aneurysms in Hospitalized-Patients. J Vasc Surg 1995;22:409-16.

[85] Assar AN, Zarins CK. Ruptured abdominal aortic aneurysm: a surgical emergency with many clinical presentations. Postgraduate Medical Journal 2009;85:268-73.

[86] Bederson JB, Awad IA, Wiebers DO, Piepgras D, Haley EC, Jr., Brott T, et al. Recommendations for the management of patients with unruptured intracranial aneurysms: A statement for healthcare professionals from the Stroke Council of the American Heart Association. Circulation 2000;102:2300-8.

[87] Walker TG, Kalva SP, Yeddula K, Wicky S, Kundu S, Drescher P, et al. Clinical practice guidelines for endovascular abdominal aortic aneurysm repair: written by the Standards of Practice Committee for the Society of Interventional Radiology and endorsed

by the Cardiovascular and Interventional Radiological Society of Europe and the Canadian Interventional Radiology Association. Journal of Vascular and Interventional Radiology: JVIR 2010;21:1632-55.

[88] Alguire PC, Mathes BM. Chronic venous insufficiency and venous ulceration. Journal of General Internal Medicine 1997;12:374-83.

[89] Beebe-Dimmer JL, Pfeifer JR, Engle JS, Schottenfeld D. The epidemiology of chronic venous insufficiency and varicose veins. Annals of Epidemiology 2005;15:175-84.

[90] Hjelmstedt A. Pressure decrease in the dorsal pedal veins on walking in persons with and without thrombosis. A study of a fracture series. Acta Chirurgica Scandinavica 1968;134:531-9.

[91] Belcaro G, Grigg M, Rulo A, Nicolaides A. Blood flow in the perimalleolar skin in relation to posture in patients with venous hypertension. Annals of Vascular Surgery 1989;3:5-7.

[92] Browse NL. The etiology of venous ulceration. World Journal of Surgery 1986;10:938-43.

[93] Browse NL, Burnand KG. The cause of venous ulceration. Lancet 1982;2:243-5.

[94] Bhutia SG, Balakrishnan A, Lees T. Varicose veins. Journal of Perioperative Practice 2008;18:346-53.

[95] McLafferty RB, Lohr JM, Caprini JA, Passman MA, Padberg FT, Rooke TW, et al. Results of the national pilot screening program for venous disease by the American Venous Forum. J Vasc Surg 2007;45:142-8.

[96] Adhikari A, Criqui MH, Wooll V, Denenberg JO, Fronek A, Langer RD, Klauber M. The Epidemiology of Chronic Venous Diseases. Phlebology 2000;15:2-18.

[97] Robertson L, Evans C, Fowkes FG. Epidemiology of chronic venous disease. Phlebology 2008;23:103-11.

[98] Schoonover JP, King JT, Gray C, Campbell K, Sherman C. 3 alternatives to standard varicose vein treatment. The Journal of Family Practice 2009;58:522-6.

[99] Tran NT, Meissner MH. The epidemiology, pathophysiology, and natural history of chronic venous disease. Seminars in Vascular Surgery 2002;15:5-12.

[100] van den Bos RR, de Maeseneer MMG. Endovenous thermal ablation for varicose veins: strengths and weaknesses. Phlebolymphology 2012;19:163-9.

[101] Callam MJ, Ruckley CV, Harper DR, Dale JJ. Chronic ulceration of the leg: extent of the problem and provision of care. British Medical Journal 1985;290:1855-6.

[102] Coon WW, Willis PW, 3rd, Keller JB. Venous thromboembolism and other venous disease in the Tecumseh community health study. Circulation 1973;48:839-46.

[103] Dalen JE, Paraskos JA, Ockene IS, Alpert JS, Hirsh J. Venous thromboembolism. Scope of the problem. Chest 1986;89:370S-3S.

[104] Nicolaides AN, Cardiovascular Disease E, Research T, European Society of Vascular S, Organization TIASAC, International Union of A, et al. Investigation of chronic venous insufficiency: A consensus statement (France, March 5-9, 1997). Circulation 2000;102:E126-63.

[105] Kapoor A, Kapoor A, Mahajan G. Endovenous Ablation of Saphenofemoral Insufficiency: Analysis of 100 Patients Using RF Closure Fast Technique. Indian J Surg 2010;72:458-62.

[106] Deatrick KB, Wakefield TW, Henke PK. Chronic venous insufficiency: current management of varicose vein disease. The American Surgeon 2010;76:125-32.

[107] Darvall KA, Bate GR, Adam DJ, Silverman SH, Bradbury AW. Duplex ultrasound outcomes following ultrasound-guided foam sclerotherapy of symptomatic recurrent great saphenous varicose veins. European Journal of Vascular and Endovascular Surgery : the Official Journal of the European Society for Vascular Surgery 2011;42:107-14.

[108] Negus D. Recurrent varicose veins: a national problem. The British Journal of Surgery 1993;80:823-4.

[109] Min RJ, Khilnani N, Zimmet SE. Endovenous laser treatment of saphenous vein reflux: long-term results. Journal of Vascular and Interventional Radiology 2003;14:991-6.

[110] Kumar V, Abbas AK, Aster JC, Robbins SL. Robbins basic pathology. 9th ed. Philadelphia, PA: Elsevier/Saunders; 2013.

[111] Kasper W, Geibel A, Tiede N, Just H. Patent foramen ovale in patients with haemodynamically significant pulmonary embolism. Lancet 1992;340:561-4.

[112] Kerut EK, Norfleet WT, Plotnick GD, Giles TD. Patent foramen ovale: a review of associated conditions and the impact of physiological size. Journal of the American College of Cardiology 2001;38:613-23.

[113] Reisman M, Christofferson RD, Jesurum J, Olsen JV, Spencer MP, Krabill KA, et al. Migraine headache relief after transcatheter closure of patent foramen ovale. Journal of the American College of Cardiology 2005;45:493-5.

[114] Leong MC, Uebing A, Gatzoulis MA. Percutaneous patent foramen ovale occlusion: Current evidence and evolving clinical practice. Int J Cardiol 2013;169:238-43.

[115] Strunk BL, Cheitlin MD, Stulbarg MS, Schiller NB. Right-to-left interatrial shunting through a patent foramen ovale despite normal intracardiac pressures. Am J Cardiol 1987;60:413-5.

[116] Knerr M, Bertog S, Vaskelyte L, Hofmann I, Sievert H. Results of percutaneous closure of patent foramen ovale with the GORE((R)) septal occluder. Catheterization and Cardiovascular Interventions : Official Journal of the Society for Cardiac Angiography & Interventions 2014;83:1144-51.

[117] Meier B. Current best practice in interventional cardiology. Chichester, UK ; Hoboken, NJ: Wiley-Blackwell; 2010.

[118] Agarwal S, Bajaj NS, Kumbhani DJ, Tuzcu EM, Kapadia SR. Meta-analysis of transcatheter closure versus medical therapy for patent foramen ovale in prevention of recurrent neurological events after presumed paradoxical embolism. JACC Cardiovascular Interventions 2012;5:777-89.

[119] Meier B. Stroke and migraine: a cardiologist's headache. Heart 2009;95:595-602.

[120] Taaffe M, Fischer E, Baranowski A, Majunke N, Heinisch C, Leetz M, et al. Comparison of three patent foramen ovale closure devices in a randomized trial

(Amplatzer versus CardioSEAL-STARflex versus Helex occluder). Am J Cardiol 2008;101:1353-8.

[121] Pavithra D, Doble M. Biofilm formation, bacterial adhesion and host response on polymeric implants - issues and prevention. Biomedical Materials 2008;3.

[122] Ratner BD. The catastrophe revisited: blood compatibility in the 21st Century. Biomaterials 2007;28:5144-7.

[123] Filion TM, Xu J, Prasad ML, Song J. In vivo tissue responses to thermal-responsive shape memory polymer nanocomposites. Biomaterials 2011;32:985-91.

[124] Bakhshi R, Darbyshire A, Evans JE, You Z, Lu J, Seifalian AM. Polymeric coating of surface modified nitinol stent with POSS-nanocomposite polymer. Colloids and surfaces B, Biointerfaces 2011;86:93-105.

[125] Sokolowski W. Potential bio-medical and commercial applications of cold hibernated elastic memory (CHEM) self-deployable foam structures. P Soc Photo-Opt Ins 2005;5648:397-405.

[126] Cabanlit M, Maitland D, Wilson T, Simon S, Wun T, Gershwin ME, et al. Polyurethane shape-memory polymers demonstrate functional biocompatibility in vitro. Macromolecular Bioscience 2007;7:48-55.

[127] Wilson TS, Bearinger JP, Herberg JL, Marion JE, Wright WJ, Evans CL, et al. Shape memory polymers based on uniform aliphatic urethane networks. J Appl Polym Sci 2007;106:540-51.

[128] Singhal P, Rodriguez JN, Small W, Eagleston S, de Water JV, Maitland DJ, et al. Ultra low density and highly crosslinked biocompatible shape memory polyurethane foams. J Polym Sci Pol Phys 2012;50:724-37.

[129] Chen H, Yuan L, Song W, Wu ZK, Li D. Biocompatible polymer materials: Role of protein-surface interactions. Prog Polym Sci 2008;33:1059-87.

[130] Furie B, Furie BC. Mechanisms of disease: Mechanisms of thrombus formation. New Engl J Med 2008;359:938-49.

[131] Gorbet MB, Sefton MV. Biomaterial-associated thrombosis: roles of coagulation factors, complement, platelets and leukocytes. Biomaterials 2004;25:5681-703.

[132] Esmon CT. Basic mechanisms and pathogenesis of venous thrombosis. Blood Reviews 2009;23:225-9.

[133] Ratner BD. Biomaterials science : an introduction to materials in medicine. 2nd ed. Amsterdam ; Boston: Elsevier Academic Press; 2004.

[134] Anderson JM. Biological responses to materials. Ann Rev Mater Res 2001;31:81-110.

[135] Dvorak HF, Harvey VS, Estrella P, Brown LF, Mcdonagh J, Dvorak AM. Fibrin Containing Gels Induce Angiogenesis - Implications for Tumor Stroma Generation and Wound-Healing. Lab Invest 1987;57:673-86.

[136] Hall WA, Oldfield EH, Doppman JL. Recanalization of spinal arteriovenous malformations following embolization. Journal of Neurosurgery 1989;70:714-20.

[137] Cho YD, Lee JY, Seo JH, Lee SJ, Kang HS, Kim JE, et al. Does Stent Implantation Improve the Result of Repeat Embolization in Recanalized Aneurysms? Neurosurgery 2012;71:253-9.

[138] Pierot L, Leclerc X, Bonafe A, Bracard S, Registry FM. Endovascular treatment of intracranial aneurysms with matrix detachable coils: Midterm anatomic follow-up from a prospective multicenter registry. Am J Neuroradiol 2008;29:57-61.

[139] Raymond J, Guilbert F, Metcalfe A, Gevry G, Salazkin I, Robledo O. Role of the endothelial lining in recurrences after coil embolization: prevention of recanalization by endothelial denudation. Stroke 2004;35:1471-5.

[140] Kroon ME, van Schie ML, van der Vecht B, van Hinsbergh VW, Koolwijk P. Collagen type 1 retards tube formation by human microvascular endothelial cells in a fibrin matrix. Angiogenesis 2002;5:257-65.

[141] Guo XB, Fan YM, Zhang JN. HydroSoft coil versus HydroCoil for endovascular aneurysm occlusion study: A single center experience. Eur J Radiol 2011;79:E42-E6.

[142] Nambiar AP, Bozlar U, Angle JF, Jensen ME, Hagspiel KD. Initial clinical experience with biopolymer-coated detachable coils (Hydrofoil) in peripheral embolization procedures. Journal of Vascular and Interventional Radiology 2008;19:995-1001.

[143] Margolis J. Initiation of Blood Coagulation by Glass and Related Surfaces. J Physiol-London 1957;137:95-109.

[144] Beilvert A, Chaubet F, Chaunier L, Guilois S, Pavon-Djavid G, Letourneur D, et al. Shape-memory starch for resorbable biomedical devices. Carbohyd Polym 2014;99:242-8.

[145] Filion TM, Xu JW, Prasad ML, Song J. In vivo tissue responses to thermal-responsive shape memory polymer nanocomposites. Biomaterials 2011;32:985-91.

[146] Davis KA, Burke KA, Mather PT, Henderson JH. Dynamic cell behavior on shape memory polymer substrates. Biomaterials 2011;32:2285-93.

[147] Neuss S, Blomenkamp I, Stainforth R, Boltersdorf D, Jansen M, Butz N, et al. The use of a shape-memory poly(is an element of-caprolactone)dimethacrylate network as a tissue engineering scaffold. Biomaterials 2009;30:1697-705.

[148] Sousa JE, Serruys PW, Costa MA. New frontiers in cardiology - Drug-eluting stents: Part I. Circulation 2003;107:2274-9.

[149] Brieger D, Topol E. Local drug delivery systems and prevention of restenosis. Cardiovasc Res 1997;35:405-13.

[150] Mani G, Feldman MD, Patel D, Agrawal CM. Coronary stents: A materials perspective. Biomaterials 2007;28:1689-710.

[151] Chen MC, Chang Y, Liu CT, Lai WY, Peng SF, Hung YW, et al. The characteristics and in vivo suppression of neointimal formation with sirolimus-eluting polymeric stents. Biomaterials 2009;30:79-88.

[152] Nagahama K, Ueda Y, Ouchi T, Ohya Y. Biodegradable Shape-Memory Polymers Exhibiting Sharp Thermal Transitions and Controlled Drug Release. Biomacromolecules 2009;10:1789-94.

[153] Jabara R, Chronos N, Robinson K. Novel bioabsorbable salicylate-based polymer as a drug-eluting stent coating. Catheter Cardio Inte 2008;72:186-94.

[154] Schwartz RS, Chronos NA, Virmani R. Preclinical restenosis models and drug-eluting stents - Still important, still much to learn. Journal of the American College of Cardiology 2004;44:1373-85.

[155] Cheng H, Hill PS, Siegwart DJ, Vacanti N, Lytton-Jean AKR, Cho SW, et al. A Novel Family of Biodegradable Poly(ester amide) Elastomers. Adv Mater 2011;23:H95-H100.

[156] Dvir T, Timko BP, Brigham MD, Naik SR, Karajanagi SS, Levy O, et al. Nanowired three-dimensional cardiac patches. Nat Nanotechnol 2011;6:720-5.

[157] Feng YK, Zhao HY, Behl M, Lendlein A, Guo JT, Yang DZ. Grafting of poly(ethylene glycol) monoacrylates on polycarbonateurethane by UV initiated polymerization for improving hemocompatibility. J Mater Sci-Mater M 2013;24:61-70.

[158] Friess F, Nochel U, Lendlein A, Wischke C. Polymer Micronetworks with Shape-Memory as Future Platform to Explore Shape-Dependent Biological Effects. Adv Healthc Mater 2014;3:1986-90.

[159] Heller DA, Levi Y, Pelet JM, Doloff JC, Wallas J, Pratt GW, et al. Modular 'Click-in-Emulsion' Bone-Targeted Nanogels. Adv Mater 2013;25:1449-54.

[160] Kolewe ME, Park H, Gray C, Ye XF, Langer R, Freed LE. 3D Structural Patterns in Scalable, Elastomeric Scaffolds Guide Engineered Tissue Architecture. Adv Mater 2013;25:4459-65.

[161] Lendlein A, Neffe AT, Jerome C. Advanced functional polymers for medicine. Adv Healthc Mater 2014;3:1939-40.

[162] Mizrahi B, Shankarappa SA, Hickey JM, Dohlman JC, Timko BP, Whitehead KA, et al. A Stiff Injectable Biodegradable Elastomer. Adv Funct Mater 2013;23:1527-33.

[163] Mizrahi B, Stefanescu CF, Yang C, Lawlor MW, Ko D, Langer R, et al. Elasticity and safety of alkoxyethyl cyanoacrylate tissue adhesives (vol 7, pg 3150, 2011). Acta Biomaterialia 2012;8:458-.

[164] Neal RA, Jean A, Park H, Wu PB, Hsiao J, Engelmayr GC, et al. Three-Dimensional Elastomeric Scaffolds Designed with Cardiac-Mimetic Structural and Mechanical Features. Tissue Eng Pt A 2013;19:793-807.

[165] Nochel U, Kumar UN, Wang K, Kratz K, Behl M, Lendlein A. Triple-Shape Effect with Adjustable Switching Temperatures in Crosslinked Poly[ethylene-co-(vinyl acetate)]. Macromol Chem Phys 2014;215:2446-56.

[166] Nochel U, Reddy CS, Uttamchand NK, Kratz K, Behl M, Lendlein A. Shape-memory properties of hydrogels having a poly(epsilon-caprolactone) crosslinker and switching segment in an aqueous environment. Eur Polym J 2013;49:2457-66.

[167] Pereira MJN, Ouyang B, Sundback CA, Lang N, Friehs I, Mureli S, et al. A Highly Tunable Biocompatible and Multifunctional Biodegradable Elastomer. Adv Mater 2013;25:1209-15.

[168] Schmidt C, Behl M, Lendlein A, Beuermann S. Synthesis of high molecular weight polyglycolide in supercritical carbon dioxide. Rsc Adv 2014;4:35099-105.

[169] Tekin H, Sanchez JG, Tsinman T, Langer R, Khademhosseini A. Thermoresponsive Platforms for Tissue Engineering and Regenerative Medicine. Aiche J 2011;57:3249-58.

[170] Ullm S, Kruger A, Tondera C, Gebauer TP, Neffe AT, Lendlein A, et al. Biocompatibility and inflammatory response in vitro and in vivo to gelatin-based biomaterials with tailorable elastic properties. Biomaterials 2014;35:9755-66.

[171] Wang J, Boutin KG, Abdulhadi O, Personnat LD, Shazly T, Langer R, et al. Fully Biodegradable Airway Stents Using Amino Alcohol-Based Poly(ester amide) Elastomers. Adv Healthc Mater 2013;2:1329-36.

[172] Wischke C, Schneider C, Neffe AT, Lendlein A. Polyalkylcyanoacrylates as in situ formed diffusion barriers inmultimaterial drug carriers. J Control Release 2013;169:321-8.

[173] Yang J, Lv J, Behl M, Lendlein A, Yang D, Zhang L, et al. Functionalization of polycarbonate surfaces by grafting PEG and zwitterionic polymers with a multicomb structure. Macromolecular Bioscience 2013;13:1681-8.

[174] Bruggeman JP, de Bruin BJ, Bettinger CJ, Langer R. Biodegradable poly(polyol sebacate) polymers. Biomaterials 2008;29:4726-35.

[175] Murayama Y, Vinuela F, Tateshima S, Song JK, Gonzalez NR, Wallace MP. Bioabsorbable polymeric material coils for embolization of intracranial aneurysms: a preliminary experimental study. Journal of Neurosurgery 2001;94:454-63.

[176] Min CC, Cui WJ, Bei JZ, Wang SG. Biodegradable shape-memory polymer-polylactideco-poly(glycolide-co-caprolactone) multiblock copolymer. Polym Advan Technol 2005;16:608-15.

[177] Xue LA, Dai SY, Li Z. Biodegradable shape-memory block co-polymers for fast self-expandable stents. Biomaterials 2010;31:8132-40.

[178] Laborda A, Medrano J, de Blas I, Urtiaga I, Carnevale FC, de Gregorio MA. Endovascular treatment of pelvic congestion syndrome: visual analog scale (VAS) long-term follow-up clinical evaluation in 202 patients. Cardiovasc Intervent Radiol 2013;36:1006-14.

[179] Masson P, Brannigan RE. The varicocele. The Urologic Clinics of North America 2014;41:129-44.

[180] Enriquez J, Javadi S, Murthy R, Ensor J, Jr., Mahvash A, Abdelsalam ME, et al. Gastroduodenal artery recanalization after transcatheter fibered coil embolization for prevention of hepaticoenteric flow: incidence and predisposing technical factors in 142 patients. Acta Radiologica 2013;54:790-4.

[181] Dudeck O, Bulla K, Wieners G, Ruehl R, Ulrich G, Amthauer H, et al. Embolization of the Gastroduodenal Artery Before Selective Internal Radiotherapy: A Prospectively Randomized Trial Comparing Standard Pushable Coils with Fibered Interlock Detachable Coils. Cardiovasc Intervent Radiol 2011;34:74-80.

[182] Emmert MY, Venbrux A, Rudakov L, Cesarovic N, Radvany MG, Gailloud P, et al. The endovascular occlusion system for safe and immediate peripheral vessel occlusion during vascular interventions. Interactive Cardiovascular and Thoracic Surgery 2013;17:882-5.

[183] Wang W, X. Zhu, M.D. Tam, G. Pierce, G. McLennan, M.J. Sands. Advantages and limitations of the Amplatzer vascular plug: a comparison study with conventional coil

technique in splenic artery embolization. Journal of Vascular and Interventional Radiology 2010;21:S78.

[184] Hwang W, Singhal P, Miller MW, Maitland DJ. In Vitro Study of Transcatheter Delivery of a Shape Memory Polymer Foam Embolic Device for Treating Cerebral Aneurysms. J Med Devices 2013;7.

[185] Ortega JM, Hartman J, Rodriguez JN, Maitland DJ. Virtual Treatment of Basilar Aneurysms Using Shape Memory Polymer Foam. Annals of Biomedical Engineering 2013;41:725-43.

[186] Rodriguez JN, Miller MW, Boyle A, Horn J, Yang CK, Wilson TS, et al. Reticulation of low density shape memory polymer foam with an in vivo demonstration of vascular occlusion. J Mech Behav Biomed Mater 2014;40:102-14.

[187] Rodriguez JN, Yu YJ, Miller MW, Wilson TS, Hartman J, Clubb FJ, et al. Opacification of shape memory polymer foam designed for treatment of intracranial aneurysms. Annals of Biomedical Engineering 2012;40:883-97.

[188] Rodriguez JN, Clubb FJ, Wilson TS, Miller MW, Fossum TW, Hartman J, et al. In vivo response to an implanted shape memory polyurethane foam in a porcine aneurysm model. J Biomed Mater Res A 2014;102:1231-42.

[189] Bavinzski G, Talazoglu V, Killer M, Richling B, Gruber A, Gross CE, et al. Gross and microscopic histopathological findings in aneurysms of the human brain treated with Guglielmi detachable coils. Journal of Neurosurgery 1999;91:284-93.

[190] Molyneux AJ, Ellison DW, Morris J, Byrne JV. Histological findings in giant aneurysms treated with Guglielmi detachable coils. Report of two cases with autopsy correlation. Journal of Neurosurgery 1995;83:129-32.

[191] Singhal P, Rodriguez JN, Small W, Eagleston S, Van de Water J, Maitland DJ, et al. Ultra Low Density and Highly Crosslinked Biocompatible Shape Memory Polyurethane Foams. Journal of Polymer Science Part B, Polymer Physics 2012;50:724-37.

[192] Friedrich P, Reininger AJ. Occlusive Thrombus Formation on Indwelling Catheters - in-Vitro Investigation and Computational Analysis. Thromb Haemostasis 1995;73:66-72.

[193] Caivano D, Birettoni F, Fruganti A, Rishniw M, Knafelz P, Moise NS, et al. Transthoracic echocardiographically-guided interventional cardiac procedures in the dog. J Vet Cardiol 2012;14:431-44.

[194] Porciello F, Caivano D, Giorgi ME, Knafelz P, Rishniw M, Moise NS, et al. Transesophageal Echocardiography as the Sole Guidance for Occlusion of Patent Ductus Arteriosus using a Canine Ductal Occluder in Dogs. J Vet Intern Med 2014;28:1504-12.

[195] Nguyen TT, Biadillah Y, Mongrain R, Brunette J, Tardif JC, Bertrand OF. A method for matching the refractive index and kinematic viscosity of a blood analog for flow visualization in hydraulic cardiovascular models. Journal of Biomechanical Engineering 2004;126:529-35.

[196] Adcock DM, Kressin DC, Marlar RA. Effect of 3.2% vs 3.8% sodium citrate concentration on routine coagulation testing. American Journal of Clinical Pathology 1997;107:105-10.

[197] Riley JH, Lassen ED. Activated coagulation times of normal cows. Veterinary Clinical Pathology / American Society for Veterinary Clinical Pathology 1979;8:31-3.

[198] Kim SW, Lee RG, Oster H, Coleman D, Andrade JD, Lentz DJ, et al. Platelet adhesion to polymer surfaces. Transactions - American Society for Artificial Internal Organs 1974;20 B:449-55.

[199] Neumann T, Nicholson BS, Sanders JE. Tissue engineering of perfused microvessels. Microvascular Research 2003;66:59-67.

[200] Zweens J, Schiphof P. Permanent catheterization of aorta and pulmonary artery in the dog. Pflugers Archiv : European Journal of Physiology 1976;362:201-2.

[201] Konig G, McAllister TN, Dusserre N, Garrido SA, Iyican C, Marini A, et al. Mechanical properties of completely autologous human tissue engineered blood vessels compared to human saphenous vein and mammary artery. Biomaterials 2009;30:1542-50.

[202] Kipshidze N, Sadzaglishvili K, Panarella M, Rivera EA, Virmani R, Leon MB. Evaluation of a novel endoluminal vascular occlusion device in a porcine model: early and late follow-up. Journal of Endovascular Therapy : an Official Journal of the International Society of Endovascular Specialists 2005;12:486-94.

[203] Zamboni P, Menegatti E, Galeotti R, Malagoni AM, Tacconi G, Dall'Ara S, et al. The value of cerebral Doppler venous haemodynamics in the assessment of multiple sclerosis. J Neurol Sci 2009;282:21-7.

[204] Gao Z, Guo W, Liu X, Huang W, Zhang H, Tan N, et al. Automated detection framework of the calcified plaque with acoustic shadowing in IVUS images. PloS One 2014;9:e109997.

[205] Wilson TS, Bearinger JP, Herberg JL, Marion JE, Wright WJ, Evans CL, et al. Shape memory polymers based on uniform aliphatic urethane networks. J Appl Polym Sci 2007;106:540-51.

[206] Yu YJ, Hearon K, Wilson TS, Maitland DJ. The effect of moisture absorption on the physical properties of polyurethane shape memory polymer foams. Smart Materials & Structures 2011;20.

[207] Kallmes DF, Fujiwara NH. New expandable hydrogel-platinum coil hybrid device for aneurysm embolization. AJNR American Journal of Neuroradiology 2002;23:1580-8.

[208] Abdel-Aal AK, Elsabbagh A, Soliman H, Hamed M, Underwood E, Saddekni S. Percutaneous Embolization of a Postnephrectomy Arteriovenous Fistula With Intervening Pseudoaneurysm Using the Amplatzer Vascular Plug 2. Vasc Endovasc Surg 2014;48:516-21.

[209] Ozyurtlu F, Acet H, Ozpelit ME, Pekel N. Optimal treatment of unligated side branch of internal mammary artery: Coil, amplatzer vascular plug or graft stent? A case report and literature review. Turk Kardiyoloji Dernegi Arsivi : Turk Kardiyoloji Derneginin Yayin Organidir 2015;43:376-80.

[210] Abdel Aal AK, Hamed MF, Biosca RF, Saddekni S, Raghuram K. Occlusion time for Amplatzer vascular plug in the management of pulmonary arteriovenous malformations. AJR American Journal of Roentgenology 2009;192:793-9.

[211] Ferro C, Rossi UG, Bovio G, Petrocelli F, Seitun S. The Amplatzer vascular plug 4: preliminary experience. Cardiovasc Intervent Radiol 2010;33:844-8.

[212] Mordasini P, Gralla J, Brekenfeld C, Schroth G, Hoppe H. Preliminary Experimental Evaluation of the Immediate Angiographic Occlusion Time with Use of the AMPLATZER Vascular Plug II for Carotid Artery Occlusion. Journal of Vascular and Interventional Radiology 2010;21:1873-7.

[213] Kauvar DS, Lefering R, Wade CE. Impact of hemorrhage on trauma outcome: an overview of epidemiology, clinical presentations, and therapeutic considerations. The Journal of Trauma 2006;60:S3-11.

[214] Kheirabadi B. Evaluation of topical hemostatic agents for combat wound treatment. US Army Medical Department Journal 2011:25-37.

[215] Ong SY, Wu J, Moochhala SM, Tan MH, Lu J. Development of a chitosan-based wound dressing with improved hemostatic and antimicrobial properties. Biomaterials 2008;29:4323-32.

[216] Devlin JJ, Kircher S, Kozen BG, Littlejohn LF, Johnson AS. Comparison of ChitoFlex(R), CELOX, and QuikClot(R) in control of hemorrhage. The Journal of Emergency Medicine 2011;41:237-45.

[217] Kozen BG, Kircher SJ, Henao J, Godinez FS, Johnson AS. An alternative hemostatic dressing: comparison of CELOX, HemCon, and QuikClot. Academic Emergency Medicine : Official Journal of the Society for Academic Emergency Medicine 2008;15:74-81.

[218] Wedmore I, McManus JG, Pusateri AE, Holcomb JB. A special report on the chitosan-based hemostatic dressing: experience in current combat operations. The Journal of Trauma 2006;60:655-8.

[219] Littlejohn LF, Devlin JJ, Kircher SS, Lueken R, Melia MR, Johnson AS. Comparison of Celox-A, ChitoFlex, WoundStat, and combat gauze hemostatic agents versus standard gauze dressing in control of hemorrhage in a swine model of penetrating trauma. Academic Emergency Medicine : Official Journal of the Society for Academic Emergency Medicine 2011;18:340-50.

[220] Johnson D, Agee S, Reed A, Gegel B, Burgert J, Gasko J, et al. The effects of QuikClot Combat Gauze on hemorrhage control in the presence of hemodilution. US Army Medical Department Journal 2012:36-9.

[221] Sairaku A, Nakano Y, Oda N, Makita Y, Kajihara K, Tokuyama T, et al. Rapid hemostasis at the femoral venous access site using a novel hemostatic pad containing kaolin after atrial fibrillation ablation. J Interv Card Electr 2011;31:157-64.

[222] Murray CK, Hsu JR, Solomkin JS, Keeling JJ, Andersen RC, Ficke JR, et al. Prevention and management of infections associated with combat-related extremity injuries. The Journal of Trauma 2008;64:S239-51.

[223] Mueller GR, Pineda TJ, Xie HX, Teach JS, Barofsky AD, Schmid JR, et al. A novel sponge-based wound stasis dressing to treat lethal noncompressible hemorrhage. The Journal of Trauma and Acute Care Surgery 2012;73:S134-9.

[224] Kragh JF, Jr., Aden JK, Steinbaugh J, Bullard M, Dubick MA. Gauze vs XSTAT in wound packing for hemorrhage control. The American Journal of Emergency Medicine 2015;33:974-6.

[225] Rodriguez JN, Miller MW, Boyle A, Horn J, Yang CK, Wilson TS, et al. Reticulation of low density shape memory polymer foam with an in vivo demonstration of vascular occlusion. Journal of the Mechanical Behavior of Biomedical Materials 2014;40:102-14.

[226] Cutting KF. Managing wound exudate using a super-absorbent polymer dressing: a 53-patient clinical evaluation. Journal of Wound Care 2009;18:200, 2-5.

[227] Kear TM. Does the Direct Application of Povidone-Iodine Hasten Hemostasis of the Cannulation Site After The Removal of Hemodialysis Needles? Nephrol Nurs J 2012;39:409-12.

[228] Xie T. Recent advances in polymer shape memory. Polymer 2011;52:4985-5000.

[229] de Faria DLA, Gil HAC, de Queiroz AAA. The interaction between polyvinylpyrrolidone and I-2 as probed by Raman spectroscopy. J Mol Struct 1999;478:93-8.

[230] Gilliland EL, Nathwani N, Dore CJ, Lewis JD. Bacterial colonisation of leg ulcers and its effect on the success rate of skin grafting. Annals of the Royal College of Surgeons of England 1988;70:105-8.

[231] Robson MC, Duke WF, Krizek TJ. Rapid bacterial screening in the treatment of civilian wounds. The Journal of Surgical Research 1973;14:426-30.

[232] Burnett LR, Richter JG, Rahmany MB, Soler R, Steen JA, Orlando G, et al. Novel keratin (KeraStat) and polyurethane (Nanosan(R)-Sorb) biomaterials are hemostatic in a porcine lethal extremity hemorrhage model. Journal of Biomaterials Applications 2014;28:869-79.

[233] Kabiri K, Omidian H, Hashemi SA, Zohuriaan-Mehr MJ. Synthesis of fast-swelling superabsorbent hydrogels: effect of crosslinker type and concentration on porosity and absorption rate. Eur Polym J 2003;39:1341-8.

[234] Omidian H, Rocca JG, Park K. Advances in superporous hydrogels. J Control Release 2005;102:3-12.

[235] Chung YC, Su YP, Chen CC, Jia G, Wang HI, Wu JCG, et al. Relationship between antibacterial activity of chitosan and surface characteristics of cell wall. Acta Pharmacol Sin 2004;25:932-6.

[236] No HK, Park NY, Lee SH, Meyers SP. Antibacterial activity of chitosans and chitosan oligomers with different molecular weights. International Journal of Food Microbiology 2002;74:65-72.

[237] Ahearn DG, Grace DT, Jennings MJ, Borazjani RN, Boles KJ, Rose LJ, et al. Effects of hydrogel/silver coatings on in vitro adhesion to catheters of bacteria associated with urinary tract infections. Current Microbiology 2000;41:120-5.

[238] Yu HJ, Xu XY, Chen XS, Lu TC, Zhang PB, Jing XB. Preparation and antibacterial effects of PVA-PVP hydrogels containing silver nanoparticles. J Appl Polym Sci 2007;103:125-33.

[239] Singhal P, Boyle A, Brooks ML, Infanger S, Letts SD, Small WD, et al. Controlling the Actuation Rate of Low-Density Shape-Memory Polymer Foams in Water. Macromol Chem Phys 2013;214:1204-14.

[240] Kim DB, Choi H, Joo SM, Kim HK, Shin JH, Hwang MH, et al. A comparative reliability and performance study of different stent designs in terms of mechanical properties: foreshortening, recoil, radial force, and flexibility. Artificial Organs 2013;37:368-79.